Towards implementing impedance control in sensorimotor neuroprostheses

A thesis submitted to the faculty of

The School of Graduate Studies

State University of New York Downstate Medical Center and

Polytechnic Institute of New York University

In partial fulfillment of the requirements

for the degree of Doctor of Philosophy

by

Pratik Y. Chhatbar

Joint program in Biomedical Engineering

Date: April 28, 2011

Thesis advisors:

Joseph T. Francis, Ph.D

John K. Chapin, Ph.D.

Department of Physiology and Pharmacology

Acknowledgements

I deeply appreciate this wonderful opportunity to be a part of joint Biomedical Engineering program between State University of New York Downstate Medical Center and Polytechnic Institute of New York University. As a graduate student under joint mentorship of Drs. Joseph T. Francis and John K. Chapin, I enjoyed rich hands-on experience on how research is conducted, pursued and communicated in multitude of ways ranging from research papers, posters, presentations and personal communications in formal as well as informal setup. I am grateful to Dr. Chapin and past dean Dr. Susan Schwartz-Giblin for finding me fit and encouraging me to join the graduate school. I thank Dr. Francis for providing perfect blend of independence and guidance as we worked together closely on variety of projects and towards numerous grants, papers, conference posters and presentations and finally making of this thesis document.

Guidance from Drs. Farshad Khorrami and Prashanth Krishnamurthy from NYU-Poly has been instrumental in applying and troubleshooting the Robotics concepts used throughout this thesis document. I thank Dr. Saha for persuading me to review current state, future projections and ethical implications related to Neuroprosthetics, which resulted a couple of platform presentations and a research paper 'The future of implantable neuroprosthetic devices: ethical considerations'. Dr. Nandor Ludvig and Dr. Mark Stewart have been very supportive, interested and available as a next-door laboratory for fruitful discussions, help and guidance that helped a lot towards superior quality of this thesis. Dr. Stewart, as a dean of School of Graduate studies, has always stood by the side of graduate students and helped everyone as

needed. Dr. Stephen Onesti always served as a source of inspiration and enthusiasm apart from keeping me abreast of clinical aspects and implications of the basic science research that we pursue intensely in our setup.

I am fortunate to have wonderful lab mates who have been of great help on everything we do in the lab ranging from simplest technical tasks to involved scientific discussions. I specially thank Emerson Hawley, Lee von Kraus, Mulugeta Semework, Shaohua Xu, Lei Li, Anna Rozenboym, Hai Tang and Dave Rodriguez for teaching me simplest laboratory how-to's to scientific way of thinking, especially during my early days in graduate school. Marcello DiStasio, Jordan Iordanou, John Choi, Brandi Marsh, Aditya Tarigoppula are awesome colleagues to have around. New post-doctoral lab members Weiguo Song, Kwangtaek Kim, Janina Farbinteanu have helped me with thinking, doing and communicating science with their post-doctoral experience and expertise. Sandra Gourdet has been helping a lot with taking care of never-ending administrative work. Thanks to Shamik Chakraborty, Gregory Perrin, Waheed Abdul, Charlie Wray, Josh Papandreadis and all rotating students who have helped out in the lab work.

I thank Division of Laboratory Animal Resources for guidance, help and supervision on the experiments and surgeries. I thank Drs. Carol Novotney, Samuel Adams and Bruce Scharf for providing wonderful platform to conduct all the experiments and acute/chronic surgery. Drs. Jean Charchaflieh and Hai Tang have always lent a helping hand during surgeries with their anesthesiology skills in case of occasional intra-operative complications. Special thanks to Elizabeth Rivera, Kerel Ferguson, Allison Maurice, Cora Kaiser, Neal Grant and other staff towards superior animal care and assistance.

Downstate body of faculties with their broad graduate program affiliation has been very friendly and supportive. I never felt awkward approaching any faculty from any graduate program track for discussing related work and have always received encouraging response and productive feedback. Graduate student colleagues at Downstate have always been fun to be around and so are the graduate school officers. I thank Ed Throckmorton, Ellen Telesca, Sharon Reid-Spence, Denise Sheares and Lila Lande for their help and encouragement.

I would like to take an opportunity to thank our collaborators Drs. William Lytton, Randall Barbour, Justin Sanchez, Jose Carmena, Jose Principe, Jose Fortes, Reza Shadmehr and their lab members for their help and support. I also would like to thank Dr. Ashesh Mehta at Long Island Jewish Northshore Healthcare System for the opportunity to work with epilepsy patients and Electro-corticography (ECoG) signals towards realizing the ECoG-based Brain-Machine Interfaces. This was my first hands-on experience to clinical research in BMI and I look forward to do more work in this direction in future.

I am extremely grateful to my family, especially my wife Namrata, for their continuous support and understanding throughout this endeavor. During my graduate school years my family has gone through most joyous moments like our marriage to most stressful situations of my mother's diagnosis of breast cancer and her consequent sad demise in a short span of 3 years. Throughout these tough times, Namrata, her parents, my brother Deepak, sister Ritu and my parents never gave me a slightest hint of the stress they are experiencing and supported me and my work. They have pure faith that the research I am pursuing will help the disabled to be more independent. Namrata has served literally as my alter-ego, taking care of my mom, my family and home back in India with her unfaltering enthusiasm even if that meant months of separation from me as I continued my research here at Downstate. My heartfelt thanks to my

extended family and friends also for supporting us here and my family back in India, filling my void as I continued my research.

Table of contents

Table of figures

1 Introduction

1.1 Sensorimotor neuroprosthetics and current state of the technology

1.1.1 What is it?

Broadly, sensorimotor Neuroprosthetics is a discipline related to neuroscience and biomedical engineering concerned with developing neural prostheses. Neural prostheses are a series of devices that can substitute a motor, sensory or cognitive modality that might have been damaged as a result of an injury or a disease (Wikipedia). It includes variety of sensory modalities including vision, hearing, touch etc. The introductory discussion of it has been given in the chapter, Ethical considerations on implantable neuroprosthetics. For the purpose of this discussion, we will limit it to the science of neural control of movements such as reaching, grasping and locomotion.

The science of neuroprosthetics related to neural control of movement entered the domain of closed-loop systems with demonstration that the robotic arm can be moved by cortical neural signals recorded through microelectrode arrays (Chapin et al. 1999). This was followed by many groups demonstrating real-time control of cursor or robotic arm using variety of decoders predicting kinematic variables in real-time (Taylor, Tillery, and Schwartz 2002; Serruya et al. 2002; Carmena et al. 2003; Wessberg et al. 2000). All this work was done using spiking activity from contralateral motor cortex. Recently our collaborators have demonstrated use of ipsilateral motor cortex for real-time control of kinematic variables, which might be of crucial importance in patients with contralateral motor cortical loss or damage (Ganguly et al. 2009). These results offer an alternate potential site of recording neural signals in case of damage or destruction of the contralateral brain region primarily involved with the sensorimotor function. All this real-

time control of robotic arm or cursor has been done using predictions of variables of kinematics like position or velocity, but use of dynamics-related parameters for such real-time control has not been demonstrated.

1.1.2 Dynamics versus kinematics

Dynamics is a branch of mechanics that is concerned with the effects of forces on the motion of a body or system of bodies, especially of forces that do not originate within the system itself. It is also called Kinetics. Kinematics, on the contrary, is the branch of mechanics that studies the motion of a body or a system of bodies without consideration given to its mass or the forces acting on it (American Heritage Dictionary of the English Language).

Figure 1.1: Same kinematics doesn't mean same dynamics. To make the same movement with the objects of different inertial properties or in different environmental conditions, we generate different amount of forces/joint torques/muscle activations.

As mentioned before, majority, if not all, of the real-time, closed-loop control of movements literature focused on kinematics behaviors. But in day-to-day reaching and grasping tasks we use forces, control impedance and co-contractions of antagonist muscles to move about and

maneuver objects (Figure 1.1). This can be best achieved by real-time control of Brain-Machine Interface (BMI) using dynamics (kinetics)-related variables such as forces and torques. By getting direct control of dynamics the user can decide how much forces to apply on the object, making impedance control possible as described below. This makes the reaching and grasping tasks less dependent, if not independent, on the inverse-dynamic algorithms of the neuroprosthetic device in case of pure kinematic control.

1.2 Significance of impedance control

Mechanical impedance (impedance implies mechanical impedance, unless specified otherwise, for the scope of this discussion) is the ratio of the mechanical force, acting in the direction of motion, to the velocity of the resulting vibration (Collins English Dictionary). In other words, it is a measure of how much a structure resists motion when subjected to a given force. It is described by symbol Z (specifically, Z_m). For the scope of this discussion, it should not be confused with acoustic impedance (Z_a, the ratio of sound pressure in a medium ot the rate of alternating flow of the medium through a specified surface due to the sound wave) or electrical impedance (Z, expressed in ohms, a measure of the opposition to the flow of an alternating current equal to the square root of the sum of the squares of the resistance and the reactance). Just like electrical impedance, the inverse of mechanical impedance is termed as admittance. Here the admittance in simple terms would mean range of mobility in response to the amount of force applied. Mechanical impedance can be explained as,

Equation 1-1

$$Z(\omega) = \frac{F(\omega)}{v(\omega)}$$

where F is the force vector, v is the velocity vector, Z is the impedance matrix and ω is the angular frequency. A simple example of impedance control would be crushing a Styrofoam cup in a controlled manner. Under pure kinematic control, the user may decide on holding the cup. But when it comes to crushing the cup, the user can only decide on pure movement aspects of it and the controller has to generate appropriate forces needed for crushing. This comes naturally if the user is controlling the robotic arm using parameters involving dynamics, which would give the user full impedance control.

Impedance control will also be the best way to control inadvertent forces generated by the robotic arm and potential damage. In the previous example if we replace Styrofoam cup with a glass or metal cup, crushing the cup under kinematic control will either break the glass cup or damage the arm in case of metal cup. This is because the robotic arm will keep trying to crush the cup as instructed by the user and might damage itself. This will not be the case with impedance control using dynamics parameters, as the amount of force applied to crush the Styrofoam cup will minimally affect the glass cup and metal cup. Also since the amount of force generation has set limits, as decided by neural activity, it will not damage the robotic arm. Similar examples can be thought of during sudden change in the environment like coming across a stiff, immobile, heavy object on the robotic arm movement trajectory or movements while submerged in water, scribbling on the chalk board with control of boldness of the writings etc.

1.3 Rationale behind invasive neural recordings

Towards achieving the goal of impedance control, we need neural signals that have high spatial and temporal resolution. We can see that BMI research claiming fine control of movements is done using intracortical recordings using microelectrode arrays (MEA). There is a

good reason behind it: the closer we are to the source of the signal, the better the signal-to-noise ratio (Figure 1.2). Other less invasive techniques of neural signal acquisition like EEG, ECoG, fMRI etc. have been used for BMI performance, but none matches the spatial and temporal resolution that is achieved with microelectrode array recordings (Felzer and Freisleben 2002; Piccione et al. 2006; Felton et al. 2007; Ganguly et al. 2009). These can thus best be used for discrete response or for simplest reaching tasks. Currently there is no technology that is non-invasive and can achieve the spatial and temporal resolution as achieved by microelectrode array recording.

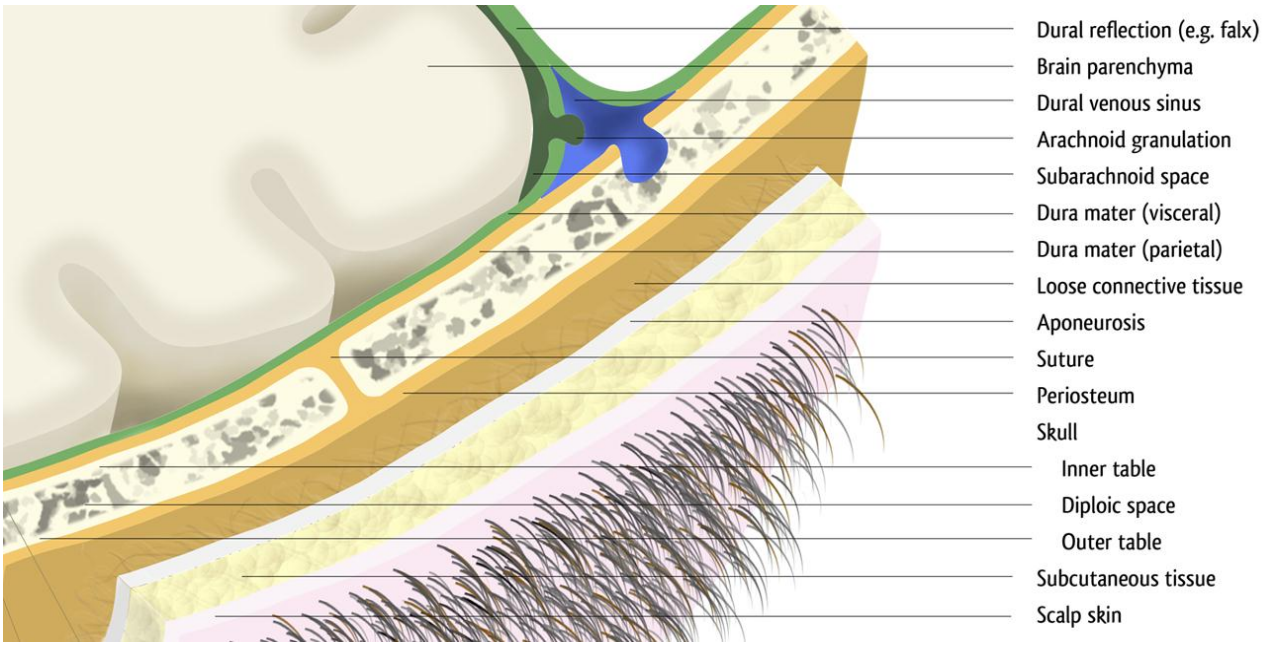

Figure 1.2: Coverings of the brain. Microelectrode arrays get implanted in gray matter and record directly from neurons immediately around the tip of the electrode. Other neural recording techniques like subdural and epidural ECoG/EEG, skin EEG have their sensors in subdural space, epidural space or on skin surface respectively and have decreased spatial resolution, and signal-to-noise ratio, in that order. Imaging techniques like MEG and fMRI technologies record the neural activity or vascular response to it, in a non-contact fashion, but lack spatial, and temporal in case of fMRI, resolution. (Image is from Wikimedia Commons)

Considering these limitations with neural signal acquisition, we settled on using invasive, but giving highest possible neural signal resolution, microelectrode array (MEA) recording method. Like any other invasive method, microelectrode implantations also have many drawbacks like inflammation, gliosis, foreign-body reaction, functional longevity issues to name a few. Efforts have been made to make implanted microelectrodes more bio-friendly by variety of coatings including nanotubes (Lovat et al. 2005; Shoval et al. 2009; Hanein 2010) but their long-term effects on the body are still not known (Shvedova et al. 2003; Köhler et al. 2008; Lam et al. 2006). Efforts have also been made towards injecting anti-inflammatory and other drugs in the vicinity of the implant site (Greger and Kateb 2004; Ludvig and Kovacs 2002; Ludvig et al. 2009). Until the availability of the technology that is non-invasive and has neural signal quality that is comparable to invasive methods, we have to make the best use of available technology in a most bio-friendly, reversible and economical manner.

1.4 Selection of implantation site, arrays and rationale

1.4.1 Motor cortex and microscopic organization of cortex in general

It has been well established that primary motor cortex (M1), along with neighboring premotor cortex anteriorly and somatosensory cortex posterior to central sulcus is directly responsible for limb and body movements. Apart from heavy connections from somatosensory cortex, structural and functional connectivity maps from other posterior parietal and supplementary motor regions have been described in details (Luppino and Rizzolatti 2000; Rizzolatti, Luppino, and Matelli 1998). These connections are established to be plastic enough to change in use-dependent and use-independent manner after M1 lesions for manual dexterous tasks (Murata et al. 2008).

Out of six neocortical layers of motor cortex, layers I-III are main targets of interhemispheric corticocortical afferents and layer III, external pyramidal layer containing primarily of small and middle-size pyramidal neurons, is the source of corticocortical efferents. Relatively thin layer IV, internal granular layer containing different types of stellate and pyramidal neurons, receives thalamic type C neuronal and intra-hemispheric corticocortical afferents (Jones 1998). Layer V, internal pyramidal layer containing large pyramidal cells and Betz cells, is the principal source of subcortical efferents. Finally the deepest Layer VI, multiform layer containing few large pyramidal neurons and many small spindle-like pyramidal and multiform neurons, sends both excitatory and inhibitory efferents to thalamus esp. in case of somatosensory cortex (Lam and Sherman 2010). Apart from such horizontal layers or laminar organization, vertical micro-columnar arrangement has also been proposed (Jones 2000). Disruption of such vertical micro-columnar disruption is found in certain diseases, for example in association cortex under Alheimer's or Lewy body dementias (Buldyrev et al. 2000).

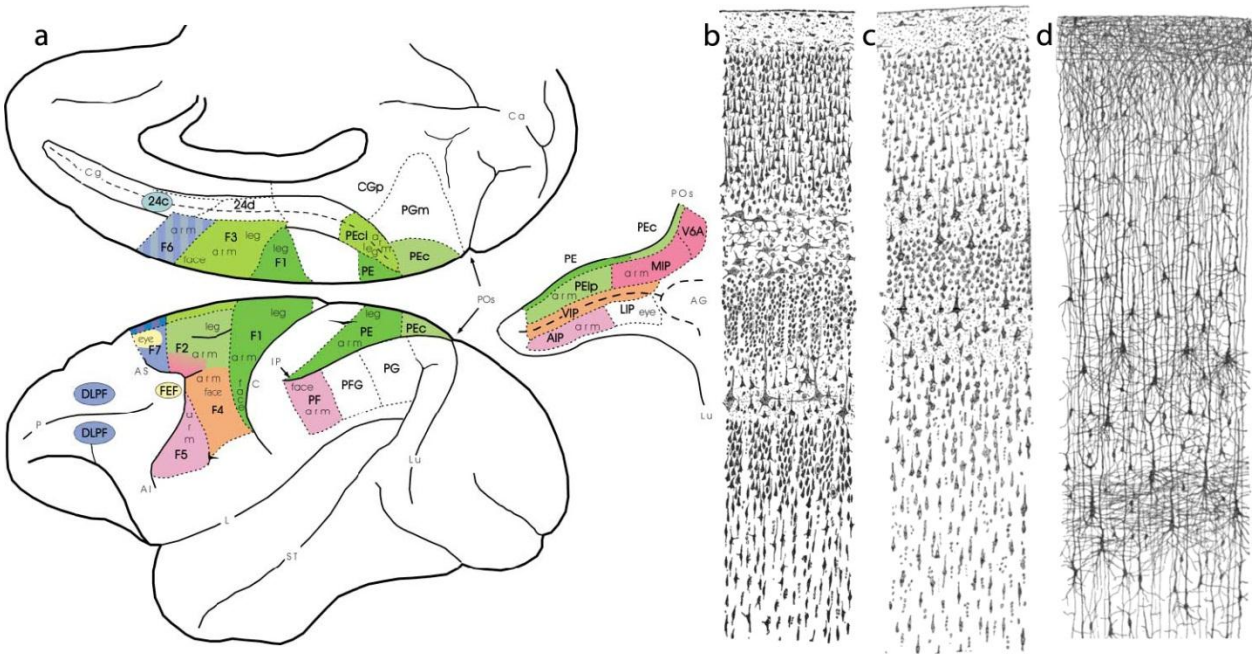

Figure 1.3: (a) Mesial and lateral view of macaque brain. Implant needs to be made in arm representative region of primary motor cortex (Brodmann 4, or area F1 as shown in the figure). AG, annectant gyrus; Ca, calcarine fissure; CGp, posterior cingulate cortex; DLPF, dorsolateral prefrontal cortex; FEF, frontal eye field; Lu, lunate sulcus; POs, parieto-occipital sulcus. (b-d) three drawings of cortical layers by Santiago Ramon y Cajal, (b) Nissl-stained adult visual cortex (c) Nissl-stained adult motor cortex and (d) Golgi-stained cortex of 1.5 months old infant. (a) is adapted with permission from (Rizzolatti, Luppino, and Matelli 1998), (b-d) is adapted from the book 'Comparative study of the sensory areas of the human cortex'.

1.4.2 Implant location and depth

In order to record the neural signal that is responsible for the movements, location of our sensor should be in the brain region that sends the signals to the lower level circuits or actuators (i.e., muscles) responsible for the movements. At the same time, consideration has to be made towards the practicality of the implantation of the sensors (in our case, microelectrode arrays). As mentioned earlier, neural signals from the microelectrode arrays implanted in motor cortex can control the BMI movements. The tips of the microelectrode arrays, or the recording sensors, are located 0.8-1.6 mm deep from the cortical surface. Considering the 1.8-2.0 mm thickness of M1 in non-human primate, this corresponds to cortical layers III-V of the motor cortex which are external/internal pyramidal cell layers sending efferents to/receiving direct or indirect afferents from subcortical or intra/inter-cortical neurons. Using the array with inter-electrode distance at tip anywhere between 250-1000 μm, we can get sparse and somewhat non-redundant representation of neural activity in both spike as well as local field potential type of recordings. This spacing with electrode thickness ranging from 30-100 μm also cause reasonably less injury and subsequent gliosis around the implant site.

The source of recorded signals can be a pyramidal cell communicating with other cells in the immediately or distally neighboring cortical region of the same area or other area of the

ipsilateral or contralateral side, or subcortical regions like thalamus or other deep nuclei. It can also be an interneuron with limited arborization and shorter axonal length which can contribute towards inhibiting a neighboring excitatory pyramidal cell. Thus, a higher firing rate of an interneuron might mean lower membrane potential and subsequent lower firing probability of a pyramidal cell it is connecting to. In any case, the linear/non-linear combination of the neural signals recorded from the arrays containing 10-100 microelectrodes has rich enough signal to decode virtually any movement-related behavioral signal (Todorov 2004; Todorov 2000).

1.4.3 Selection of microelectrode array

For intracortical neural recordings in non-human primate setup, commonly used arrays are microwires (Nicolelis et al. 2003) or Utah Intracortical Electrode Arrays (UIEA) (Nordhausen, Maynard, and Normann 1996; Maynard, Nordhausen, and Normann 1997). We compared the recording quality, in terms of signal-to-noise ratio and longevity of both the arrays and did not find one type significantly superior to the other. On the other hand, UIEA's floating nature and flexible wirebundle to the connector gives us more freedom towards improved implantation technique, especially when it comes to closure of the implantation site with the bone flap of the craniotomy and superficial scalp/galea and skin. Thus, we adhered to using UIEA for our experiments involving chronic MEA implantation procedure in M1.

1.5 Specific aims

With the discussion so far we can see the need, in chronological order, for a better microelectrode array implantation technique, a behavioral parameter that includes dynamics-related variables and performs consistently across variety of external environment and finally real-time, closed-loop control of movements that changes with changing environmental

conditions. To address these issues, the specific aims of the projects are laid out below with the details:

1.5.1 Developing a microelectrode implantation technique that is bio-friendly, reversible, repeatable and economical

For the broader scope of our research interest, we wanted neural recordings from multiple brain regions in behaving animals, which required chronic implantation of multiple microelectrode arrays. We selected bonnet macaques (*M. radiata*) for our experiments, because non-human primates have reaching movements that closely resemble human reaching movements and there is direct and high technology transfer potential for non-human primate research in clinical application. Since these animals need months of training of behavioral task, we wanted a microelectrode implantation technique that is reversible, bio-friendly and that fits in the research budget. Acrylic/cement cap method (Dolbakyan, Hernandez-Mesa, and Bures 1977; Nicolelis et al. 2003) has been the standard for chronic neural recordings with microelectrode arrays, but has disadvantage of having high infection rates and is sometimes irreversible. FDA approved microelectrode array for human use ((Nordhausen, Maynard, and Normann 1996; Hochberg et al. 2006) uses titanium pedestal making it reversible and bio-friendly implantation technique, but for the small skulls of non-human primates, the pedestal is too big, especially when we consider multiple array implants. So, we have come up with a new surgical technique of implanting 'Nesting Platform' that attaches on titanium head-post and mounts multiple microelectrode array connectors. We have successfully used this technology on 3 different monkeys (two bonnet and one rhesus macaque) to date, one of which was implanted for the third time using this technique, making a total count of 5 successful uses. Detailed explanation of this technique is included in 'Nesting Platform'.

1.5.2 Finding a behavioral signal that can control the BMI consistently across different external dynamic environments

It has been well established that neuronal activity changes with different muscle activity under different limb orientation/position in non-human primates motor, pre-motor and parietal cortical regions (Scott, Sergio, and Kalaska 1997; Scott 1997; Scott and Kalaska 1997). Since it is a group of muscles which leads to generation of torque and consequent joint movement, neuronal activity would have direct relationship with joint torques. This is demonstrated at different postures under continuous and transient load conditions (Kurtzer, Herter, and Scott 2005; Herter et al. 2007; Herter, Korbel, and Scott 2009). It has also been demonstrated that trajectory of kinetic/dynamic variables like torque, just like any kinematic variable trajectory, can be decoded using motor cortical ensembles (Fagg et al. 2009). The authors of this paper demonstrated that addition of limb state, or proprioceptive feedback, improves the prediction accuracies of joint torques. This finding suggests that limb state, or kinematic information is important for better torque predictions. Collectively, we can conclude that the optimal signal for neural control of movement should have properties of both kinematics and dynamics. We observed that Power, a product of torque and joint angular velocity or a product of end-point forces and end-point velocity gives stable prediction accuracies across different external dynamic environments with variety of gain-field conditions. Details of these results are included in 'Towards finding a generalizable BMI controller minimally influenced by external dynamic environments'.

1.5.3 Developing a real-time control of movements that has improved interaction with the external environment and is capable of impedance control

It is well known to the BMI community that the prediction accuracies of the decoder in open-loop configuration, or offline control, differ from when the loop is closed. Commonly the loop is closed by offering visual feedback of predictions to the BMI user in real-time. This way, the user can see the performance of the BMI performance and change the neuronal modulation which can work towards or against superior performance. We wanted to apply our knowledge of open-loop performance of the decoder in closed-loop real-time BMI setting. This required a hardware setup that is capable of streaming spiking neural data from the recording system device to prediction computer, predictions of behavioral variables from this neural information, sending the prediction values to the BMI plant where the monkey gets the feedback (closing the loop) and finally recording of the performance – all in real time. We were successful in building a system that is capable of simultaneously record 384 spiking neural channels, 192 field potentials/EMG/behavioral variables and task-related information and stream all the spike timestamps or 128s channel spiking neural data and 64 channels of field potentials in real-time for predictions and finally closing the loop by feeding these predictions in BMI plant to drive the task. The details of the system is more technical than scientific, but is included in abstract manner nevertheless as it might be a handy guide to a new user of the system. Details of the hardware setup is described in 'Appendix : Hardware Setup'.

We applied our knowledge of open-loop performance of the decoder in the closed-loop setup and found that the animal use torque predictions in real-time to run the task using ipsilateral or contralateral motor cortical activity. We have observed that using torque and position predictions together gives the animal superior control of the movements than torque predictions alone, which underscores the importance of combining dynamics and kinematics towards superior BMI performance. We have observed that the BMI performance changes as

the external dynamic environment changes, and that animal adapts to it. This makes our BMI controller unique, as other BMI controllers use kinematic values and have not been shown to adapt as the dynamic properties of the environment (e.g., viscosity of the medium, stiffness of the object, etc.) changes. Details of this work are described in 'Hybrid torque-position control in different viscous environments using ipsi/contra-lateral primary motor cortical signals'.

2 Nesting Platform

Below is the manuscript of the Paper titled 'A bio-friendly and economical technique for chronic implantation of multiple microelectrode arrays'; Chhatbar, P. Y., von Kraus, L. M., Semework, M., Francis, J. T.; Journal of Neuroscience Methods; 188(2): 187-194. PMID: 20153370

2.1 Abstract

Many neurophysiological experiments on rodents and non-human primates involve the implantation of more than one multi-electrode array to record from many regions of the brain. So called 'floating' microelectrode arrays are implanted in cortical regions of interest and are coupled via a flexible cable to their connectors which are fixed to the skull by a cement cap or a titanium pedestal, such as the Cereport system, which has been approved for human use. The use of bone cement has several disadvantages including the creation of infection prone areas at the interface with the skull and surrounding skin. Alternatively, the more biocompatible Cereport has a limited carrying capacity and is far more expensive.

In this paper, we describe a new implantation technique, which combines the bio-compatibility of titanium, a high carrying capacity with a minimal skull footprint, and a decreased chance of infection, all in a relatively inexpensive package. This technique utilizes an in-house fabricated 'Nesting Platform' (NP), mounted on a titanium headpost to hold multiple connectors above the skin, making the headpost the only transcutaneous object. The use of delrin, a durable, lightweight and, easily machinable material, allows easy customization of the NP for a wide variety of floating electrodes

and their connectors. The ultimate result is a longer survival time with superior neural recordings that can potentially last longer than with traditional implantation techniques.

Keywords: Brain Machine Interface, Microelectrode array, Neurophysiology, Surgical Methods

2.2 Introduction

For the past several decades, researchers have made great strides in our understanding of the brain by utilizing chronic neural recordings taken from awake behaving animals (Dolbakyan, Hernandez-Mesa, and Bures 1977; Nicolelis et al. 2003). Until recently most of these chronic implants had been conducted on rodents while primate neurophysiology had primarily been implemented using acute electrode insertion through chronically implanted recording chambers (Baker et al., 1999), allowing recording sessions of only several hours at a time on restrained animals. Today laboratories around the world are chronically implanting arrays of microelectrodes into non-human primates and even humans with good results (Donoghue et al. 2007; Hochberg et al. 2006). However, the risk of infection is still high when employing the commonly used cement 'cap' method of electrode/connector attachment in which quick drying acrylic is used in combination with skull screws.

The three major issues with chronic electrode implantations are (1) the long-term stability of the implant attachment to the skull, (2) prevention of infections and (3) the long-term stability of electrodes within the neural tissue. We will address the first two

of these difficulties. Both the acrylic/cement cap (Carmena et al. 2003; Nicolelis et al. 1998; Dolbakyan, Hernandez-Mesa, and Bures 1977) and the titanium pedestal (Fellows and Suner 2006; Normann et al. 1999; Donoghue et al. 2007; Hochberg et al. 2006) techniques are widely used for chronic electrode implantation, but each has their own limitations. Acrylic is exothermic and also believed to be toxic during the settling period (Albrektsson and Linder 1984) and the newer antibiotic (Gentamycin) impregnated bone cements like Palacose (Heraeus Medical GmbH, Wehrheim, Germany) have only limited anti-bacterial effectiveness, due to low surficial contact with surrounding bacteria. The alternative, a titanium pedestal like the Cereport (Blackrock Microsystems, Salt Lake City, UT), is bio-compatible and interfaces well with surrounding bone (Adams et al. 2007). However the limited carrying capacity of each Cereport (up to 96 channels per device) requires multiple Cereport pedestal implantations for a larger number of electrode implants. Therefore, the Cereport option ultimately provides little decrease in skin margins or required skull real estate as the number of implanted electrodes increases.

To avoid the disadvantages of these previously mentioned methods we have designed and manufactured a novel apparatus in house. This apparatus, which consists of a 'nesting platform' (NP) mounted on a single titanium post, maintains the advantages of a traditional titanium Cereport while simultaneously increasing the carrying capacity by four times (4 x 96 electrode connectors) and reducing the transcutaneous cross section and cost. This design concept is very adaptable, and with

appropriate changes in scale, could be used on animals of any size for any electrode coupled to its connector by a flexible wire; For instance floating cortical microelectrode arrays (as described here) or depth electrodes for thalamic/hippocampal implants (Behrens et al. 1994; Simuni et al. 2002). Finally, this attachment method is also very durable and does not require or impose any specific restrictions on animal movement. During the recording sessions, head movement restrictions can be imposed in order to prevent detachment of headstages from the connectors and prevent movement artifacts in the recordings, but is not required.

2.3 Methods

2.3.1 Nesting Platform (NP) Design

The goals of this project were to create an implantation technique that would allow the implantation of up to four 96-channel microelectrode arrays while maintaining a minimal skull footprint, minimal transcutaneous cross section, and would not require the use of acrylic cement. Figure 2.1 shows our final design of the NP complex, a titanium headpost (model: 6-FHP-2XF, Crist Instrument Co., Inc., Hagerstown, MD) mated with an in-house fabricated NP that holds the electrode connectors above the surface of the scalp. All designs were created using Rhinoceros v3.0 and milled out of white delrin (density 1.42 gm/ cm^3) using an EGX-300 Desktop Engraver (Roland DG Corporation). A .3dm file format model of the NP design can be found in the online supplementary information.

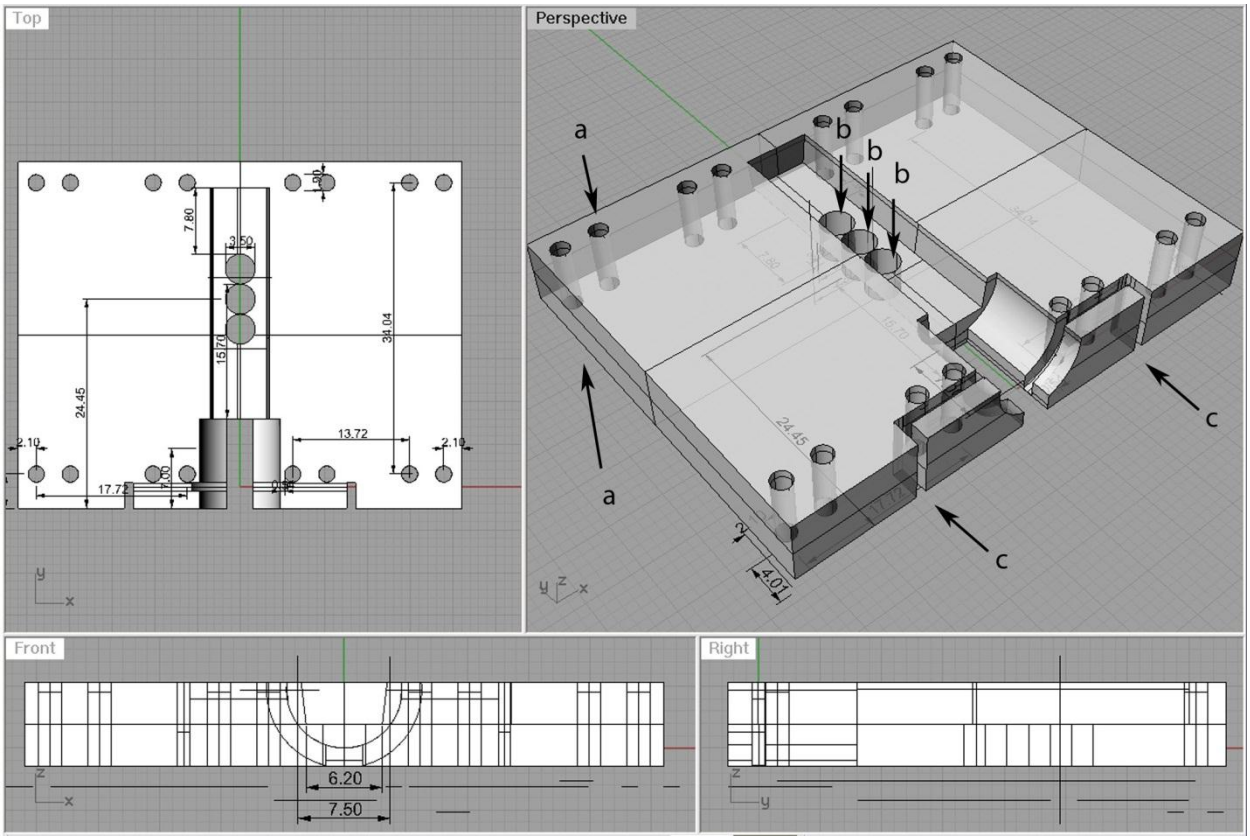

Figure 2.1: 3D drawing of the NP. Note the small screw holes (a) to snugly fit ICS-96 connector screws, big screw holes (b) in the midline to fit 6-FHP-X2F headpost screw. The 3 holes give freedom to adjust the height and clearance from the animal's skull. The horizontal channels (c) created at the bottom are for passing the wire-bundles running from the arrays to the connectors.

The NP is 5.2 cm long, 4.05 cm wide, 0.68 cm thick, and 18.07 grams in weight. This NP is mounted on a titanium headpost 6-FHP-X2F (weight 13.3 gm) using the screws supplied with the headpost. Four ICS-96 connectors are then mounted onto the NP by screwing directly into appropriately positioned holes. Each of these connectors weighs ~9 grams, making the total weight of the NP with four connectors to be ~67.4 grams. This low weight caused no problems for our usage, but should a lower weight be desired, the NP could be made thinner and nonessential material (for instance the

regions below the mounted connectors) could be removed with little effect on structural integrity. In addition, should one need to glue anything additional to the NP, we recommend CyPox glue (Gowest2 International, Arlington, OH) which, unlike most glues, bonds very effectively to delrin.

The effective grip between the NP and the ICS-96 connectors is provided by the self-tapping Ø.082 inch ICS-96 connector screws into the .075 inch diameter holes of the NP. If desired, one can modify the NP design to have slots for small nuts to keep the screws in place. However we have found over the course of a 6 month experiment that the structural integrity of the entire connector/ NP complex was very stable.

2.3.2 Implantation Technique

All animal procedures were approved by SUNY Downstate Medical Center IACUC and conformed to National Institutes of Health guidelines. Female Bonnet Macaques (Macaca radiata), weighing between 4 and 7 kg, were used for the experiments. Prior to attachment of the headpost to the skull, its four titanium foot processes were trimmed to adjust their length in accordance with the space constraints of our implantation site. For attachment to the skull we used eight 6 mm length titanium screws (2.7 mm thickness, 402.006 Synthes, Inc., West Chester, PA). Three microelectrode arrays were then implanted with the use of a pneumatic inserter following the recommended surgical protocol (Fellows and Suner 2006). In this case, however, all 3 array connectors were mounted on the NP prior to the electrode insertion. A detailed description of this assembly and a chronology of the subsequent surgical steps are defined below.

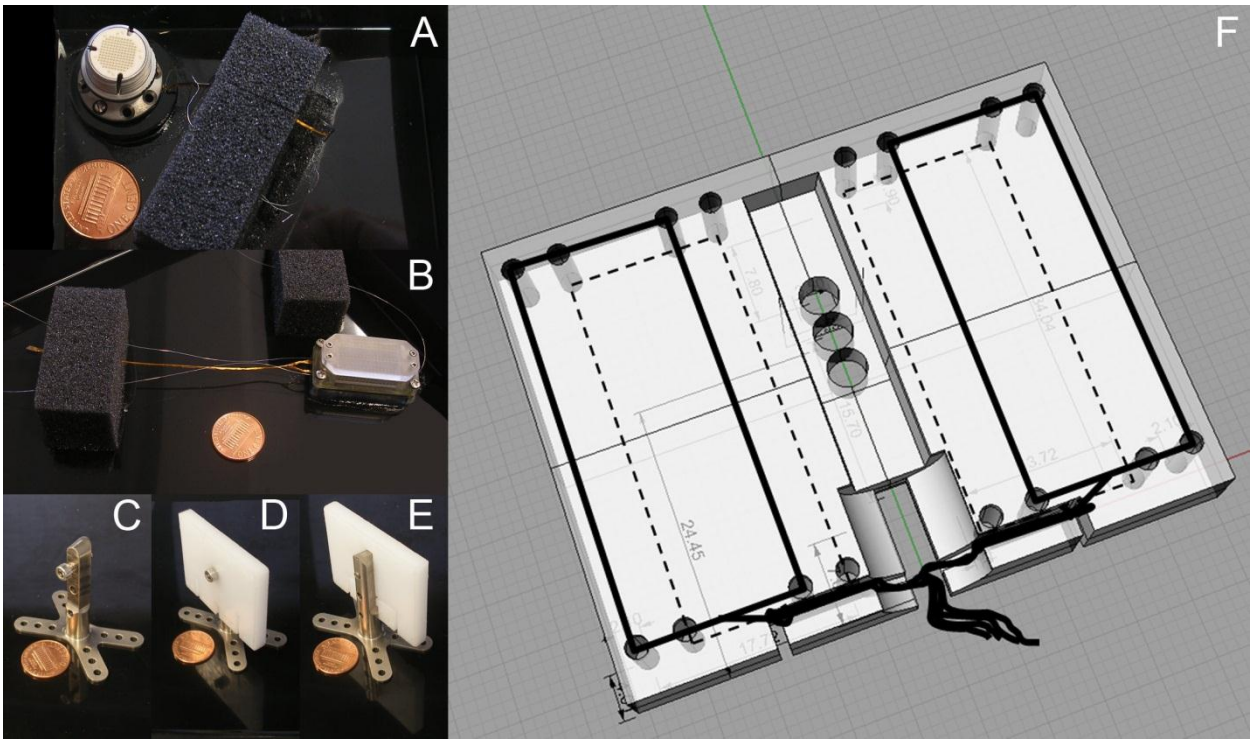

Figure 2.2: A, An array with Cereport connector; B, An array with ICS-96 connector; C, 6-FHP-2XF headpost; D and E, front and back views of headpost with NP mounted; F, Scheme showing the use of appropriate screw holes on the NP to affix ICS-96 connectors. Connector outline in dotted line suggests connector location on the other side of the view. Also note the wire-bundles passing through the channels created at the bottom of the NP.

2.3.3 Connector-NP assembly method

To fasten the connectors to the NP we first arranged the electrode-to-connector wire-bundles into their dedicated channels on the bottom of the NP and then attached the connectors to the NP using (Ø .082 inch) screws (Figure 2.2). To prevent any future intrusion of biological matter between the connectors and the NP we then applied a thin layer of cyanoacrylate along the junctions. Because cyanoacrylate does not bond very strongly to delrin this process does not interfere with future unscrewing of the connectors should it be necessary. We found it useful to label the wire bundles of each

array to easily identify the connector to array pairing during surgery. All the contact edges of the NP have been smoothened to minimize the inadvertent injury to the wire bundles. Materials like silastic (Kwik-Sil™ Silicon Elastomer, World Precision Instruments, Sarasota, FL) that are inert to the wirebundles and that can give cushion can also be used to give additional insulation and protection to the wirebundles.

Recommended chronology in surgical procedure: Although many variations can be made in the implantation technique, we found that the following chronology makes the surgery more efficient and less confusing. The steps we followed are broadly as follows:

1. Create a midline incision, with coronal plane extensions at the end, to make a wide window with a blunt dissection laterally up to the temporalis ridge.

2. Blunt dissection through the temporalis ridge in order to separate temporalis muscle inside its sheath from periosteum.

3. Open a skull window exposing cortical regions of interest, in our case primary motor cortex (M1), dorsal premotor cortex (PMd) in the left frontal lobe and primary somatosensory cortex (S1) Brodmann's areas 3b, 1 and 2 of left parietal lobe (see Figure 2.3(c)). We used the structural MRI of the same monkey to locate the exact coordinates of the window. Thin out the removed bone using an electric rotary tool and set it aside in ringer's solution.

   Note here that multiple cortical regions that are far apart anatomically can also be chosen and multiple skull windows can be drilled out. The wirebundles

can then be channeled to the NP mounting site and taken out from the base of the headpost, as described in the steps that follow.

4. Choose the orientation of implants and paths of the wire bundles (all our arrays had 10 cm wire bundle length). See Figure 2.3 to get a clear idea of the array orientation, the wire bundle path that we followed and the location of the second headpost. When choosing the mounting site for the headpost it is important to take into consideration clearance space for all of the attached wires between the connectors and the amplifier bank. We oriented the NP-headpost assembly so that the wire bundles passed through the posterior margin of the headpost, making it least accessible to the animal's fingers.

5. Mount the headpost using skull-screws at its predetermined location and connect the NP to make sure that the wire bundles can sit on the skull as planned. We did not dismount the NP until step 10 as it did not interfere with the surgical field.

6. Open the dura and perform somatotopic mapping of sensory cortex using a single sharp microelectrode to get a precise location of implantation site.

7. If implanting into multiple neighboring cortical regions, crowding of electrode arrays and wire bundles is inevitable. To facilitate the alignment and positioning of multiple arrays, we used multiple small padded alligator clips attached to malleable wires mounted on the stereotax. (See Figure 2.3.C(e)) Once in position

insert the arrays into the cortex following the procedures recommended by the surgical manual (Fellows and Suner, 2006).

8. Fix the wire bundles on the skull using titanium straps and screws (P4ST-08-48 and SCR4-04-05, Bioplate, Inc., Los Angeles, CA) and silastic (Kwik-Sil™ Silicon Elastomer, World Precision Instruments, Sarasota, FL). We recommend the use of minimum amounts of silastic, making sure there are no pockets between silastic and skull, as these can be potential sites for pathogens to thrive.

9. Use GORE PRECLUDE(R) membrane (GORE PRECLUDE(R) Pericardial membrane, W.L. Gore & Associates, Inc., Flagstaff, AZ) as described in the Blackrock Microsystems' surgical manual (Fellows and Suner, 2006).Then close the window with the thinned out bone attached (from step 3) and titanium straps. Finally, seal the open edge with a thin layer of silastic (Figure 2.4.A).

10. To allow ease of scalp closure around the headpost, temporarily dismount the NP taking care not to pull on the electrode wire bundles fixed on the skull. Maneuver the NP to get the closest possible scalp closure around the headpost.

11. After suturing and topical antibiotic application, mount the NP back on headpost (Figure 2.4), check the headpost and NP stability, and finally fill any gaps between headpost, NP, and connectors using cyanoacrylate glue to discourage microorganism growth. Be careful to avoid cyanoacrylate contact with the ICS-96 connector cover, as it can damage certain plastics.

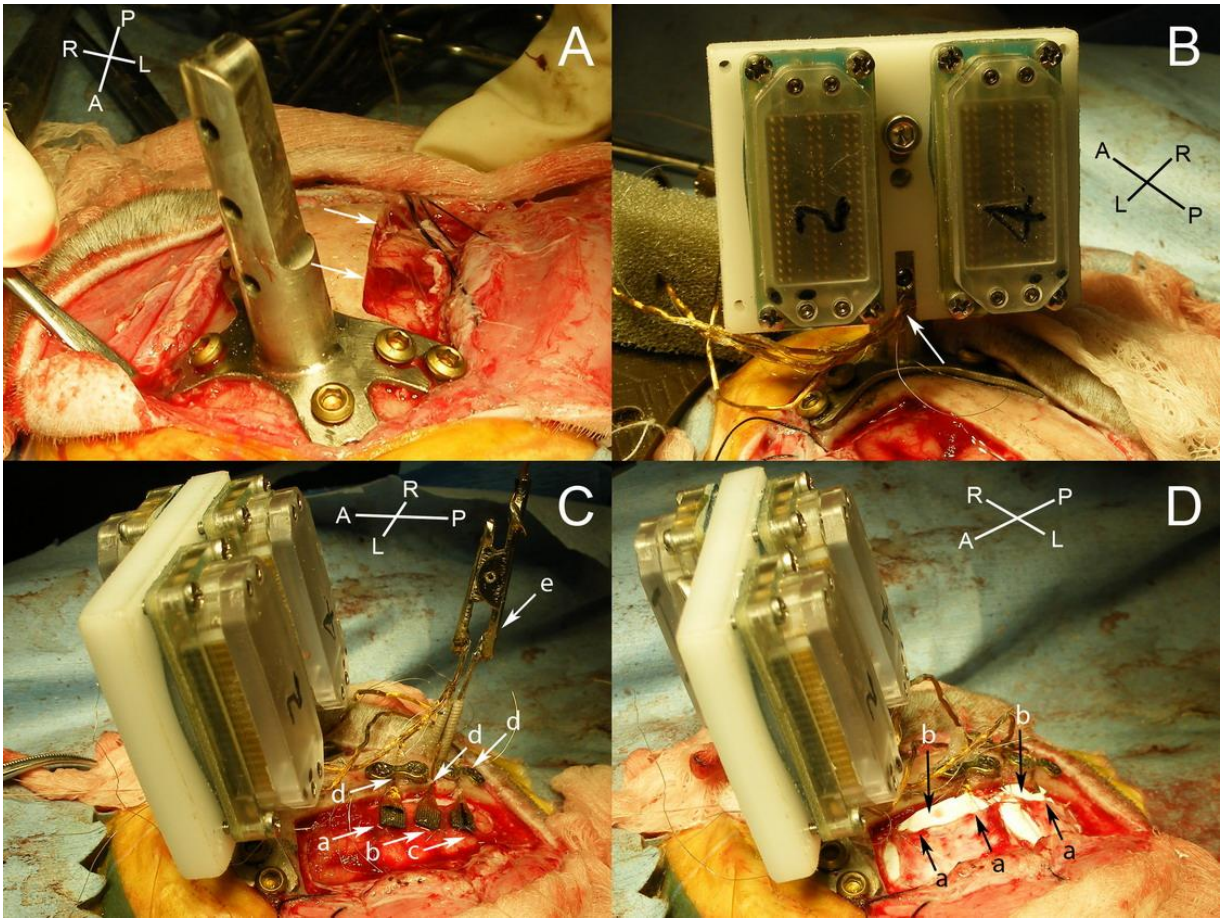

Figure 2.3: A, second headpost implanted on the anterior side of the skull – note the orientation of the headpost is such that the NP fits on it from the posterior side, so that the wire-bundles pass posterior to the headpost stem, making them less reachable to the animal. White arrows show medial margin of the skull window; B, NP-connector assembly mounted on the headpost using the headpost screw (in the middle) using the top screw-hole on the NP. The microelectrode arrays are yet to get implanted (see wire-bundle going behind (white arrow), passing through the slits created in the sponge); C, all 3 microelectrode arrays implanted in PMd(a), M1(b) and S1(c) and their wire-bundles partially fixed on the skull using titanium straps and silastic(d) and padded alligator clips(e) were used to keep the wire bundles in place until then; D, Closure is accomplished by first placing a layer of GORE PRECLUDE(R) membrane (artificial pericardium) between the array and the dura (b) followed by closing the dura (a) and placing a second layer of GORE PRECLUDE(R) membrane between the dura and the skull (shown in next figure) as instructed in the blackrock surgical manual).

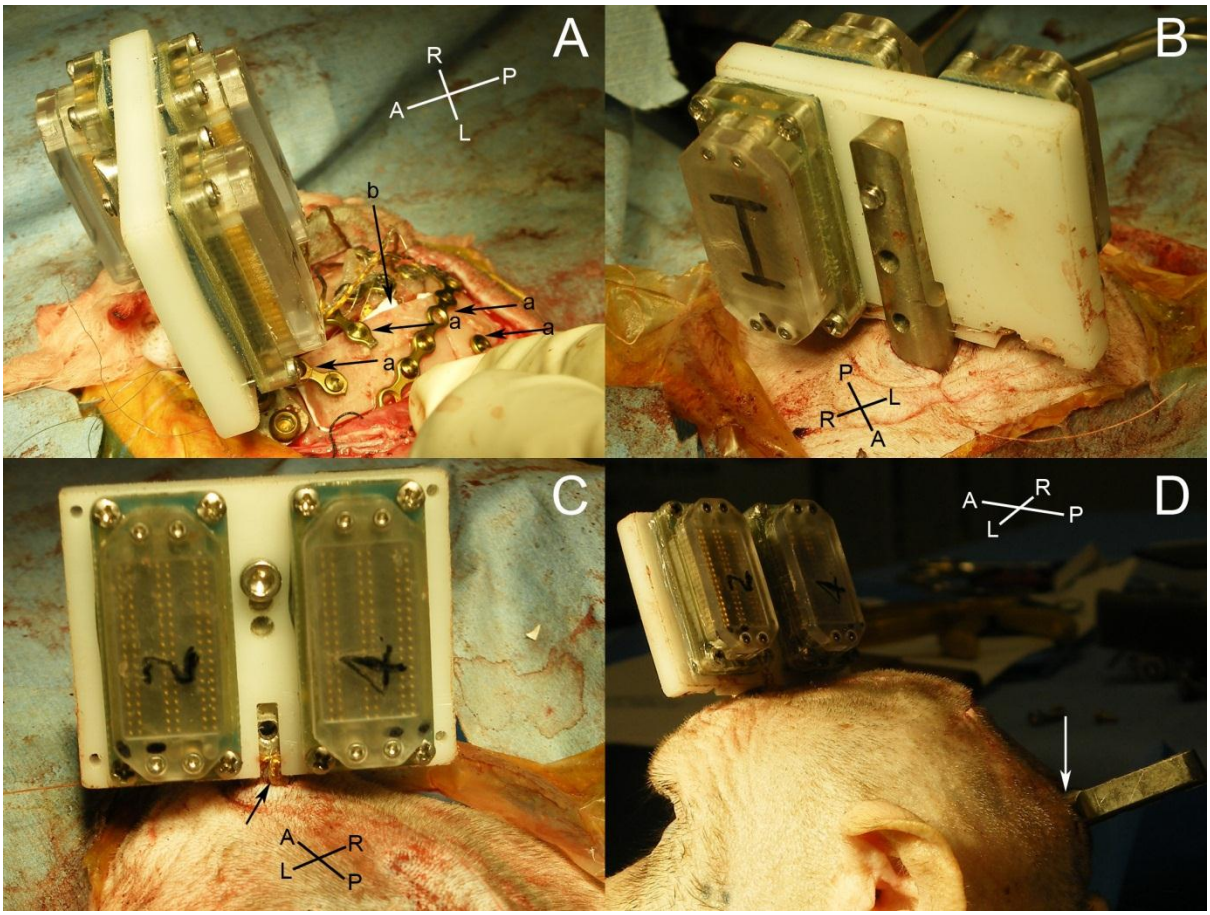

Figure 2.4: A, Closure of the implantation window created on the skull using thinned out bone flap using titanium straps(a). Note another layer of GORE PRECLUDE(R) membrane(b) sitting between the dura mater and the bone flap; B, anterior view and C, posterior view of the headpost-NP-connector assembly after closure of galea and skin. Note the wire bundles (black arrow) going under scalp posterior to the headpost stem; D, Post-operative lateral view of monkey with the NP-connector assembly sitting on the anterior headpost. Note that posterior headpost (white arrow) was implanted slightly above the occipital ridge a few months ago.

2.4 Results

We have implanted this single nesting platform with three 1.5 mm length microelectrode arrays in cortical areas PMd, M1, and S1 on a female Bonnet macaque (Macaca radiata) weighing 4.2 kg on Feb 19, 2009 and she has been completely healthy to date (August 08, 2009); See recordings in Figure 2.7. She was given systemic

antibiotics daily up to day-10 post-implantation with no later antibiotic applications needed. This animal is our third animal with the Utah array implant, but first utilizing nesting platform (see the section below for more details). Her recordings have been consistent and in fact better than our previously implanted two animals with the same type arrays (1.0 mm microelectrode length) implanted with the traditional cement cap covering (Palacos).

2.4.1 Comparison with other techniques

2.4.1.1 Cement Cap

Our lab has experience with the chronic microelectrode implantation of five non-human primates (M. radiata), and over 50 rats. Below is a summary of the non-human primate implants and prognosis.

1. Cap created with dental acrylic; microwire array implantation; infection occurred ~6-months after implantation.

2. Cap created with dental acrylic; microwire array implantation; infection occurred ~6-months after implantation.

3. Cap created with palacos cement with impregnated antibiotics; 1.0 mm Utah array, microwires and multi-site ceramic arrays implantation; infection occurred ~6-months after implantation.

4. Cap created with palacos cement with impregnated antibiotics, 1.0 mm Utah array and multi-site ceramic arrays implantation and a standard recording

chamber; lost recordings at 6 months after implantation, but the animal and the cap are healthy after 11 months.

5. See the next section for the NP implantation.

When an infection was suspected we would clean the skin margin with betadine and nolvasan and apply topical antibiotic ointment daily. In addition, systemic antibiotics were given. If an animal was healthy the skin margin was left undisturbed. Animals were individually housed in very large baboon cages conveniently situated to allow grooming between neighboring animals. In addition, the animals were given free time to run around and explore the lab space. As the cement cap is not a biological tissue, antibiotics given systemically barely reach the infection site. Also, due to the unyielding nature of the cement cap, unlike scalp, the diagnosis of infection may be delayed until behavioral changes are observed, or the infection is sensed via olfaction, visual evidence or presumed via fever, in which case it is generally too late for any effective intervention, because by then a biofilm has already been formed between the scalp and the cap. This makes it impossible to replace the cement cap as the skull underneath is not healthy enough to support the new bone screws needed to attach a new cap. In addition, the implant site would be compromised once the original cement cap is removed along with the microelectrode connectors impregnated within. There are several labs that have been successfully using cement caps in their preparations for the chronic microelectrode array implants with good results, and without the animal

becoming infected. In the above statements we are merely pointing out situations we have experienced and know others have as well (personal communications).

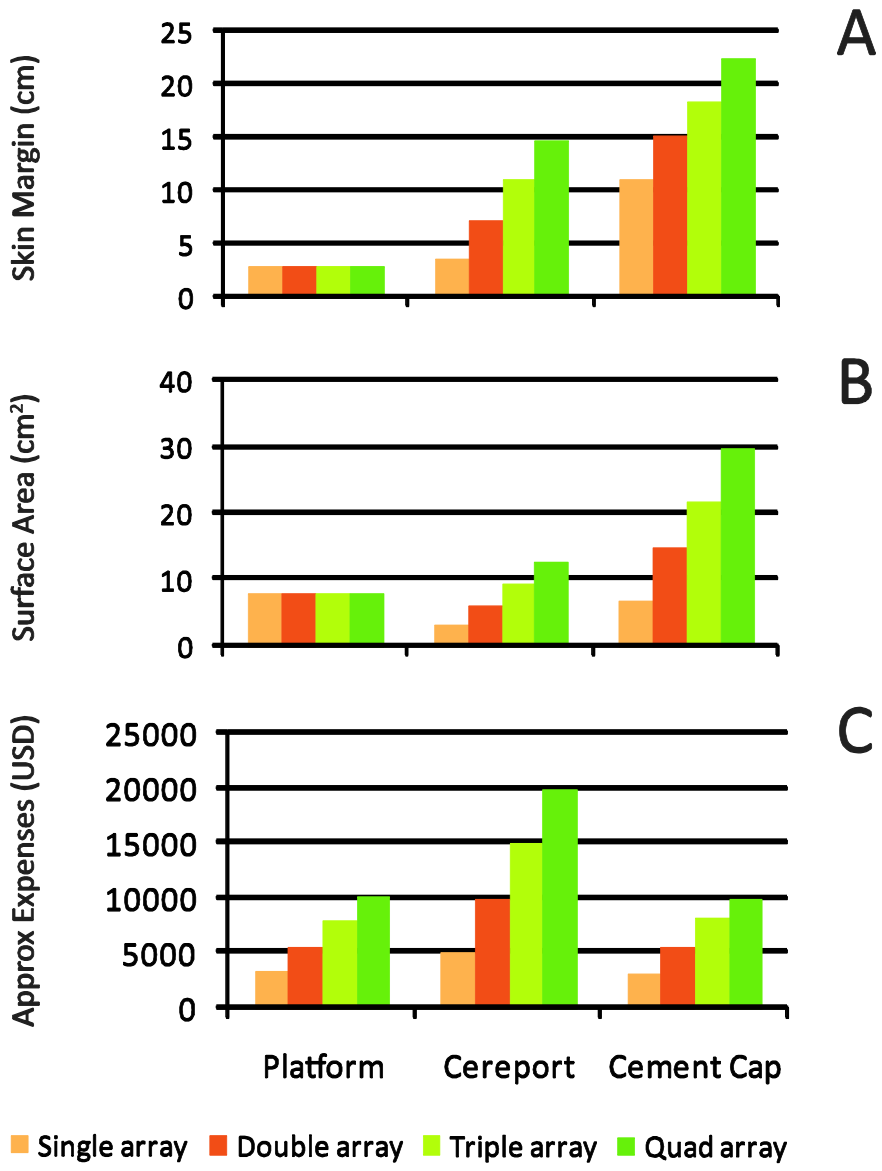

Figure 2.5: Comparison of NP method of chronic MEA implantation with other methods. A, the skin margin stays the same with NP method irrespective of number of arrays used, and that it is less than other methods. B, the surface area occupied by the feet of the titanium headpost is greater than two Cereport connectors – this will give greater stability to the assembly because of bone-friendly nature of the titanium. Note that surface area of cement cap won't positively contribute to the stability of the connector assembly impregnated into it. C, expenses

incurred by both NP and cement cap method are the same and are almost half the expenses by the Cereport method.

A second problem that our lab has encountered with the cement cap method was the lifting of our floating microelectrode arrays out of the cortex. During post mortem analysis we found that the meninges had grown under the microelectrode array and pushed it up and out of the cortex. Since the Utah arrays are floating and not fixed to the cap, as many microwire implants have been, this problem can occur when there is no structure to keep the array pressed against the cortex. However, this is not a problem with the newer techniques such as those in the Blackrock surgical instruction manual that we have expanded on. It appears that this problem can be solved by closing the dura up properly; however, this can only be done currently with floating electrodes. This last point clearly has nothing to do with what type of connector housing you are using.

2.4.1.2 Titanium Pedestal (Cereport)

Titanium's bio-friendly nature and bone-cell attracting quality (Adams et al. 2007) makes the Titanium Pedestal, such as the Cereport, the implantation method of choice when compared to the cement cap. However, when implanting multiple arrays as stated previously, one quickly ends up with a transcutaneous area comparable to that of cement caps when using multiple pedestals. It should also be noted that the manufacturing of titanium pedestal is expensive and thus the overall cost of the Cereport is almost double when compared with the same array using an ICS-96 connector type.

2.4.1.3 The nesting platform (NP)

Using the NP implantation technique with scalp closure we implanted two 1.5 mm Utah arrays and one 1.5 mm IrOx coated Utah array. We removed the implants along with NP (leaving the anterior headpost in situ) 6 months post implantation because of a local skin infection as a preventive measure to intra-cranial extension of infection, although we were still obtaining recordings from the arrays (see Figure 2.7). This animal has fully recovered from the superficial infection and will be re-implanted after several months off studies. We observed that two of the three wire bundles were cut at the headpost stem level, which we believe is in part due to vigorous cleaning of the anterior post margin by rhythmic rubbing of a piece of gauze almost daily for few weeks, although this is speculative. Dismounting the NP might have caused avulsion of the wire bundles which were tightly glued to the headpost with the help of cyanoacrylate.

Since the NP mounts on a headpost the number of arrays or connectors do not increase the exposed skin margin proportionately. By using the NP multiple Utah arrays with up to 4 ICS-96 connectors can be used while maintaining a minimal skin margin around a single headpost, which is almost 20% less than that of a single Cereport connector. Table 2-1 summarizes the comparison points between the NP we propose here with the cement cap and the titanium Cereport pedestal. We are only using the Utah array as one of many possible floating array types in this work, and do not wish to make claims as to what electrode type is best past the advantages of the floating style.

An additional feature of the NP is that one can use the headpost and NP again on another animal after removal and sterilization. We are presently developing a NP that can be mounted to the same headpost used for head restraint, thus decreasing further the surgical trauma to the animal and post-surgical skin margins. Meanwhile, the cement cap design is extremely difficult if not impossible to re-use on other animals and we do not believe that the Cereport system is designed for reuse.

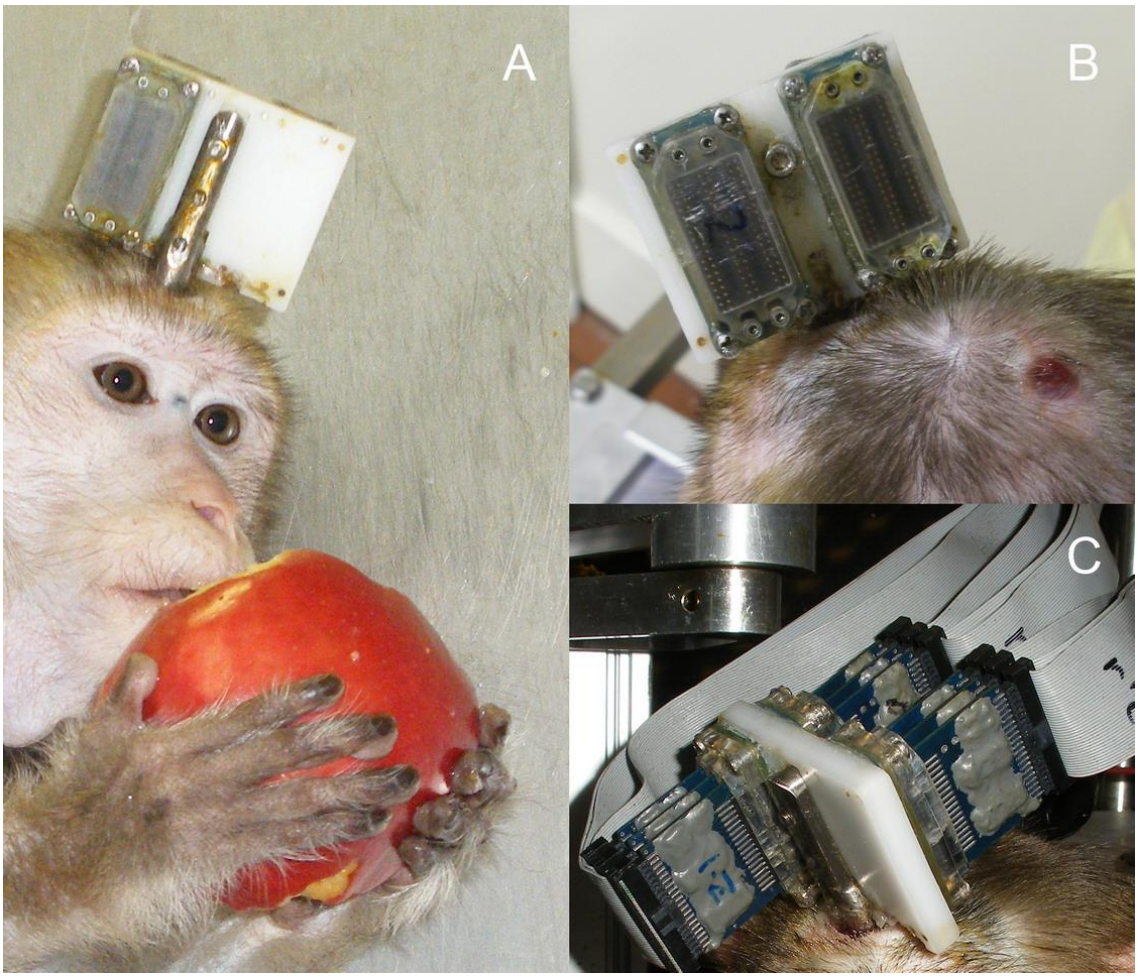

Figure 2.6: The implanted monkey, 6 months post implantation. A, while enjoying an apple; B, view from the back while seated; C, assembly with headstages plugged in.

2.5 Discussion

We demonstrate in this paper a novel technique of microelectrode array implantation that is cost-effective, bio-friendly, reusable and easy to implement in light of growing interest in the field of chronic multi-site, multichannel electrophysiological recordings. The NP design can be modified to meet the customized needs for individual research labs and with the advent of sophisticated milling and 3D printing technology can be finely tuned to a specific experimental setup. Thus the NP design can be changed according to the type of headpost used (small pinhead size headpost for rats, for example or different shape and diameter of headposts as commercially available by different companies.) and the physical properties of the connectors for a given MEA (e.g., ICS-96 connectors, Omnetics connectors etc. as well as custom made connectors.) Apart from that, different hardware, like wireless transmitter or antennas can also be mounted on NP with minimally, if at all, disturbing biological tissues. This would expand its use manifold and give an experimenter some degree of freedom in engineering the novel technology without much worrying about the installation or mounting of the required hardware straight on the skull or scalp and fixing it with less biologically friendly materials. The NP described here is a simple demonstration of this idea which is specifically designed for non-human primates with headpost model 6-FHP-2XF and connector type ICS-96. Use in different species with different headpost model and connector type would need a customized size and design of NP, which can be easily produced by use of 3D designing software and manufactured by a milling/3D printing process with a custom choice of material to use in the making of NP.

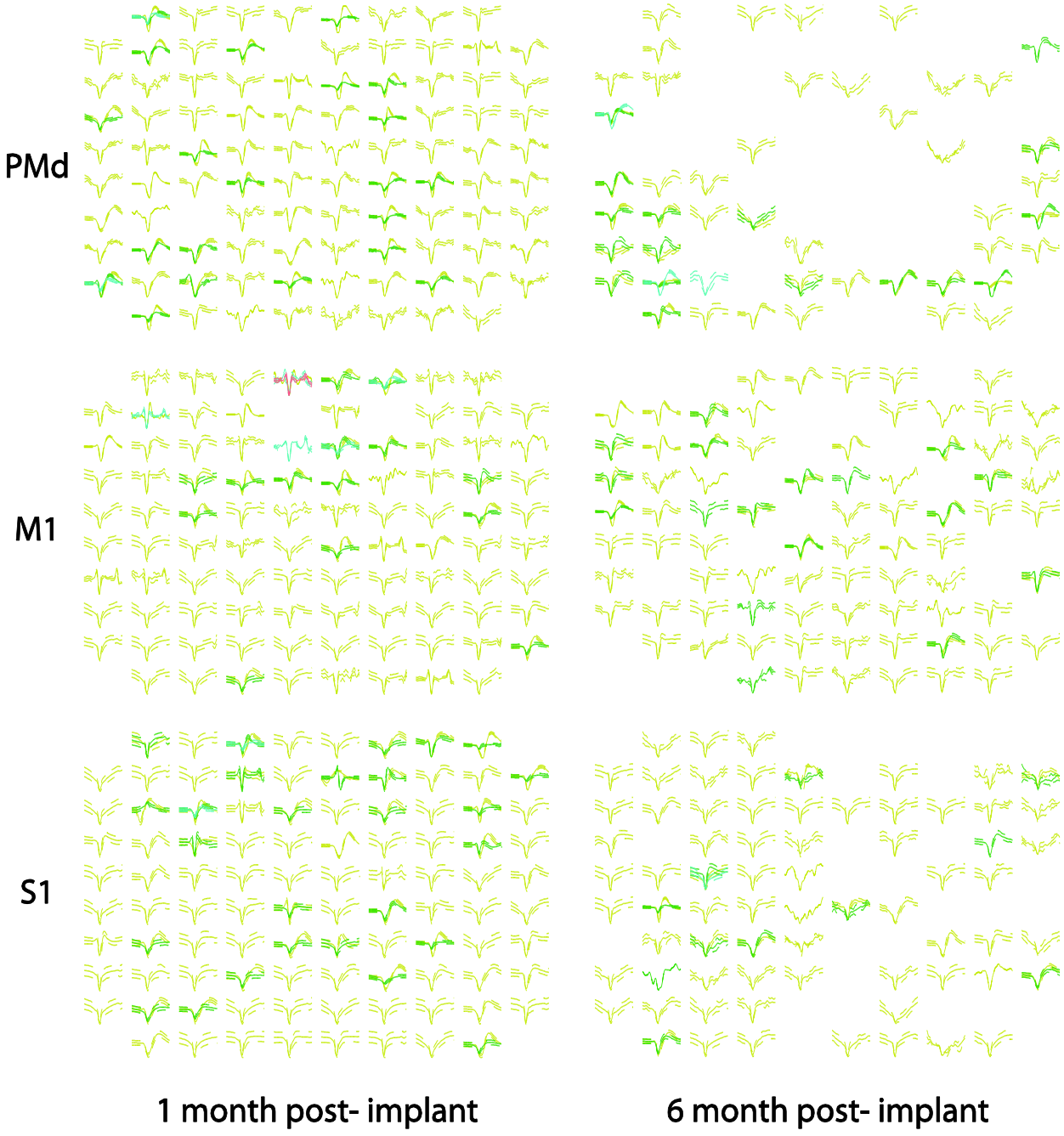

Figure 2.7: Waveform recordings from all available channels shown approximately one and six months after implantation, waveform mean (solid line) ± standard deviation (dashed lines). Recordings were made at 40 KHz digitizing frequency with appropriate gain, threshold and sorted using PCA method on recorded waveform tracings online using SortClient software (Plexon Inc., Dallas, TX). The waveform location represents actual anatomical location of the microelectrode in the arrays and the arrays are arranged as implanted (see Figure 2.3.C). So, consider left side as anterior, right as posterior, top as medial and bottom as lateral side for individual

microelectrode location in the array. Different waveform patterns with unique shade represent different unit activity (i.e. possible single neuron action potential activity in the vicinity of a given electrode) recorded from the same channel. All 3 arrays as depicted in Figure 2.3.C are shown here. Dorsal premotor (PMd), primary motor (M1) and primary somatosensory (S1) cortical array recordings are arranged in rows from top to bottom in that order.

The next generation of our NP will fit onto the same headpost needed for head restraint during awake, behaving macaque neurophysiological experiments. In our case mild head restraint is needed to keep the animal from destroying the expensive preamp headstages. Using our in house developed nesting platform we have shown that it is possible to record from hundreds of microelectrodes while greatly limiting the exposed skin margin vulnerable to infection. While the continuing development of wireless transfer technologies promise a future without the need for trans-cutaneous protrusions, realization of such implants is in its nascent stage with their capacity limited to a few channels (Song et al. 2009). In the meantime the described nesting platform allows possibly the most bio-friendly and economical means of conducting chronic neurophysiological experiments with multiple microeletrode arrays.

Acknowledgements

We would like to thank Shaohua Xu, Allison Maurice, Carol Novotney and Elizabeth Rivera for their continuous support throughout the course of the surgery and animal care. In addition we would like to thank John Chapin for allowing us the use of the EGX-300 desktop-engraver for making the NP. The work is supported by NYS

Department of Health SCIRBs # C022048, National Academies Keck Futures Initiative NAFKI SP09 and SUNY Downstate Medical Center.

Conflict of Interest Statement

At the time of publication, no authors have any real or potential conflict of interest.

Table 2-1: Showing comparison between three different chronic microelectrode array implant techniques. 6.77418 cm2 is the area of ICS-96 (1.5 x .7 in); Price calculations are based on: NP raw cost ~100$, Headpost price ~600$, single bone screw price ~50$, bone cement price ~500$; Cereport price ~4500$, ICS-96 price ~2250$.

Parameter	**NP**	**Cereport**	**Cement Cap**
Surface area (cm2) covered on skull	Foot process length dependent	Base diameter (~2 cm) dependent	Variable, at least the size of ICS-96
Single array	8.03	3.14	> 7
Double array	8.03	6.28	> 15
Triple array	8.03	9.42	> 22
Quad array	8.03	12.57	> 30
Skin margin (cm)	Post diameter dependent (~0.94	Neck diameter dependent	Variable, at least the perimeter of
Single array	2.953	3.691	> 11.2
Double array	2.953	7.383	> 15.3
Triple array	2.953	11.074	> 18.4
Quad array	2.953	14.765	> 22.5
Approximate Total Price (USD)	Platform + Headpost + Array + 10 screws	Cereport + 10 screws per array	Bone cement + 10 screws
Single array	3450	5000	3250
Double array	5700	10000	5500
Triple array	7950	15000	8250
Quad array	10200	20000	10000
Approximate savings if recycled	NP + Headpost + 10 screws	10 screws per array	10 screws
	1200	500 per array	500

3 Towards finding a generalizable BMI controller minimally influenced by external dynamic environments

Below is the manuscript of the Paper titled 'Comparison of force and power generation patterns and their predictions under different external dynamic environments'; Chhatbar, P. Y., Francis, J. T.; It was presented at Engineering in Medicine and Biology Society (EMBC), 2010 Annual International Conference of the IEEE; 1: 1686-1690. PMID: 21096397.

3.1 Abstract

Use of neural activity to predict kinematic variables such as position, velocity and direction etc of movements has been implemented in real-time control of robotic systems and computer cursors. In everyday life, however, we generate variable amounts of force to manipulate objects of different inertial properties or to follow the same trajectory under different external dynamic environments like air or water. The resultant work during such movements, and its time derivative power, should depend on the dynamics of the movement. In order to give the users of a brain-machine interface (BMI) comprehensive control of a prosthetic limb under different dynamic conditions, it is imperative to consider the dynamics-related parameters like end-effector forces, joint torques or power. In this paper, we show distribution patterns of two such dynamics parameters – force and power – and their predictive efficiency under different dynamic environmental conditions. We intend to find the force-related parameter, which has optimal predictive efficiency across different dynamic environments that is generalization. Our ultimate goal is to materialize a force-based brain-machine interface (fBMI).

Index terms—Brain-Computer Interface, Power, Force-related Parameters, Robotic Manipulandum, Chronic Microelectrode Array, Motor Learning, Reaching Movements, Neuroprosthetics

3.2 Introduction

Over the past decade several groups have shown neural activity recorded from the motor cortex can be used to control a brain-machine interface (BMI). At present all BMIs have allowed the user to control kinematic variables such as end-point/joint position or velocity. Such kinematic control may be useful for a BMI, but it is clearly different from the type of control we use on a daily basis, changing the output forces we use as a function of the situation, such as when picking up a full vs. an empty cup of coffee. It is easy to imagine how such dynamic related control may lead to a more natural feeling BMI controller. Neural prostheses have been able to predict discrete (Musallam et al. 2004; Andersen et al. 2004) and continuous (Chapin et al. 1999; Wessberg et al. 2000; Taylor, Tillery, and Schwartz 2002; Serruya et al. 2002; Carmena et al. 2003) behavioral data from neural signals. In addition researchers have generated learning based decoders (Sanchez et al. 2009; Danziger, Fishbach, and Mussa-Ivaldi 2009). Efforts have been made to include force into such work (Kim et al. 2007; Chib et al. 2009), but little is known of how well a neural decoder trained under one force-field environment could generalize to novel force-field environment.

To predict the generated force-related parameters, we used multiple linear regression models fed with the first 20 principal components calculated from neural activity recorded from hundreds of motor cortex neurons while the monkey worked on a center-out reaching task. Reaching movements were made using a block paradigm with blocks of either a high or a low gain viscous force-field. Our results show that when we train our models to predict the power

and force in a low gain viscous force-field environment, they predict these variables approximately as well under a high gain viscous force-field environment or even better, but the opposite tends to be false, except for when looking at power. We hope that by combining such generalization of power, we can provide better and more natural control of a BMI.

3.3 Methods

3.3.1 Subjects and Behavioral Task

All animal handling and experimental procedures were approved by IACUC of SUNY Downstate Medical Center and are assisted and scrutinized by Division of Laboratory Animal Resources at SUNY Downstate Medical Center. A female Bonnet Macaque (*M. radiata*) (Age 10 years, weight 4.5 kg) was trained under a modified 8-target center-out reaching task, where she had to perform the task under cycling blocks of 10 consecutive trials in a low (3 Ns/m) followed by 10 high (12 Ns/m) end-point viscous force field. A KINARM setup for non-human primates (Scott 1999) was used for the behavioral task.

3.3.2 Microelectrode Arrays and Implantation Procedure

Three floating microelectrode arrays (Rousche and Normann 1998; Normann et al. 1999) of 10x10 Iridium Oxide coated electrodes of 1.5 mm lengths (Blackrock Microsystems, Salt Lake City, UT) were implanted in primary motor cortex (M1), primary somatosensory cortex (S1) and dorsal premotor cortex (PMd), only M1 results are described in this paper. The implantation site spanned the shoulder region as confirmed by intra-operative single electrode recordings from S1. Details of surgical implantation technique and use of our Nesting Platform (NP) to hold multiple connectors from the arrays has been previously described (Chhatbar et al. 2010). A few

months before implantation a headpost implantation surgery was performed (Adams et al. 2007) to restrict head movements while the monkey performed the task.

3.3.3 Neural Recordings

Neural signals were high-pass filtered, differentially referenced, amplified and thresholded as per individual characteristics of that electrode channel and sampled at 40 KHz. Online spike sorting was used to pick off putative single unit activity, all spike timestamps and waveform data were saved for further offline analysis (Nicolelis et al. 2003). As the monkey performed the center-out reaching task, kinematic variables (joint positions, velocities, accelerations) and applied torques at each joint where recorded. Muscle activities were recorded through surface EMG leads after shaving the skin contact areas and applying conductive gel on the leads.

3.3.4 Data Processing and Analysis

Before processing the data in the offline case the recorded waveforms are sorted using Offline Sorter (Plexon Inc., Dallas, TX) using an automatic Valley Seeking algorithm (Fukunaga 1990). Matlab (Mathworks Inc., Natick, MA) was then used for all data analysis. We used 100 ms bins and neural activity from 10 bins in the past (total 1 second) for all analysis. Each of the binned neural spiking data and behavioral data were then Z-score transformed. We used multiple linear regression coefficients fit to the data to filter the incoming neural data (Wessberg et al. 2000), and found in our experimental setup that the neural activity of M1 recordings gave the best prediction values when using the first 20 principal components of the combined neural signals. Thus we will concentrate our further discussion only on M1 recordings. The general form of such a model is described below:

Equation 3-1

$$\hat{y}(T) = b + \sum_{i=1}^{m}\sum_{t=1}^{n}\left(\alpha_i(t) \cdot S_i(T-t)\right)$$

where $\hat{y}$ is the predicted variable of interest (e.g., power, force) at time T; b is the y-intercept, $a_i(t)$ are the filter coefficients for the $S_i(T-t)$ that represent the score of the ith principal component at time bins $T - t$ (we used n = 10 and m = 20 as described above). The transformation of neural activity space to principal component space is described in matrix notation by:

Equation 3-2

$$S_{(1\times n)}(T) = N_{(1\times n)}(T)Q_{(n\times n)}$$

where $S_{(1\times n)}(T)$ is the vector of principal component scores for a given time bin T; $N_{(1\times n)}(T)$ is the vector of normalized neural spike counts on each unit for the same time bin T, and $Q_{(n\times n)}$ is the principal component coefficient matrix.

Calculation of power is done by first working on the inverse dynamics of the system (Scott 1999; Fagg et al. 2009). The inertial properties of limb segments were estimated from the weight of the monkey and limb segment lengths (Cheng and Scott 2000), and those of the robotic systems were made available by the company that commercializes KINARM (BKin Technologies, Kingston, ON, Canada). The generalized form of such inverse dynamics equation can be described as:

Equation 3-3

$$\vec{\tau}_{mon} = M(\theta)\ddot{\theta} + C\left(\theta,\dot{\theta}\right)\dot{\theta} + G(\theta) - \vec{\tau}_{cmd} - \vec{\tau}_{frc}$$

where $\vec{\tau}_{mon}$ is torque generated by the monkey (with separate shoulder and elbow components), $M(\theta)$ is the inertial matrix of the whole system, $C(\theta, \dot{\theta})$ is the term for coriolis and centripetal forces, $G(\theta)$ is the gravity term (which will be 0 in our case because of planar nature of manipulandum performing movements about horizontal plane). $\theta, \dot{\theta}, \ddot{\theta}$ denote joint (in our case, shoulder and elbow) angular positions, velocities and accelerations, respectively. $\vec{\tau}_{cmd}$ is the commanded torques by attached motors in order to create the virtual environment and $\vec{\tau}_{frc}$ is the friction torques generated inside the torque motors as the monkey makes the movements. The negative sign before the last two terms is because the monkey has to overcome those torque values in order to make the movements.

We used these torque values to calculate the power,

Equation 3-4

$$P = \vec{\tau}_{sh}\dot{\theta}_{sh} + \vec{\tau}_{elb}\dot{\theta}_{elb}$$

where P is the power generated by monkey which is a linear summation of power generated at the shoulder and elbow, each of which can be calculated by the torque generated at each joint multiplied by the angular velocity of the joint.

Another way to calculate the power is to first transform the joint torques into end-point forces using the generalized formula,

Equation 3-5

$$\vec{\tau} = \vec{l} \times \vec{F}$$

where $\vec{\tau}$ is the joint torque vector, $\vec{F}$ is the end-point force vector, $\vec{l}$ is the vector joining the points where torque and force are applied. '×' denotes cross/vector product. The end-point force can then be used to calculate the power as below:

Equation 3-6

$$P = \vec{F} \cdot \vec{v}$$

which is the dot/scalar product of end-point force vector and end-point velocity vector. Note here that the power calculated by Equation 3-4 or Equation 3-6 use Polar or Cartesian coordinate frame respectively, and that the difference between these two equations is purely cosmetic. In our calculations, we found no difference in power calculated by either of these equations (R>0.99).

3.4 Results and Discussion

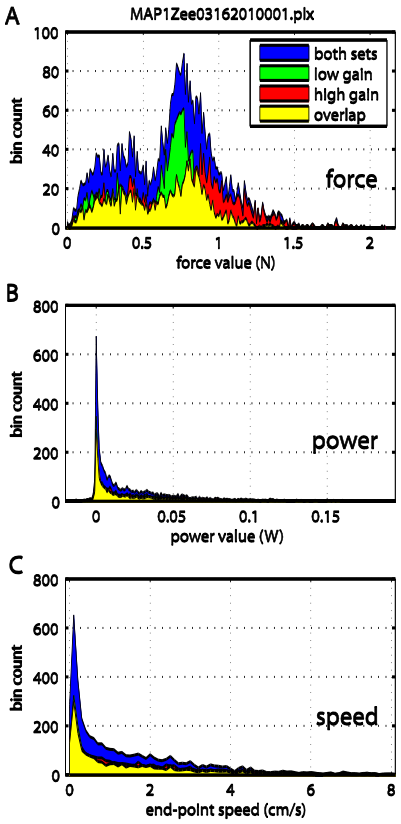

Figure 3.1: Distribution patterns of monkey-generated force magnitude (A), power (B) and speed (C) under low-gain (light gray) and high-gain (dark gray) viscous field. The overlap of the distribution is demarked by darker shade, and lightest gray represent the total distribution through the entire task consisting of the mixture of low- and high-gain viscous environments. Note the highly separate distribution patterns of force generation under different viscous field conditions, which is not the case power or speed profiles.

It is known how neural activity patterns change under loads at different joints and postures (Cabel, Cisek, and Scott 2001; Kurtzer, Herter, and Scott 2005). This suggests that limb motor control is accomplished via a group of separable controllers running in parallel, such that the existence of multiple internal models is supported. Results from bimanual tasks lead to similar conclusions (Nozaki, Kurtzer, and Scott 2006; Nozaki and Scott 2009). It has been about two decades since neural population vectors have been shown to deferrer between external static and dynamic forces (Georgopoulos et al. 1992) as well as for power and kinematic variables such as position (Graham et al. 2003; Kurtzer, Herter, and Scott 2006). It has been shown that both M1 and PMd, previously thought of as regions of execution and planning respectively, can both contribute equally well to the predictions of force-related variables (Gupta and Ashe 2009). Here we try to address two questions. First, whether we can generalize our assumptions of motor control under different external dynamic environmental conditions. Secondly, under

such conditions which parameter of motion will make the most consistent candidate for the control of a BMI.

We found comparable speed profiles under two viscous gain field conditions (-3 Ns/m and -12 Ns/m gains on end-point velocity) suggesting that the monkey's task performance was similar under both conditions (see Figure 3.1(C)). The forces generated by the monkey under high-gain field conditions were increased, explaining the maintenance of such comparable speed profiles (see Figure 3.1(A)). However, the distribution of monkey-generated power, which is displacement per unit time multiplied by the force component in the direction of displacement, remained similar under both gain field conditions. With these findings we believe that that monkey-generated power remains consistent at least under different external viscous environments.

We have also observed that power predictions remain reliable and consistent under different external viscous environments irrespective of the environmental condition of training data-set (Figure 3.2 (B)). We found similar results for speed (Figure 3.2(C)) and other kinematic variables like joint position and velocity (not shown here). On the other hand, we noticed improved force prediction performance in the environments with higher gain fields than those of training data-set ($p<0.05$) but poorer prediction performance in the low gain field compared to training data ($p<0.001$, Figure 3.2(A)). We believe that this is due to the fact that inverse dynamics has been used for calculations of kinetic variables, leading to minute inaccuracies in the derived force variable. Under high gain field conditions increased force generation leads to improved signal-to-noise ratio (SNR), where signal can be seen as generated force and the signal-independent noise as numerical inaccuracies associated with such derivation of force, and thus improved force predictions.

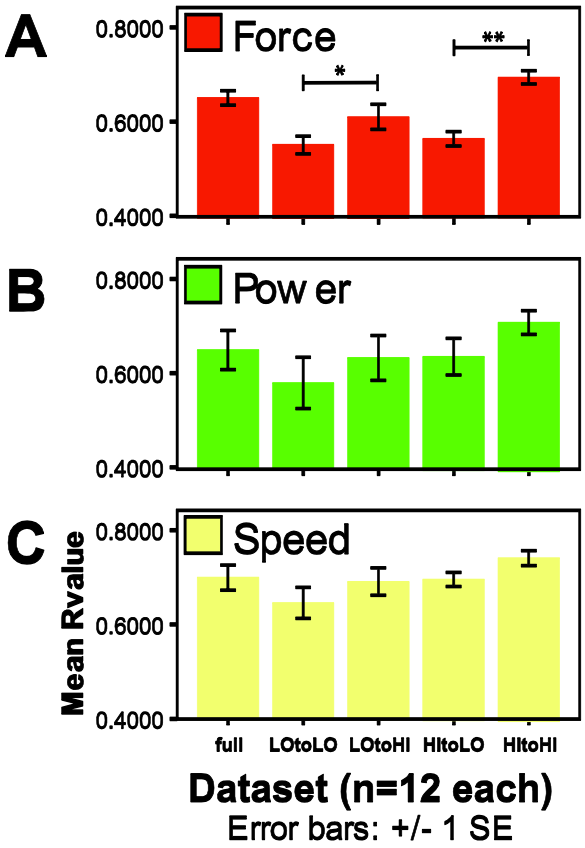

Figure 3.2: Comparison of prediction correlation coefficients trained under one gain field environment and tested under same or another gain viscous field environment. Shown here are results on force (A), power (B) and speed (C) from 12 datasets. Full-model trained from the mixed data consisting of both low- and high-gain viscous field environments to predict the variable under same mixed environments. LOtoLO-model trained in low-gain environment to predict in low-gain environment. LOtoHI-model trained in low-gain environment to predict in high-gain environment. HItoLO-model trained in high-gain environment to predict in low-gain environment. HItoHI-model trained in high-gain environment to predict in high-gain environment. Note that force predictions differ when the model trained under one gain field environment is used to predict in different gain field environment (post-hoc t-test; *p<0.05, **p<0.001). Statistically we failed to find the difference between predictive efficiency of power or speed values for models that are trained under various viscous environments and tested on the others (ANOVA).

These results favor the possibility of using force related variables, such as power, for controlling BMIs under different dynamical environments. Unlike kinematic variables, power contains the kinetic information of the movement; therefore, power might give users superior control over a prosthetic device. Using a dynamics related parameter such as power that incorporates kinematic and force information should allow for more natural BMI control and prove invaluable while working under differing dynamical conditions. Such force related control is also very important for writing on the chalkboard or driving the robotic arm under environmental boundary conditions like stiff wall etc. to prevent potential damage caused by limitations of kinematic controllers. This might make such dynamics-related control a superior choice over traditional kinematics-based BMI algorithms. Further experiments are needed to demonstrate similar findings under a variety of dynamic environments. We are presently working on having the animals working against a continuum of different weight objects to be

transported and various static and dynamic force field conditions. Such experiments should give us comprehensive insights to force and power distribution patterns and more thoroughly interpret the results we have presented here.

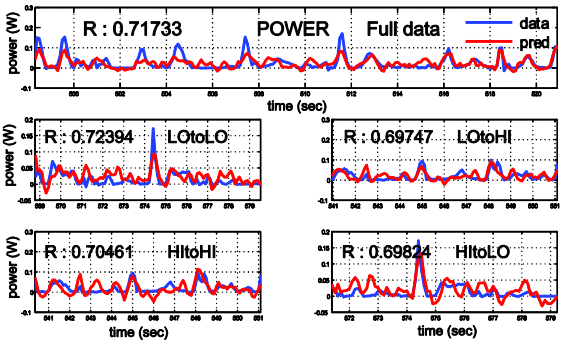

Figure 3.3: Comparison of measured (dark) and predicted (light) power under different gain field conditions for models trained under different gain fields, using the same data set as shown in Fig. 1. Note that power prediction accuracies remain comparable unlike force (not shown) which we found to differ when the external environmental properties change. Refer to Figure 3.2 for abbreviations used here.

Acknowledgments

We would like to thank our lab members for fruitful discussions and help with the experiments and setup. We also thank DLAR staff for their constant support throughout the animal care, implantation and experimentation.

4 Hybrid torque-position control in different viscous environments using ipsi/contra-lateral primary motor cortical signals

4.1 Summary

In real life, limbs generate a variety of end-point forces and joint torques to achieve the same movement profile under different external dynamic environments. The motor cortices have been shown to contain such information, but less is known about ipsilateral motor cortical contribution in force/torque generation. Here we demonstrate the use of ipsilateral, as well as contralateral, motor cortical activity to perform simultaneous joint torque and joint position predictions for a brain-machine interface. We also show changes in the performance under a variety of force-field conditions, when used continually for a few minutes and across different days. Our results suggest that simple mathematical approach combined with inertial dynamics of the system can provide real-time control of joint torques. This might play a crucial role in sensorimotor neuroprostheses, for impedance control at each joint of the prosthetic device will bring us closer to the ultimate goal of a majority of the dexterous movements - reaching and grasping.

4.2 Introduction

Real-life use of brain-controlled robotic manipulator requires impedance control at end-effector for tasks like grasping. Movements with exact same kinematic profiles under different external dynamical conditions, swinging bats of different weights/dimensions for example, require different amount of force/torque generation at manipulator links. This may be achieved by velocity control using force-controllers embedded in the robotic manipulator, but the advantages of giving the user direct control of force-related parameters would be two-fold.

First, user can define the impedance thus giving superior control of the action. Second, the manipulator would have fewer chances of unforeseen behavior, and possible damage, when interacting with high stiffness coefficient objects like wall or metal pole. Other challenge for patients with damaged (e.g., stroke) or resected (e.g., tumor removal surgery) contralateral motor cortex is to extract motor command signals from other healthy cortical region of the brain. It has been shown that ipsilateral motor cortex has position information in both humans and non-human primates and that real-time control of kinematic parameters is possible from ipsilateral motor cortex (Ganguly et al. 2009). Here we demonstrate for the first time the real-time hybrid control of combined joint torques and positions using Utah intracortical array(Maynard, Nordhausen, and Normann 1997; Chhatbar et al. 2010) implanted in ipsilateral motor cortex of bonnet macaque.

Two monkeys were trained on planar random target jump task using kinarm(Scott 1999) (BKin Technologies, Kingston, ON, Canada), where animal has to move to the target displayed at random location in the workspace. Water reward was given at random reward schedule (30%-70% for manual tasks, 70%-100% for BMI tasks) on successful reach. Variety of Joint velocity dependent viscous force fields were applied as monkey performed the task (See Table 4-2), which cycle between low and high gain fields every 10 trials. The torques generated by the monkey were calculated using equations of inverse dynamics (Scott 1999; Fagg et al. 2009; Chhatbar and Francis 2010). Inertial estimates of the animal limb segments were done using linear regression equations based on limb segment lengths and animal weight (Cheng and Scott 2000).

Reconstruction of variety of kinematics and dynamics related parameters was then done using linear filter, or multiple linear regression, method using first 20 principal components of

the firing rate of neural population recorded from ipsilateral or contralateral motor cortex (Chhatbar and Francis 2010). We used previous 1 second of activity with the bin size of 100 ms. These reconstructions were fed continuously to the BMI plant which used single pair of behavioral parameters (joint torques, joint velocities or joint positions) or any combination of the two to come up with the final cursor predictions (see methods).

During BMI mode the monkey was either allowed to move the arm (BMIfree) or arm movements were restricted by a locking pin (BMIlock). Eye movements and bilateral surface EMGs from muscles responsible for shoulder and elbow were recorded and used to qualitatively classify the animal attention and task performance but not used for analysis. We didn't notice any significantly task-related movements or EMG activity in left upper limb in either manual or BMI tasks.

The task was made stringent by limiting trial length to 5 seconds and the trial was considered unsuccessful if the monkey fails to hit the target during this period. Looking at the workspace was important because there is no task-relevant proprioceptive information in BMI task unlike in manual task, making visual feedback the only available task-relevant information for closing the loop.

4.3 Results

4.3.1 Prediction accuracies in open-loop condition

We used multiple linear regression algorithm on binned spiking neural data. The spikes were binned at 100 ms bins and past 10 bins were used for training the algorithm and for prediction. First 20 principal components (PCs) of all the channels were used for the algorithm, because we found best correlation coefficient (R) values at these many PCs. On increasing the

number of PCs the R-values plateaued or even slightly decreased. 20 PCs also gave us superior performance than cosine tuning or selection of units based on behavior-dependent spiking modulation, especially for torque predictions (Figure 4.2, a-b). On comparing R-values for different behavioral variables for different cortical regions, Left M1 performed superiorly for monkey AG3, while Right M1 performed better for monkey Z6. Note that both the animals perform the manual task using right upper limb kinarm apparatus, making right M1 ipsilateral and left M1 contralateral side. The reason for superior fit/prediction performance of ipsilateral M1 neural activity in monkey Z6 can be poor contralateral implantation and/or damage of cortex from previous implantation procedures. During previous two implants (on contralateral side only), we have observed comparable fit/prediction performance from contralateral M1 recordings.

4.3.2 Closed-loop BMI algorithms

In Brain-Control mode (BMI), the loop is closed by visual feedback through the workspace. We tried motor cortex from either side in running closed-loop BMI, but were successful with only Left M1 for monkey AG3 (Figure 4.4, a-e) and Right M1 for monkey Z6. So we will focus majority of results on AG3 with left M1 performance and Z6 with Right M1 performance. We tried multiple decoders on the same day on multiple instances and observed comparable findings. In case of position predictions driven BMI (pBMI) (Figure 4.3, a), we noticed that after presentation of the target, the first sub-movement peak velocity (FSPV) occurs very close to the start point itself, with mean direction of of FSPV not in general direction of the target. This is possibly because of slightly jittery/wavy position predictions. On causal smoothing (not shown), we found that intention-execution lag increased and thus the virtual BMI cursor seem

like having high inertia, difficult to maneuver and it failed to respond to newer predictions instantaneously.

Using velocity-predictions based BMI (vBMI, Figure 4.3, b), the FSPV directionality looks more angled towards the target. On using hybrid velocity-position BMI with 0.001% position influence (hvp1e-5, Figure 4.3, c), we found no statistically significant difference in FSPV distribution (dotted black circle), directionality (thin black circle) or span (size of the black circles) of them (see methods for explanation of the terms; two-sample Kuiper test and Kolmogorov-Smirnov test, $p<0.05$). This suggests that 0.001% position is too small for vBMI to influence.

When we used torque positions in hybrid torque-position BMI with 0.001% (htp1e-5, Figure 4.3, d), we found significant difference from hvp1e-5 in FSPV distribution, directionality and span ($p<0.001$), with non-significant change in the mean angle of FSPV directions, possibly because of expanded directionality span. This suggests that pure torque BMI might be too much out of control (at least on certain days, as we will appreciate in following results) and needs more position influence to 'tame' it down. We found exactly the same: on using 0.005% position influence (htp5e-5, Figure 4.3, e), the FSPV distribution, directionality and span became statistically non-differentiable from hvp1e-5, while when compared with vBMI, Kuiper statistics couldn't find difference in FSPV distribution and directionality, suggesting non-significant change in the mean angle of FSPV locations/directions. Span differences between them were also statistically non-significant.

On comparing htp5e-5 closed-loop performance with open-loop performance (htp5e-5Open, Figure 4.3, f), we found significant differences in FSPV distribution, directionality and spans

(Kuiper and K-S tests, $p<0.05$), demonstrating now well-known fact that open-loop performance doesn't match when the loop is closed. We have also observed that there was no statistically significant difference in magnitude of mean FSPV velocities and distribution span between htp5e-5 performance and manual task performance for the same day (figure not shown).

4.3.3 Changes in performance over time and across days

When animal AG3 used ipsilateral (Right) M1 cortical activity for BMI performance, he couldn't perform the task satisfactorily and soon gave up on BMI control as evident by progressive decrease in rewarded trials (Figure 4.4, a-b). On switching to contralateral (Left) M1 control, the monkey started working on the task and progressively getting more and more involved and proficient as demonstrated by increased trial success rates (Figure 4.4, c-e). The FSPV directionality improved over time (between c and e, $p<0.05$).We didn't observe any statistical difference found between c and d (except change in distribution span, which we noticed between c and e also, $p<0.05$) or d and e.

On using same decoder with same weights used the day before, we have observed some decrease in the performance with change in FSPV distribution, directionality and spans ($p<0.05$), but non-significant difference in the angle of the mean FSPV direction ($p>0.1$, Kuiper test). Similarly, on day 1 the monkey was on pure torque BMI (no position influence; tBMI) controller, when the performance at the beginning and end of the session was fairly consistent with no significant difference in FSPV profile (except spans; Figure 4.4 h,i). On day 2, on using tBMI controller with same prediction coefficients, we noticed no significant difference between h and j (except FSPV distribution span, $p<0.05$). On comparing i and j, we couldn't find significant difference between mean FSPV direction ($p>0.1$, Kuiper test), even though all other FSPV parameters were statistically significant ($p<0.05$, Kuiper and K-S tests).

4.3.4 *Effect of position predictions influence under hybrid torque-position control*

As we have seen earlier in Figure 4.3(d-e), position predictions greatly influence the performance of hybrid torque-position BMI. On putting the monkey on such a hybrid BMI with 0.01% position influence (htp1e-4, Figure 4.5, a), we can see the FSPV trends that are similar to pBMI (peaks very near to the start point, direction of the peak velocity away from the target, constricted span etc). On decreasing the position influence to 0.005% (htp5e-5, Figure 4.5, b) we observed change in mean FSPV location towards the target and constricted FSPV directionality span (Figure 4.5a-b, $p<0.05$). Further decrease in position influence to 0.001% (htp1e-5) was followed by expansion of FSPV distribution span and changed FSPV location and direction angles (Figure 4.5c-d, real arm was locked in 75° shoulder and 85° elbow angle in both the instances; $p<0.05$). When the arm restrain was released, there was some readjustment of mean FSPV location ($p<0.005$) and improved performance. We didn't find any statistical differences in the performance when the kinarm was pinned under htp5e-5 condition (Figure 4.5b-c).

We also locked the kinarm at the center of the workspace (25° shoulder, 85° elbow) and let the monkey perform the BMI task (Figure 4.5f-j). The relatively low reward percentage under this condition when compared with other instance (Figure 4.5a-e) was because of stringent task conditions and expanded boundary, making it harder for the animal to successfully complete the trial. We only noticed FSPV directionality span changing ($p<0.05$, Figure 4.5f-h) as the monkey works with the hybrid htp1e-5 controller. On switching to pure torque controller, the performance decreased, angle of mean FSPV location and direction changed ($p<0.05$, Kuiper test) and FSPV distribution span expanded ($p<1e-3$, K-S test; figure 5 h-i). Within a couple of minutes, the monkey adapted to the task as demonstrated by higher success rate. We didn't find any significant difference in the FSPV profile though (Figure 4.5i-j).

4.3.5 Adaptation through novel task conditions

On increasing task difficulty (by expanding BMI movement boundaries, increasing target stay time and decreasing random reward schedule), we have observed that monkey has sped up the movements as demonstrated by expansion in FSPV distribution and directionality span and mean FSPV location and direction vector ($p<0.05$, compare Figure 4.5d-e with Figure 4.6a). On unlocking the kinarm (from 75° sh, 85° elb) we observed reversal of expansion in FSPV spans with changed FSPV directionality ($p<1e-5$, Figure 4.6a-b), but no statistically significant difference in the FSPV profile when compared with the previous easy task when the arm was freely moving (Figure 4.5e with Figure 4.6b).

Introducing high viscocity environment (from equal to high, see Table 4-2) didn't immediately lead to significant difference in FSPV profile (Figure 4.6,f, compare with Figure 4.5, i-j), but after a few minutes it led to decrease in both FSPV distribution and directionality (Figure 4.6,f-g). This resulted in relatively slower movements and thus possibly better control and higher success rate. On the other hand, on introducing novel viscous gain fields within the bounds of the low and high viscous fields that the animal is currently experiencing (from routine to novel, see Table 4-2) during tBMI, we didn't find significant differences in the FSPV distribution or directionality, even under freely moving actual arm versus locked arm (75,85 degrees) configurations. (Figure 4.6, c-e; h-j).

4.4 Discussion

Here we demonstrate torque-driven brain-machine interface (tBMI) using real-time predictions of torque from the spiking neural data from ipsilateral or contralateral M1. To give the user the advantage of its position expectation, we combined torque predictions with position predictions as a hybrid torque-position control (htpBMI). Influence of position

predictions on BMI in small amounts gives stability to the movements of BMI, by adding expectation of limb state and thus superior prediction performance and hence improved BMI function. It has been documented that information of limb state or proprioception leads to superior offline torque predictions (Fagg et al. 2009) and that torques when combined with kinematic variables (Power) lead to stable performance across different dynamic environments (Chhatbar and Francis 2010). Our results of hybrid torque-position BMI echo these phenomena in real-time, closed-loop setup.

Dynamics-related parameters like torques and forces give user the most direct control of robotic device in brain-machine interface. Use of pure kinematics-related parameters like positions and velocities for impedance control might be sub-optimal, since the user can only have control over kinematic properties of the robotic device and it is totally up to the state of inverse dynamics algorithm to determine the amount of force to be exerted at end-effector level. Other advantage of including torque control is that the BMI will have a capacity to interact external dynamic conditions and learn and adapt to them, as shown in the results.

On the other hand, use of torques for brain-machine interface might not be as accurate as torque generation involves inertial properties of the system, and the external objects that it interacts with, leading to propagation and accumulation of errors as the information is converted from kinematics to dynamics and vice versa. One possible way of addressing it is to include the position-related predictions in the system which leads to decrease in the error, as we demonstrate here with an acceptable trade-off of decreasing torque-predictions influence on the BMI. For future, tactile and/or proprioceptive feedback can be fed directly into the brain regions using micro-stimulation or otherwise to make the closed-loop controller more efficient

and less dependent on vision (O'Doherty et al. 2009; Suminski et al. 2010; London et al. 2008; Francis, Xu, and Chapin 2008; Venkatraman et al. 2009).

In spite of static nature of the decoder we have observed behavioral adaptations in the closed-loop BMI performance involving torque predictions, as demonstrated by others under different BMI setups (Chase, Schwartz, and Kass 2009; Ganguly and Carmena 2009; Ganguly et al. 2009; Jarosiewicz et al. 2008). This can further improved by using coadaptive, learning decoders (Taylor, Tillery, and Schwartz 2002; Digiovanna et al. 2010; Sanchez et al. 2009; Heliot et al. 2010) or using BMI training algorithms (Gilja, Nuyujukian, Chestek, et al. 2010; Gilja, Nuyujukian, Cunningham, et al. 2010). With this learning algorithm, it is crucial to determine when to make changes in the decoder, which can be guided by internal reward state of the system (Khamassi et al. 2008), state of the BMI user (attentive, distracted, asleep etc.) (Velliste et al. 2010; Mahmoudi, Principe, and Sanchez 2009) and/or use of other behavioral information like eye-tracking. Changes in performance across the days can be made favorable by selecting a subset of stable units for performance (Ganguly and Carmena 2009).

Our results suggest that simple mathematical approach combined with inertial dynamics of the system can provide real-time control of joint torques. More experiments are required to test the long-term performance and adaptation rates of the decoder to novel external dynamic environments, under restrained versus freely moving arm conditions. All in all, hybrid torque-position BMI might play a crucial role in sensorimotor neuroprostheses, as impedence control at each joint of the prosthetic device will bring us closer to the ultimate goal of majority of the dexterous movements - reaching and grasping.

4.5 Methods

4.5.1 Behavioral task

Two bonnet macaques (*M.radiata*, one male (AG3) and one female (Z6), weights 3.7 – 4.0 kg) were trained on were trained on the random target pursuit (RTP) task. We used 2-degree-of-freedom planar robotic robotic manipulandum (KINARM, BKin Technologies, Kingston, ON, Canada) as a right hand exoskeletal system exoskeletal system to train the bonnet macaques (*M. radiata*)(Scott 1999). The animals were trained to hit the trained to hit the target that is randomly displayed in the workspace (Serruya et al. 2002). Target was circular in was circular in shape and radius was 1.5 cm for easy task and 1 cm for difficult task. Target was displayed in a displayed in a manner that its center falls inside the workspace spanned by shoulder angle between 10 and 50 between 10 and 50 (easy) or 65 (routine) degrees and shoulder+elbow angle (elbow angle in global space) between global space) between 85 and 125 degrees (Table 4-2). As the monkey performs the task, one of the sets of joint angular velocity-dependent (viscous) torque fields were applied (

Table 4-1). The loads cycle between low and high gains at every 10 trials (Figure 4.1(a)).

Once reached the target, the subject has to stay in the target for 40 ms-160 ms for the trial to become successful. On successful completion of trial, monkey was rewarded with a few drops of water (~0.25 ml). To control the water intake amount and keep the monkey doing the task for more than an hour, the monkey was rewarded 40% of correctly performed trials in manual task. . As the monkey is newly exposed to BMI task, 100% of correctly performed trials are rewarded to keep the monkey motivated and engaged in the task.

The boundary conditions for the manual task was physical restrains of the kinarm apparatus, which commonly gives movement range of -30 to 100 degrees at shoulder angle and 0 to 160 degrees in elbow angle (local coordinates). For the virtual BMI arm, we have set boundaries to be 5 to 75 degrees for shoulder angle, 0 to 150 degrees for elbow angle and 0 to 160 degrees for shoulder+elbow angle (i.e., elbow angle in global space), as long as the virtual

BMI arm doesn't go out of the display screen of the paradigm. For easier task, the boundary conditions were used as the random target generation boundaries plus 5-10 degrees on each border.

Behavioral data, specifically joint angular positions and torques applied by the kinarm robot on each joint was recorded along with neural recordings at 2 KHz sampling rate. Task specific information was also saved with the same recording system as strobed word events.

4.5.2 Microelectrode implantation

All the behavioral and surgical procedures were approved by IACUC of SUNY Downstate Medical Center and closely supervised and assisted by Division of Laboratory Animal Resources. The subjects were trained on the task with head restraint using footed head-post (6-FHP-X2F, Crist Instrument, Hagerstown, MD) previously implanted in midline slightly superior to occipital ridge . Once the animal reached the proficiency level of 90% task performance we implanted the animals bilaterally in primary motor cortex (M1) of shoulder representative region using Utah intra-cortical arrays (10x10 electrode grid, 450 μm inter-electrode distance at tip, 1.5 (Z6) or 1.0 (AG3) mm shank length, Platinum (Z6) or Iridium oxide (AG3) coating at tip; Blackrock Microsystems, Salt Lake City, UT) (Maynard, Nordhausen, and Normann 1997). Monkey AG3 was also implanted bilaterally in primary somatosensory cortex area 1 and 2 of hand representative region and area PE (6x6 electrode grid S1, 1.5 mm shank length, Platinum coating at tip; Blackrock Microsystems, Salt Lake City, UT). Monkey Z6 was implanted bilaterally in S1 area 1-2 of shoulder representative region (10x10 electrode grid, 1.5 mm shank length and Platinum coated tip on left side, 1.0 mm shank length and Iridium Oxide coated tip on right side). We used Nesting Platform method to minimize the trans-cutaneous area and the costs associated with the implant (Chhatbar et al. 2010).

Monkey Z6 was implanted for the third time in contralateral (left) M1 and S1 cortices with 1.5 mm shank length arrays (previous two implantations also covered dorsal premotor cortex), but we were not successful with the neural recordings from these regions with current implant. This might be because of previous surgical insults to gray matter and/or consequent healing and gliosis that led to superficial fibrosis, keeping the array tips from close enough contact with the neurons. Right sided S1 array for Z6 (fresh implant) also didn't give any recordings, possibly due to poor implantation method leading to high wire-bundle strain and eventual spontaneous explantation of the array post-operatively (Figure 4.1).

We will only be using neural recordings of bilateral M1 cortex from monkey AG3 and right sided (ipsilateral) M1 cortex from monkey Z6 for closed-loop experiments. For open-loop performance,

4.5.3 Neural recordings

After implantation surgery, the monkey was allowed to recover for 2-3 weeks after which, recordings of single unit activity were taken while the animal performed the reaching task. Recordings were made using externally synched multiple multichannel acquisition processor systems (MAPs). Neural signals were amplified, band-pass filtered (170 Hz – 8 KHz), sampled at 40 KHz, thresholded and single/multiple units were sorted based on their waveforms using principal-component-based methods in the Sort-Client software (Plexon Inc., Dallas, TX). Neural spike timestamps were streamed online using TCP/IP protocol through PlexNetConc (Plexon Inc., Dallas, TX) to the computer where spike-based-predictions are made based on previously calculated weights from manual task. LFP recordings were also made from 32 channels of each array, (0.7 Hz – 300 Hz band-pass filtering), apart from EMG recordings (bilateral pectoralis major, latissimus dorsi, anterior and posterior heads of deltoid, biceps

brachii, triceps brachii) using surface electrodes (Grass Technologies, West Warwick, RI) at 2 KHz sampling rate, but were not used for analyzing the data.

4.5.4 BMI algorithm

The torques generated by the monkey were calculated using equations of inverse dynamics (Scott 1999; Fagg et al. 2009; Chhatbar and Francis 2010). Inertial estimates of the animal limb segments were done using linear regression equations based on limb segment lengths and animal weight (Cheng and Scott 2000) and those of the robotic systems were made available by the company that commercializes KINARM (BKin Technologies, Kingston, ON, Canada). The generalized form of such inverse dynamics equation can be described as:

Equation 4-1

$$\vec{\tau}_{mon} = M(\theta)\ddot{\theta} + C\left(\theta, \dot{\theta}\right)\dot{\theta} + G(\theta) - \vec{\tau}_{cmd} - \vec{\tau}_{frc}$$

where $\vec{\tau}_{mon}$ is torque generated by the monkey (with separate shoulder and elbow components), $M(\theta)$ is the inertial matrix of the whole system, $C\left(\theta, \dot{\theta}\right)$ is the term for coriolis and centripetal forces, $G(\theta)$ is the gravity term (which will be 0 in our case because of planar nature of manipulandum performing movements about horizontal plane). $\theta, \dot{\theta}, \ddot{\theta}$ denote joint (in our case, shoulder and elbow) angular positions, velocities and accelerations, respectively. $\vec{\tau}_{cmd}$ represents commanded torques by attached motors in order to create the virtual environment. All these variables are sampled at 2 KHz and then low-pass filtered at 10 Hz using 6-pole (3 pole forward + 3 pole backward) Butterworth filter. $\vec{\tau}_{frc}$ represents friction torques generated inside the torque motors as the monkey makes the movements, which were calculated as a function of tanh function of joint velocity times static friction parameter, as supplied by BKin

technologies. The negative sign before the last two terms is because the monkey has to overcome those torque values in order to make the movements.

First 20 principal components were used to make predictions(Chhatbar and Francis 2010). The general form of such a model is described below:

Equation 4-2

$$\hat{y}\,(T) = b + \sum_{i=1}^{m}\sum_{t=1}^{n}\left(a_i(t)S_i(T-t)\right)$$

where $\hat{y}\,(T)$ is the predicted variable of interest (e.g., torque, position in our case) at time T; b is the y-intercept, $a_i(t)$ are the filter coefficients for the $S_i(T-t)$ that represent the score of the ith principal component at time bins $T - t$ (we used n = 10 and m = 20 as described above). These filter coefficients were derived from multiple linear regression methods from the data collected from manual task (using backslash '\' operator in Matlab). The transformation of neural activity space to principal component space can be described in matrix notation by:

Equation 4-3

$$S_{(1\times n)}(T) = N_{(1\times n)}(T)Q_{(n\times n)}$$

where $S_{(1\times n)}(T)$ is the vector of principal component scores for a given time bin T; $N_{(1\times n)}(T)$ is the vector of normalized neural spike counts on each unit for the same time bin T, and $Q_{(n\times n)}$ is the principal component coefficient matrix.

Thus predicted shoulder and elbow joint torques and positions (total four variables) were sent to the behavioral paradigm plant running at 1 KHz on xPC target (Dexterit-E v2.2, BKin

Technologies, Kingston, ON, Canada), which then calculates the consequent virtual BMI arm positions by weighted sum of arrived predictions using following formula:

Equation 4-4

$$\Theta_{plant}(t) = \left(2\Theta_{plant}(t-\Delta t) - \Theta_{plant}(t-2\Delta t)\right) + (1-\alpha)\left(\left(inv\big(M(t-\Delta t)\big)\left(\hat{\tau}(t) - C(t-\Delta t) - G(t-\Delta t)\right)\right)\frac{(\Delta t)^2}{2}\right) + \alpha\left(\widehat{\Theta_{pos}}(t) - \left(2\Theta_{plant}(t-\Delta t) - \Theta_{plant}(t-2\Delta t)\right)\right)$$

where $\Theta_{plant}(t)$ is joint position values of virtual BMI arm in the plant at time t, $\hat{\tau}(t)$ and $\widehat{\Theta_{pos}}(t)$ are joint torque and position predictions respectively fed to the plant, and α is the weight given to the joint position predictions. This can be put simply as,

Equation 4-5

$$\theta_{plant}(t) = (1-\alpha)\left(\widehat{\Theta_{tor}}(t)\right) + \alpha\left(\widehat{\Theta_{pos}}(t)\right)$$

where $\widehat{\Theta_{tor}}(t)$ is joint position values calculated by plant based on joint torque prediction values given joint position values of the plant in previous state or iteration and $\widehat{\Theta_{pos}}(t)$ is joint position values based on joint position predictions. We used α in the range of 0 to 1e-2, or 0 to 1%, which is the weight given to joint position predictions. This gives rest of 99 to 100% weightage to position values derived from joint torque predictions. The weighted sum of them is then used to calculate final joint position values of virtual BMI arm in the plant. We also tried such a hybrid control using combination of velocity and position also, where the $\widehat{\Theta_{tor}}(t)$ is replaced with $\widehat{\Theta_{vel}}(t)$in the equation above and it means joint position values calculated by plant based on joint velocity prediction values, given joint position values of the plant in previous state or iteration. The slight contribution of joint position seems to prevent the plant of accumulating and propagating the errors that comes with joint torque predictions and

consequent dynamics-to-kinematics transformations as the joint position values are being calculated in the plant, as mentioned in the results section.

4.5.5 FSPV plot

The reaching task is commonly accomplished by a single movement or a combination of multiple sub-movements. Latter is the case more commonly, and that makes the first sub-movement since the presentation of the target gets crucial importance in appreciating the performance. Peak velocity at a given sub-movement is considered representative for the whole sub-movement. Since the task was random target pursuit, we have come up with this first sub-movement peak velocity (FSPV) plot to generalize each movement to a level that it can be compared again each other. Detailed explanation of the plot is provided below.

4.5.5.1 Finding the movement peaks

Shoulder and Elbow angular position data was collected at 2 KHz sampling rate. It was low-pass filtered at 10 Hz using 6-pole (3 forward, 3 backward) Butterworth filter. End-point position was then calculated using trigonometry and numerically differentiated to come up with end-point velocities and speed. Peaks and troughs of the speed were then found using simple calculus (when second differential of speed (jerk) is zero and the sign first differential (acceleration)). Only trials that were considered in the analysis have (i) peak values of the speed higher than 5 cm/sec, (ii) start of the movement (trough immediately before the peak) at least 100 ms after the presentation of the target (iii) peak of the speed at least 200 ms after the presentation of the target and finally (iv) start of the movement point is at least 1 cm away from the margin of the target in workspace.

4.5.5.2 Normalizing the movements

All the considered trials are normalized by using start-to-target vector, the start of the movement being point 0 and center of the target being point 100. Notice that this distance in reality is always greater than 1 cm + target radius (making total of 2-3 cm) considering the inclusion criteria that we have used, and can go as high as 15 cm in cases of targets presented at the extremes of the workspace. Now first sub-movement peak velocity (FSPV) is located on workspace and perpendicular and parallel displacement is found out using trigonometry, as a fraction of this distance. Similarly, velocity in x- and y-direction is also rotated and scaled to this start-to-target vector.

4.5.5.3 FSPV distribution, directionality, span and plot legends

The distribution of FSPV locations in normalized workspace is defined as FSPV distribution and the distribution of FSPV directions in normalized workspace as FSPV directionality. Span of FSPV distribution and dimensionality is defined as the spread of the FSPV locations/directions after subtraction of mean FSPV location/direction. Normalized start-to-target vector is plotted as vertical yellow bar of length 100 and mean target size is plotted as green circle with standard deviation as dashed circle bigger and smaller than the green circle. Individual FSPV locations are plotted as blue or red dots in case of manual or BMI task, respectively, and individual FSPV directions as blue or red arrows in case of real arm or virtual arm movements, respectively (scaled to 0.01 of original). Unsuccessful trials are marked by black plus (+) sign on individual FSPV locations. The mean and standard deviation of FSPV distribution is plotted as dashed circle/oval with center in mean and the margin as a standard deviation. The mean and standard deviation of the FSPV directionality is plotted as dashed arrow and thin circle respectively (scaled to 0.1 of original).

We used non-parametric Kuiper two-sample test (circular statistic analogue of Kolmogorov-Smirnov two-sample test) to compare the mean angles of distribution and directionality of the FSPV. To compare the mean vector lengths or sparseness (that is FSPV locations/directions minus mean distribution/directionality vector) of distribution or directionality, we used non-parametric Kolmogorov-Smirnov two-sample test statistic.

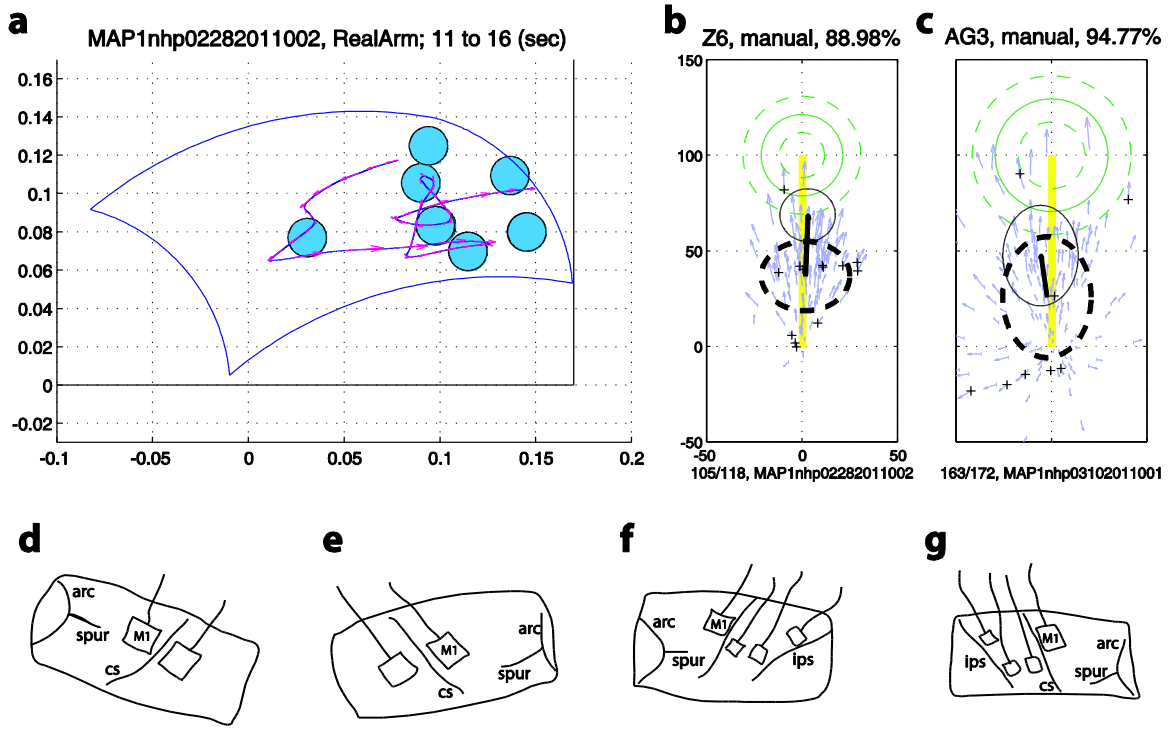

Figure 4.1: Task, FSPV plots and microelectrode array implant locations: (a) random target pursuit (RTP) task during manual/BMI performance. (b,c) normalized first sub-movement peak velocity (FSPV) plots: Title shows animal ID, task type as manual and percent successful trials. Actual numbers of successful and total considered trials are presented in the bottom, next to the recorded file name. Further explanation can be found in the methods section. (d-k) Array placement for the two animals based on digital photographs taken at the time of surgery. Top of the figures always represent rostral/medial direction towards sagittal sulcus. Anterior is direction of junction of arcuate sulcus and its spur (arrow head) relative to central sulcus (arrow). (d) Z6 left and (e) right brain M1 and S1 (area 1-2) implant (96 channels) in shoulder representative region. Animal Z6 was implanted for the third time in left M1 and S1 regions at the same implant location. (f) AG3 left and (g) right brain implant in

M1 (96 channels) shoulder representative region, S1 area 1, 2 hand representative regions and area PE (32 channels each).

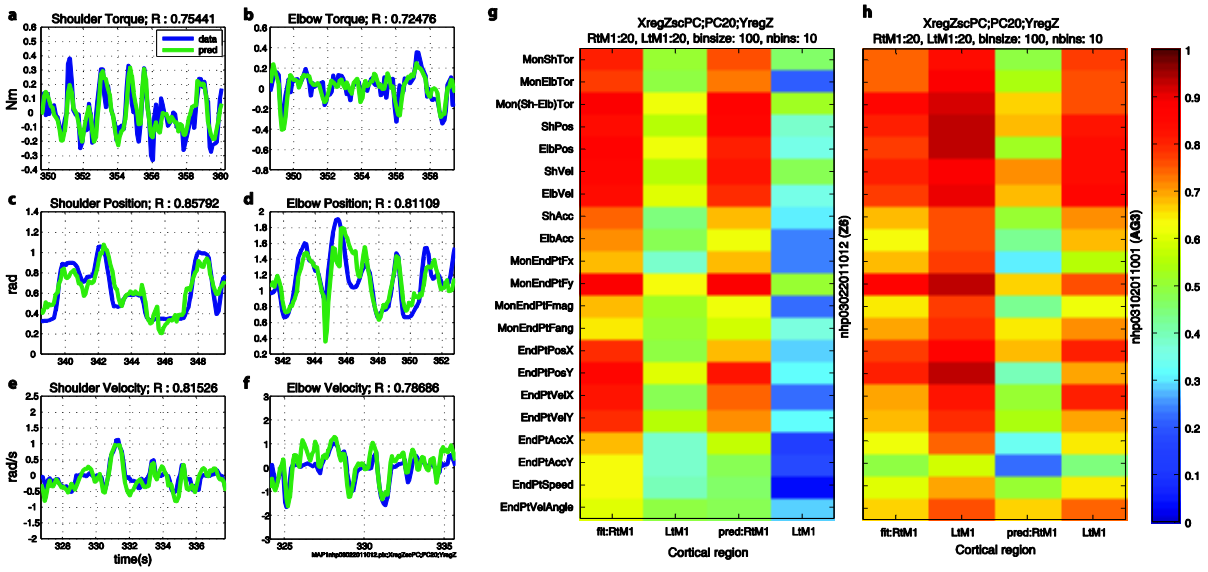

Figure 4.2: Open loop performance of the decoder: (a-f) Sample plot of prediction values (green) overlaid on actually recorded or calculated joint torques, positions and velocities during manual task. R-values are shown along with the respective parameter in the title of the subplot. About 10 seconds of data is shown for each parameter. Predictions are made on a new dataset using coefficients calculated by multiple linear regression of first 20 principal components of all units recorded from M1 (ipsilateral, in this case, on monkey Z6) against the behavioral parameter from different dataset Data was binned at 100 ms and past 10 bins were used for predictions. (g-h) summary R-value plots of fits (estimates on same dataset, left 2 columns) and predictions (estimates on new dataset, right 2 columns) on multiple behavioral variables using first 20 principal components. (g) Z6 and (h) AG3. Acronym key: fit = fit values, pred = prediction values, Rt = Right side, M1 = primary motor cortex, shoulder-representative region; Mon = monkey generated, Sh = shoulder, Elb = elbow, Tor = torque, Pos = position, Vel = velocity, Acc = acceleration, EndPt = End-point/end-effector - about the tip of middle finger of the monkey, F = force, x = X-direction, y = y-direction, mag = magnitude, ang = angle.

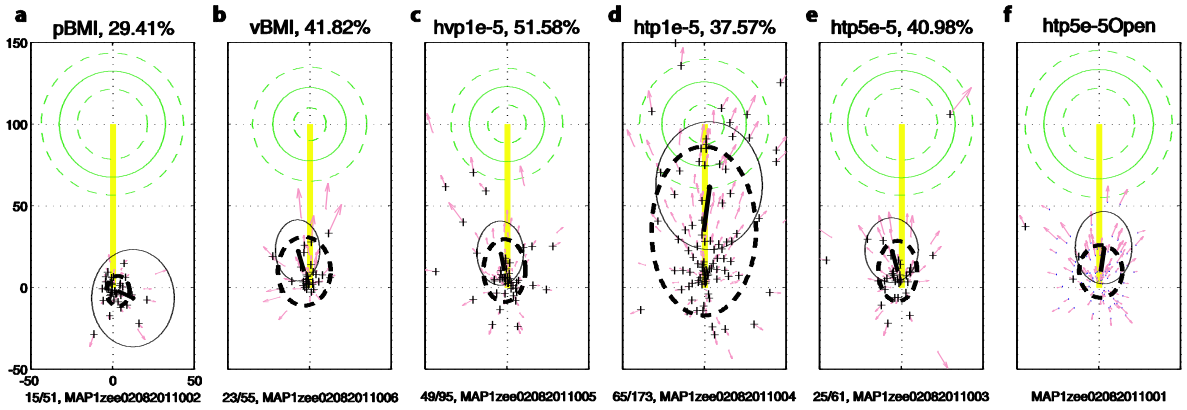

Figure 4.3: Effect of position prediction influence on the first sub-movement peak-velocity (FSPV) under variety of closed-loop BMI controllers on a single day (loop is closed by vision of the workspace), animal Z6. (a) position BMI (pBMI) (b) velocity BMI (vBMI) (c) hybrid velocity-position BMI, 0.001% position influence (hvp1e-5) (d) hybrid torque-position BMI, 0.001% position influence (htp1e-5) (e) hybrid torque-position BMI, 0.005% position influence (htp5e-5) (f)open-loop htp5e-5 (htp5e-5Open) without animal's knowledge while doing manual task. Please refer to Figure 4.1 and methods and results for detailed explanation of the plots for this and the following figures.

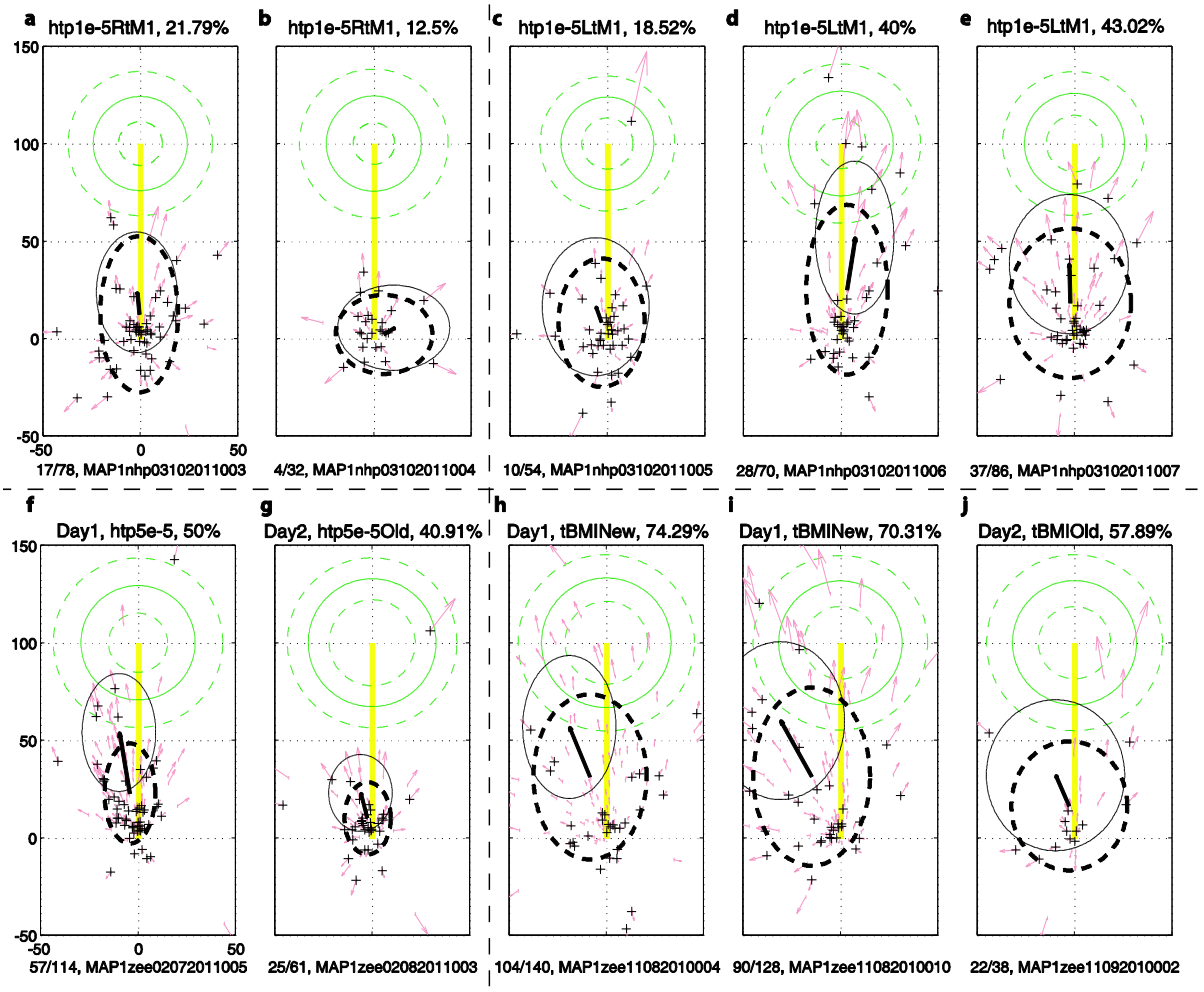

Figure 4.4: Changes in the performance with continued usage of BMI over time. (a-e) animal AG3: (a,b) using ipsilateral M1 hybrid torque-position BMI with 0.001% position influence (htp1e-5RtM1). (c,d,e) using contralateral M1 (htp1e-5LtM1). (f-j) animal Z6 across days: (f,g) htp5e-5 controller with set of coefficients across the day led to slightly decreased success rate, more constricted FSPV distribution and directionality ($p<0.05$) but similar mean FSPV direction ($p>0.1$). (h,i) Using pure torque controller (tBMI) with fresh coefficients from same day manual task (j) using same decoder from previous day led to no significant difference in mean FSPV direction ($p>0.1$, Kuiper test).

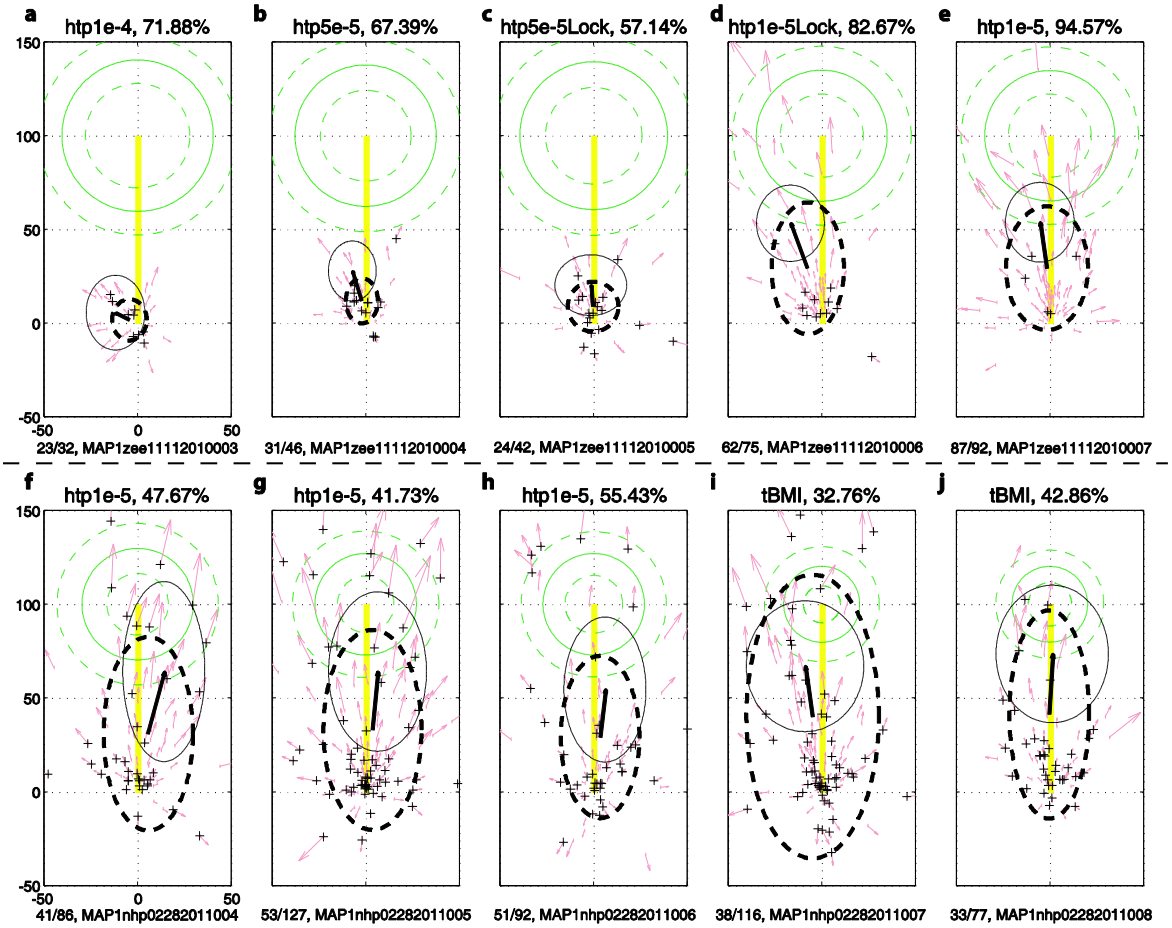

Figure 4.5: Effect of position influence in hybrid torque-position BMI: (top row) decreasing position influence from 0.01% (a) to 0.005% (b-c) to 0.001% (d-e). Real arm was locked in (c,d) at 75° shoulder and 85° elbow. (bottom row, f-j) Decreasing position influence from 0.001% to 0% (pure torque control). The real arm was locked at the center of the workspace, at 25° shoulder and 85° elbow.

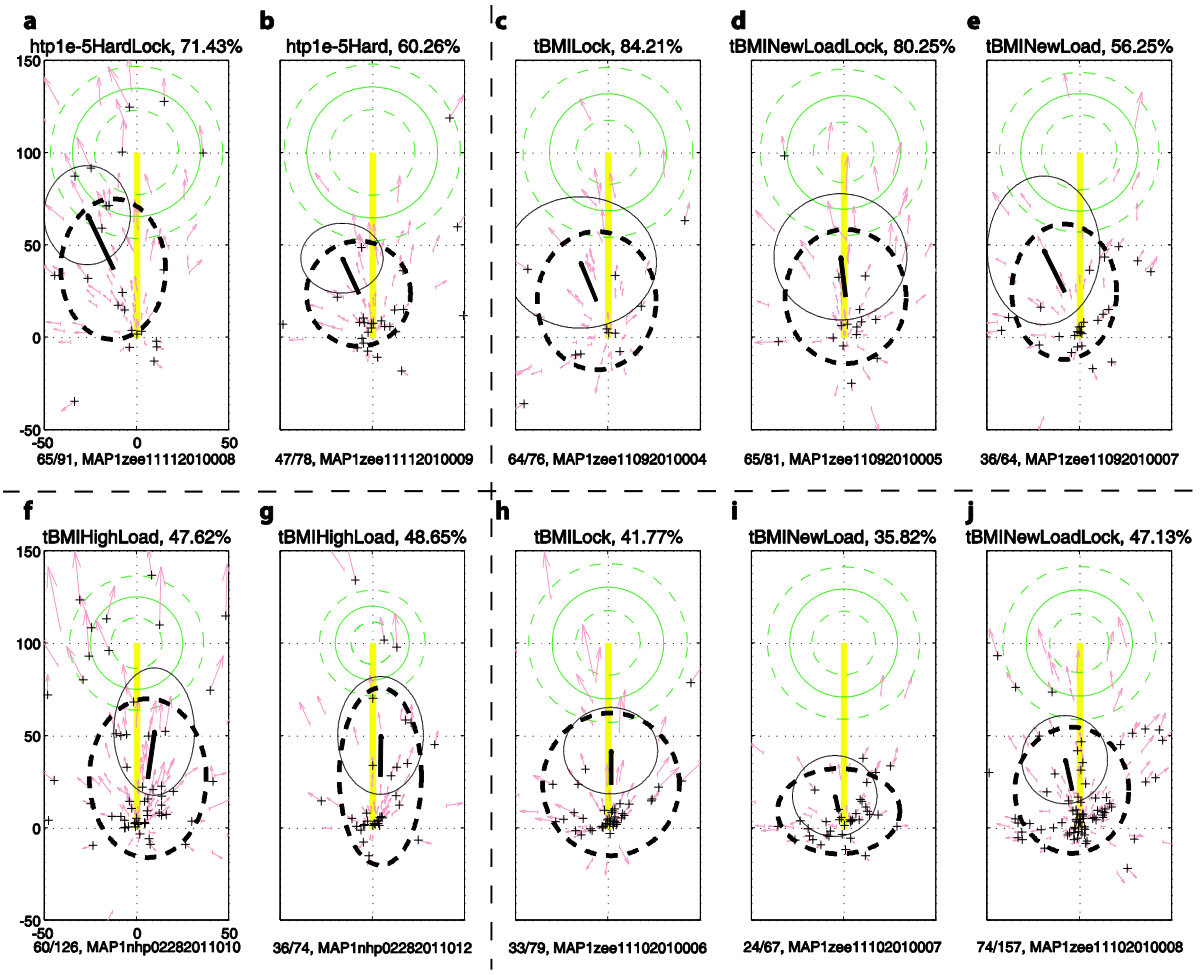

Figure 4.6: Adaptation through novel task conditions: (a,b – htp1e-5) Increased task difficulty led to faster movements and decreased success-rate (a, compare with Figure 4.5,d-e). followed by slowing down by the animal (b, decrease in FSPV distribution and directionality). (f-g, tBMI) Increased viscous gain-fields (joint-angular velocity-dependent resistive torques, equal versus high, see Table 4-2) led to slower movements and improved the success-rate ($p<0.05$, g, compare with Figure 4.5,i,j). (c-e; h-j tBMI) Introduction of novel viscous gain-fields inside the bounds of ongoing low- and high- gain fields (routine versus novel, see Table 4-2), no significant difference in FSPV distribution or directionality found even under freely moving actual arm versus locked arm (75,85 degrees) configurations.

Table 4-1: Applied loads on the real or virtual arm as the animal performs the reaching task. The loads cycle between low load condition and high load condition every 10 trials, and the current load condition is displayed through the size of the cursor, which is proportional to the summed resistive gains for a given load condition, i.e. smaller cursor size under low loads and larger cursor size under high loads.

Load set name	Joint velocity-dependent resistive load gains (Nms/rad)			
	Low load condition		High load condition	
	shoulder	elbow	shoulder	elbow
Routine	-0.01	-0.05	-0.04	-0.20
Novel	-0.02	-0.10	-0.03	-0.15
Equal	-0.05	-0.05	-0.15	-0.15
High	-0.10	-0.10	-0.20	-0.20

Table 4-2: Random target generation limits in shoulder and elbow angle space. The target is generated in uniformly distributed fashion in joint angular space to ensure uniform sampling of global shoulder and elbow joint angular position.

Target set name	Location of the target center in joint-angular coordinate system (degrees, global)			
	Lower limit		Upper limit	
	shoulder	elbow	shoulder	elbow
Routine	10	85	65	125
Easy	10	85	50	125

5 Discussion and possible future directions

Towards achieving the aims laid out above, we have demonstrated that our microelectrode array implantation technique provides an efficient way of microelectrode implantation under 'Nesting Platform'. We also demonstrated how the vector dot product of force and velocity, or power, can be a superior candidate in terms of consistent prediction accuracies in different environments over speed or force for offline predictions under 'Towards finding a generalizable BMI controller minimally influenced by external dynamic environments'. Finally we have showed real-time control of BMI using combination of kinematic and dynamic parameter predictions and how it is superior to current kinematics-based BMI technology under 'Hybrid torque-position control in different viscous environments using ipsi/contra-lateral primary motor cortical signals'. Further discussion, updates and possible future directions are laid out in the following sections. Finally, the last section of this chapter introduces a broad discussion of implantable neuroprosthetics and ethical considerations, covered in one of the chapters below.

5.1 Nesting platform – current uses and future possibilities

As described in 'Nesting Platform' (NP) above, we have been using this technology successfully on multiple subjects. To date, we have successfully implanted the same animal for 3 times with no post-surgical complications. Total of 3 different animals have been implanted with this NP alone or with other technologies like chambers and different microelectrode array connectors.

If we extend the generic concept of the NP, the same idea can be used to make different NP design that can be function-specific. To illustrate, we have designed an NP that can carry up to 8 ICS-96 connectors or can have changed connector mounting orientation.

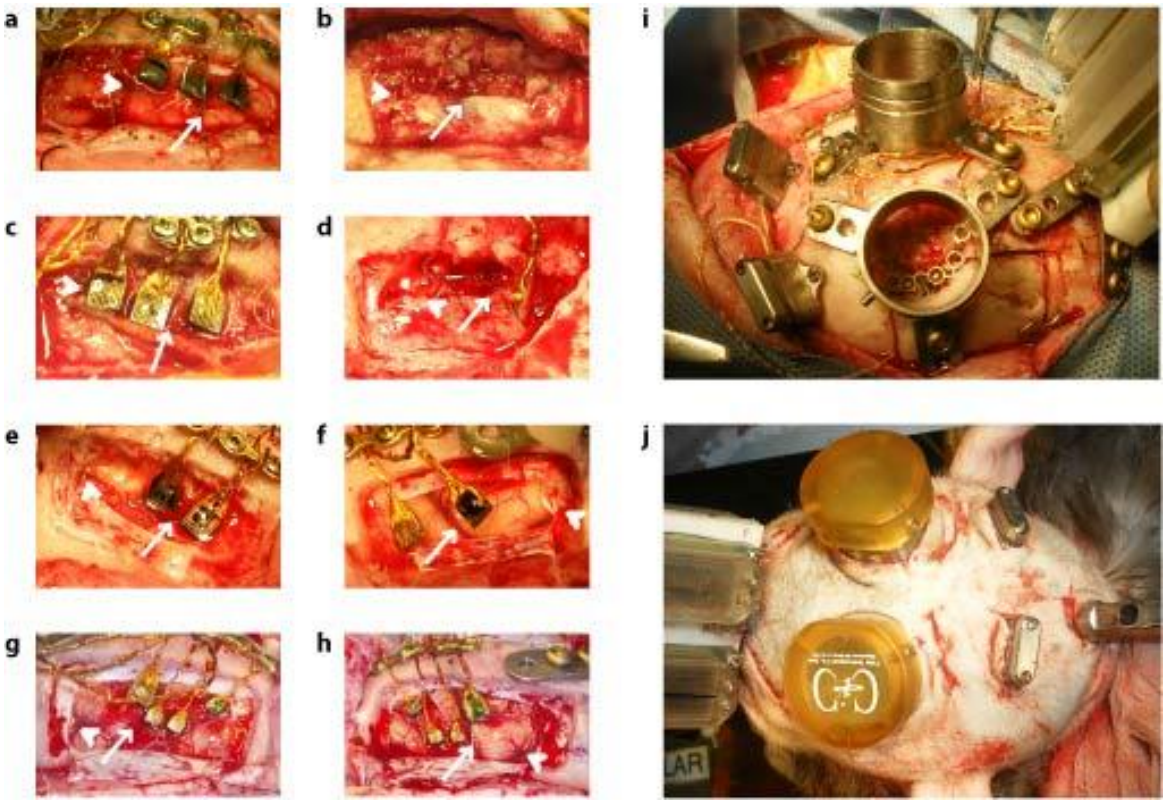

Figure 5.1: Use of Nesting Platform (NP) for microelectrode array (MEA) implant surgeries. (a-h) implant on same subject for 3 times. (a) first implant, (b) first implant removal, (c) second implant, (d) second implant removal, currently active third implant on (e) right and (f) left sensorimotor cortex. (g-h) implant on another subject on (g) right and (h) left sensorimotor cortex. Arrow and arrow head show central sulcus and arcuate sulcus, respectively. (i-j) use of NP in combination with 2 chambers and other set of MEA connectors. (i) just after installing all the hardware and (j) after complete closure.

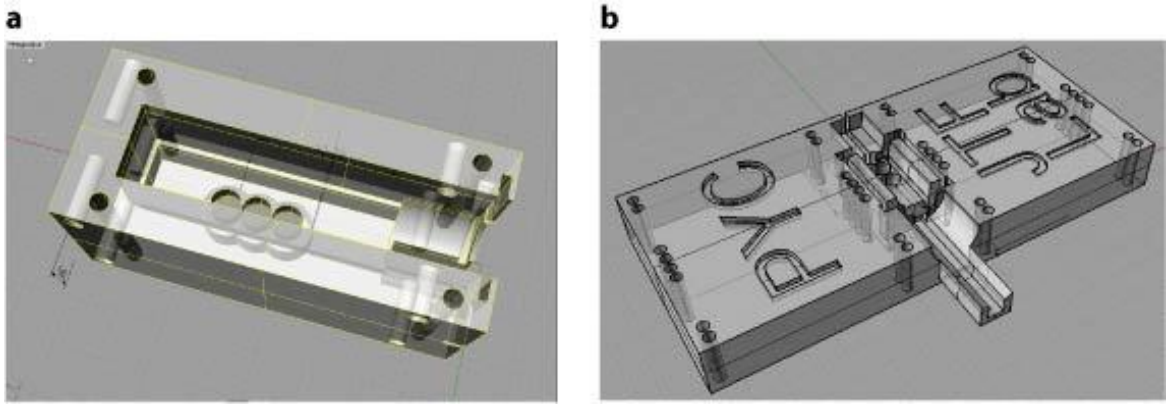

Figure 5.2: Newer NP designs. (a) NP with capacity to connect four ICS-96 MEA connectors on all four sides. (b) NP with capacity to connect eight ICS-96 MEA connectors.

5.2 Power and its closest closed-loop approximation

As demonstrated in 'Towards finding a generalizable BMI controller minimally influenced by external dynamic environments' above, Power gives consistent prediction accuracies across different external dynamic environments (like speed/velocity) and contains properties of dynamic variables (like force/torque). Kinematic variables, as the name suggests, don't take into account the dynamic properties and thus their predictions don't get affected by changed dynamic environment. On the other side, pure dynamic variables like force predictions give different behavioral performance under changed environmental dynamics. Considering both these issues, power contains qualities of both kinematic and dynamic properties making it superior to using only kinematic/dynamic variable.

For real-time use, using power becomes impractical because it requires both force/torque and consequent velocity vector. So, mimicking it by using both dynamic and kinematic parameters simultaneously will be one of the work-around. It has also been shown that including kinematic parameter (limb state) improves torque (dynamic parameter) predictions (Fagg et al. 2009), encouraging such dynamic+kinematic combination.

5.3 Hybrid BMI controller equations and generalization to neurally predicted signal

5.3.1 Derivation of hybrid BMI controller equations

For a given time t, the joint position values of the plant running at discrete sufficiently high sampling rate/frequency Fs (and sufficiently small sampling interval Δt) will be,

Equation 5-1

$$\theta_{plant}(t) = \theta(t - \Delta t) + \dot{\theta}(t - \Delta t)\Delta t + \frac{1}{2}\ddot{\theta}(t)(\Delta t)^2$$

Where, $\theta_{plant}(t)$ is joint position values at time t, which depends on previous position $\theta(t - \Delta t)$ and velocity $\dot{\theta}(t - \Delta t)$ values and the acceleration $\ddot{\theta}(t)$ applied to the plant. Also,

Equation 5-2

$$\dot{\theta}(t) = \frac{\theta(t) - \theta(t - \Delta t)}{\Delta t}$$

Equation 5-3

$$\ddot{\theta}(t) = \frac{\dot{\theta}(t) - \dot{\theta}(t - \Delta t)}{\Delta t} = \frac{\theta(t) - 2\theta(t - \Delta t) + \theta(t - 2\Delta t)}{(\Delta t)^2}$$

Under no external forces/torques, acceleration on the plant will be zero, making the third term in Equation 5-1 to be 0.

Equation 5-4

$$\tilde{\theta}_{plant}(t) = \theta(t - \Delta t) + \dot{\theta}(t - \Delta t)\Delta t = 2\theta(t - \Delta t) - \theta(t - 2\Delta t)$$

$$\tilde{\dot{\theta}}_{plant}(t) = \dot{\theta}_{plant}(t - \Delta t)$$

$$\ddot{\tilde{\theta}}_{plant}(t) = 0$$

Where $\tilde{\theta}_{plant}(t)$ suggests plant positions at time t without any acceleration influence or, in other words, plant state without external torques/forces. Similarly, $\dot{\tilde{\theta}}_{plant}(t)$ is defined as plant velocities at time t without any external torques/forces, which essentially would be the same velocity as in previous iteration. $\ddot{\tilde{\theta}}_{plant}(t)$ is the acceleration at time t without torques/forces acting, explaining its value 0. Plugging Equation 5-4 into Equation 5-1 gives us,

Equation 5-5

$$\theta_{plant}(t) = \tilde{\theta}_{plant}(t) + \frac{1}{2}\ddot{\theta}(t)(\Delta t)^2$$

Thus the plant state at time t (left hand side, LHS) is defined by summation of two terms (right hand side, RHS). Plant state that is acquired without any force/torque contribution $\tilde{\theta}_{plant}(t)$, and the change due to collective influence of all forces/torques applied on the plant $\ddot{\theta}(t)(\Delta t)^2$.

For the generalized hybrid control that depends on, for instance, weighted sum of joint position, joint velocity and joint torque from neural predictions, Equation 5-5 can be written as,

Equation 5-6

$$\theta_{plant}(t) = \tilde{\theta}_{plant}(t) + \frac{1}{2}\left(\alpha_{pos}\widehat{\ddot{\theta}_{pos}(t)} + \alpha_{vel}\widehat{\ddot{\theta}_{vel}(t)} + \alpha_{tor}\widehat{\ddot{\theta}_{tor}(t)}\right)(\Delta t)^2$$

Where $\widehat{\ddot{\theta}_{\iota}(t)}$ is acceleration value derived from neural predictions of a behavioral variable and α_i is the coefficient or weight assigned to each acceleration value. This can be also shown as,

Equation 5-7

$$\theta_{plant}(t) = \tilde{\theta}_{plant}(t) + \alpha_{pos}\widehat{\delta_{pos}(t)} + \alpha_{vel}\widehat{\delta_{vel}(t)} + \alpha_{tor}\widehat{\delta_{tor}(t)}$$

Where $\widehat{\delta_{\iota}(t)} = \frac{1}{2}\widehat{\ddot{\theta}_{\iota}(t)}(\Delta t)^2$ is the change in the position value that happened due to influence of each neural prediction, given previous plant position and velocity values. If $\sum \alpha_i = 1$ then,

$$\theta_{plant}(t) = \alpha_{pos}\left(\tilde{\theta}_{plant}(t) + \widehat{\delta_{pos}(t)}\right) + \alpha_{vel}\left(\tilde{\theta}_{plant}(t) + \widehat{\delta_{vel}(t)}\right) + \alpha_{tor}\left(\tilde{\theta}_{plant}(t) + \widehat{\delta_{tor}(t)}\right)$$

Replacing $\tilde{\theta}_i + \hat{\delta}_{\iota}$ with $\hat{\theta}_{\iota}$,

Equation 5-8

$$\theta_{plant}(t) = \alpha_{pos}\widehat{\theta_{pos}(t)} + \alpha_{vel}\widehat{\theta_{vel}(t)} + \alpha_{tor}\widehat{\theta_{tor}(t)}$$

Where $\widehat{\theta_{pos}(t)}$, $\widehat{\theta_{vel}(t)}$ and $\widehat{\theta_{tor}(t)}$ are defined as the position values derived from neural predictions of position, velocity and torque, respectively. Note here that the derived position values $\widehat{\theta_{\iota}(t)}$ are dependent on the plant state, namely previous position, velocity and frequency at which the plant runs (see Equation 5-4).

5.3.2 Normalizing the coefficient values for used behavioral predictions

In this discussion we use joint angular position and its first two time differentials, joint angular velocity and acceleration. Suppose Neural predictions for joint angular position, velocity and acceleration are $\widehat{S_{pos}(t)}$, $\widehat{S_{vel}(t)}$ and $\widehat{S_{tor}(t)}$, respectively, and the change theey bring about in the plant position, velocity and acceleration in unit time Δt are $\widehat{d_{pos}(t)}$, $\widehat{\dot{d}_{vel}(t)}$ and $\widehat{\ddot{d}_{tor}(t)}$, respectively. The relationship between these neural predictions and the difference they bring about is explained by,

Equation 5-9

$$\widehat{d_{pos}(t)} = \widehat{S_{pos}(t)} - \tilde{\theta}_{plant}(t)$$

$$\widehat{\dot{d}_{vel}(t)} = \widehat{S_{vel}(t)} - \tilde{\dot{\theta}}_{plant}(t)$$

$$\widehat{\ddot{d}_{tor}(t)} = inv\big(\tilde{M}(t)\big)\widehat{S_{tor}(t)} - \tilde{C}(t) - \tilde{G}(t)$$

Where $\tilde{M}(t)$, $\tilde{C}(t)$ and $\tilde{G}(t)$ are the inertial, coriolis and gravitational terms of the plant at time t. In order to feed these difference values in Equation 5-6 we will first convert $\widehat{d_{pos}(t)}$ and $\widehat{\dot{d}_{vel}(t)}$ values of Equation 5-9 into acceleration terms.

Equation 5-10

$$\widehat{\ddot{\theta}_{pos}(t)} = \frac{2}{(\Delta t)^2}\widehat{d_{pos}(t)}$$

$$\widehat{\ddot{\theta}_{vel}(t)} = \frac{1}{\Delta t}\widehat{\dot{d}_{vel}(t)}$$

$$\widehat{\ddot{\theta}_{tor}(t)} = \widehat{\ddot{d}_{tor}(t)}$$

Plugging these acceleration values of Equation 5-10 into Equation 5-6 gives us,

Equation 5-11

$$\theta_{plant}(t) = \tilde{\theta}_{plant}(t) + \frac{1}{2}\left(\frac{2\alpha_{pos}}{(\Delta t)^2}\widehat{d_{pos}(t)} + \frac{\alpha_{vel}}{\Delta t}\widehat{\dot{d}_{vel}(t)} + \alpha_{tor}\widehat{\ddot{d}_{tor}(t)}\right)(\Delta t)^2$$

Which is the equation of plant update similar to Equation 5-5 and Equation 5-6, but now normalized to the changes brought about by the position, velocity and torque predictions in the plant. Rearranging notations will give us,

Equation 5-12

$$\theta_{plant}(t) = \tilde{\theta}_{plant}(t) + \frac{1}{2}\left(\gamma_{pos}\widehat{d_{pos}(t)} + \gamma_{vel}\widehat{\dot{d}_{vel}(t)} + \gamma_{tor}\widehat{\ddot{d}_{tor}(t)}\right)(\Delta t)^2$$

And the relationship of γ_i and α_i is,

Equation 5-13

$$\gamma_{pos} = \frac{2\alpha_{pos}}{(\Delta t)^2}$$

$$\gamma_{vel} = \frac{\alpha_{vel}}{\Delta t}$$

$$\gamma_{tor} = \alpha_{tor}$$

If interested, the relationship between $\widehat{\theta_i(t)}$ in Equation 5-8 and $\widehat{S_i(t)}$ is,

Equation 5-14

$$\widehat{\theta_{pos}(t)} = \widehat{S_{pos}(t)} - \tilde{\theta}_{plant}(t) + \tilde{\theta}_{plant}(t) = \widehat{S_{pos}(t)}$$

$$\widehat{\theta_{vel}(t)} = \left(\widehat{S_{vel}(t)} - \tilde{\dot{\theta}}_{plant}(t)\right)\Delta t + \tilde{\theta}_{plant}(t)$$

$$\widehat{\theta_{tor}(t)} = \frac{1}{2}\left(\left(inv(\tilde{M}(t))\widehat{S_{tor}(t)} - \tilde{C}(t) - \tilde{G}(t)\right) - \tilde{\ddot{\theta}}_{plant}(t)\right)(\Delta t)^2 + \tilde{\theta}_{plant}(t)$$

5.3.3 Hybrid torque+position control plant running at 1 kHz

In case of a hybrid torque+position BMI, $\alpha_{vel} = 0$. If we consider $\alpha_{pos} = \alpha$ then $\alpha_{tor} = (1 - \alpha)$. This converts Equation 5-8 into,

Equation 5-15

$$\theta_{plant}(t) = \alpha\widehat{\theta_{pos}(t)} + (1-\alpha)\widehat{\theta_{tor}(t)}$$

Corresponding changes in Equation 5-6 will be,

Equation 5-16

$$\theta_{plant}(t) = \tilde{\theta}_{plant}(t) + \frac{1}{2}\left(\alpha\widehat{\ddot{\theta}_{pos}(t)} + (1-\alpha)\widehat{\ddot{\theta}_{tor}(t)}\right)(\Delta t)^2$$

Also, changes in Equation 5-12 will be,

Equation 5-17

$$\theta_{plant}(t) = \tilde{\theta}_{plant}(t) + \frac{1}{2}\left(\gamma_{pos}\widehat{d_{pos}(t)} + \gamma_{tor}\widehat{\ddot{d}_{tor}(t)}\right)(\Delta t)^2$$

Where $\gamma_{pos} = \frac{2\alpha}{(\Delta t)^2}$ and $\gamma_{tor} = 1-\alpha$ based on Equation 5-13. Different values of α with related γ_{pos} and γ_{tor} values are listed in Table 5-1 for 1 kHz plant frequency ($Fs = 1000;\ \Delta t = 0.001$).

Table 5-1: Relationship of α with γ_{pos} and γ_{tor} at plant frequency of 1 kHz ($Fs = 1000;\ \Delta t = 0.001$)

α at $Fs = 1000$	$\alpha_{pos} = \alpha$	$\gamma_{pos} = 2\alpha/(\Delta t)^2$	$\alpha_{tor} = 1-\alpha$	$\gamma_{tor} = 1-\alpha$
0.01% or 10^{-4}	10^{-4}	200	0.9999	$0.9999 \approx 1$
0.005% or $5\text{x}10^{-5}$	$5\text{x}10^{-5}$	100	0.99995	$0.99995 \approx 1$
0.001% or 10^{-5}	10^{-5}	20	0.99999	$0.99999 \approx 1$
0	0	0	1	1

5.4 From hybrid control to impedance control

We have discussed the performance of hybrid (torque+position) control in 'Hybrid torque-position control in different viscous environments using ipsi/contra-lateral primary motor

cortical signals' above. The unique quality of this control, unlike kinematic BMI control in currently prevailing literature, is that it changes its behavior under different external dynamic environment (see Figure 4.6). The magnitude of this change heavily depends on position predictions contribution in hybrid control. This contribution is controlled by variable α as described in Equation 4-4 and Equation 4-5.

We have seen that as we decrease the α (or α_{pos} or γ_{pos}) value, the influence of position predictions decreases, increasing the influence of torque predictions on the movements as we observed in Figure 4.5 and Figure 4.3 as an increase in FSPV (first sub-movement peak velocity) distribution and directionality away from the movement start-point. This can be seen as increased admittance or decreased impedance (see Equation 1-1). Thus by varying the position prediction influence in hybrid BMI controller we get a handle towards impedance control of the BMI arm, changing the sensitivity of the arm towards torques/forces applied. In simplistic terms, this can be exemplified by a stiff/rigid arm versus a relaxed arm.

In order to exploit the full functionality of this hybrid control feature, α value needs to be controlled using neural signals. This can implemented by discrete neural control of α value, if not continuous control, along with simultaneous torque and position controls using neural predictions. This way the user can decide on the compliance/admittance of the prosthetic arm, keeping it high (low α or α_{pos} or γ_{pos} value) during routine movements and making it low (high α or α_{pos} or γ_{pos} value, increased impedance) once the object grasp has occurred. Fine tuning α value will also determine amount of force applied on the object, making it convenient to manipulate objects with wide variety of physical properties from delicate, fragile ones to stiff, brittle objects.

In natural acts of reaching and grasping, we routinely increase the impedance of the proximal joints (shoulder, elbow) towards providing stability to distal links (wrist and hand/finger joints) which in turn have low impedance as the act of grasping progresses. Once the grasp action completes, the impedance of the joints involved in holding the object (commonly, finger joints) is determined by the physical properties of the object like dimension, smoothness, softness, fragility, stiction (static friction) etc. Towards achieving such a proficient level of impedance control at multi-joint level, the α value can be predicted for each and every joint of the prosthetic manipulator involved and used towards impedance control of individual joints, with common trend of high impedance (high α or α_{pos} or γ_{pos} value) at proximal joints that provide stability to distal joints, low impedance (low α or α_{pos} or γ_{pos} value) at joints involved with actual act of grasping and finally individualized impedance values depending on the physical properties of the object once the grasp has completed and the act of holding the object continues.

5.5 Thoughts on future of the technology in general and ethical issues

As the field of Neuroprosthetics advances, non-clinical uses of the neuroprosthetic devices will be explored. This has already begun by use of neural signals for video games (Dawson 2004; Mason et al. 2004; Qiang, Sourina, and Khoa). The possible applications of neuroprosthetics have gained tremendous attention as demonstrated in TV series and movies like Matrix, Ironman, Spiderman 2 (Carmena 2004), Six million dollar man, Bionic woman etc. It seems that the realization of such applications is a question of when than if. Its use can easily extend from restoration of lost modality like amputated or paralyzed limb in clinical setting to supplementation like increased strength of limb using neurally controlled exoskeletal system. A totally new neurally controlled modality like multiple limbs/tentacles, well projected in

character named ‘Dr. Octopus’ is movie Spiderman 2 for example, might be very attractive functionality for many able-bodied persons. As we can see, there is tremendous potential in this new technology to get misused or even abused if fallen in wrong hands. Ethical and legal standards need to be in place before this rapidly emerging technology goes out of control. ‘Ethical considerations on implantable neuroprosthetics’ goes over the current state and future projections of the technology, potential issues and ethical considerations.

6 Ethical considerations on implantable neuroprosthetics

Below is the manuscript of the Paper titled 'The future of implantable neuroprosthetic devices: ethical considerations'; Chhatbar, P. Y., Saha, S.; Journal of Long-term Effects of Medical Implants; 19(2): 123-137; PMID: 20666712.

This paper was presented in part at 'The Fifth International Conference on Ethical Issues in Biomedical Engineering'; Brooklyn, NY on April 5, 2009 and at 'The 6th Annual World Congress of IBMISPS On Brain Mapping and Image Guided Therapy'; Boston, MA on August 28, 2009.

6.1 Abstract

From the well-established results of cochlear implants to the advent of implantable microelectrode arrays, the implantable neuroprosthetic devices have gained increasing attention of healthcare professionals, scientists, engineers and population in general. With recent depictions and projections of these neuroprostheses by news media and movies, the confusion about their current state and concern for their future use has increased tremendously among the public. Many government agencies and non-government organizations are also concerned regarding the safety and efficacy of these devices. We plan to discuss the present state of development of some of these implantable neuroprostheses, the possible future use of this technology and the associated ethical issues that can be of concern and sometimes alarming. This would include the process of manufacturing, animal experimentation, human trials, scope of the use, and the individual and societal concerns associated with the use of such devices.

Keywords: neuroprosthetics, neural prostheses, ethics, newer technologies, medical implants

6.2 Introduction

A neural prosthetic device or a neural prosthesis can be defined as a device implanted in the central or peripheral nervous system for the purpose of restoring or improving a lost or altered neural function. A neural prosthesis can work as a stimulating device (e.g. cochlear implant in neural deafness, subthalamic implant in drug-refractory parkinsonism, stimulation based functional mapping of the cortex using subdural surface electrodes) or a recording device (e.g. subdural surface electrodes to localize epileptogenic focus, multi-electrode implant to control cursor/robotic devices using motor cortex activity). As of today multitudes of such neural prostheses are available commercially and many of them are being investigated for modifying the existing technology, or as a de-novo technology. We have observed an increasing interest in the field as objectively evidenced by the publication trends in scientific journals for past few years (Figure 6.1).

The cochlear implant, developed in 1950s, is perhaps the first commercially used neural prosthesis that is helping thousands of deaf children and adults around the globe every year to restore hearing, albeit partially(House and Willstedt 1957). The development from a single channel initially to today's 32-channel cochlear implant has empowered it with a lot more functionality and access on the user's end to actually be able to understand a simple, day-to-day conversation just by 'listening' without using any gestures(Loizou 1999).

The use of a subthalamic implant as a therapy for drug-refractory Parkinsonism is based on the same principle of micro-stimulation as a cochlear implant (Simuni et al. 2002). While the

latter stimulates the cochlea, a part of the peripheral nervous system, a subthalamic implant stimulates the deep brain structures. This in turn stimulates/inhibits selected pathways in the brain network responsible for impairment of motor function that allows easy initiation of movements and also minimizes resting tremors in the patients.

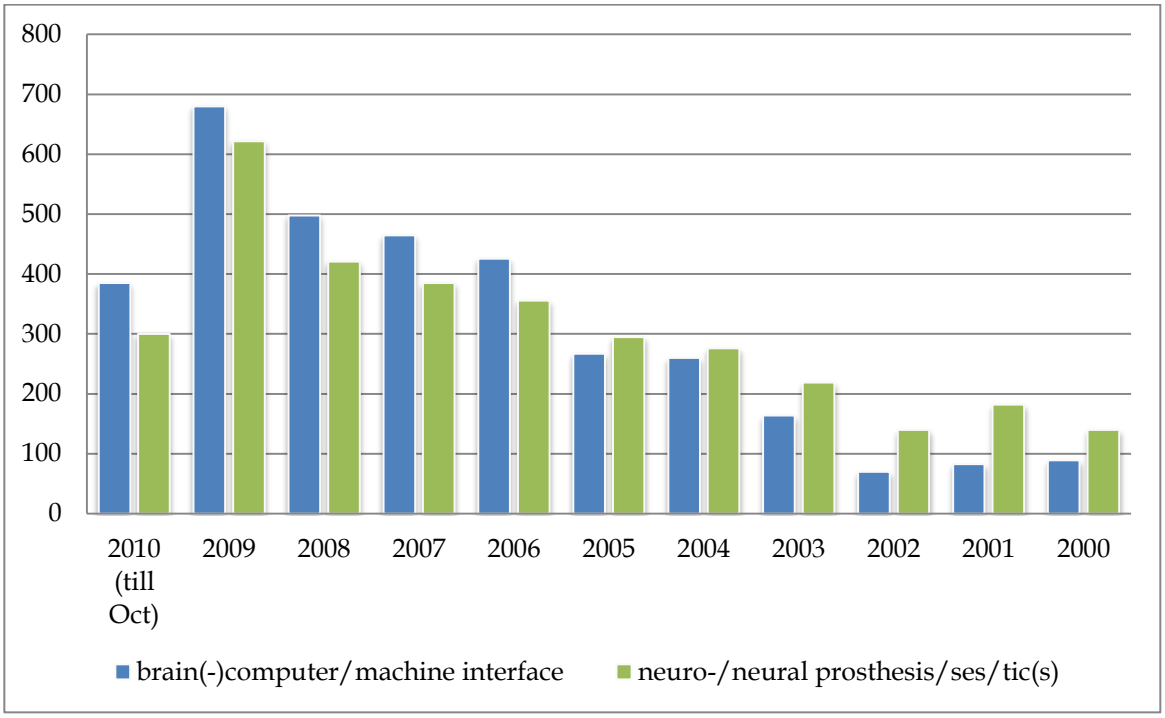

Figure 6.1: Number of publications based on PubMed database for different keywords related to neural prostheses up to October 2010.

A widely used surgical technique in cases of epilepsy can be classified as temporary neural prosthetics, which comprises of subdural electrode strip or grid electrodes or depth electrodes reaching deep into the hippocampal region of the temporal lobe(Spencer et al. 1990). Patients with recurrent seizures with poor medical response or compliance can be candidates for the resection of the epileptogenic focus that is commonly located in or around the temporal lobe. Before the actual resection, these patients undergo an implantation surgery of such electrodes and are followed up for days to weeks without anti-epileptic medications in order to locate the

exact site of seizure origin. The second use of these implanted electrodes is to determine possible functional impairment caused by resection of underlying or surrounding brain region(Behrens et al. 1994). The electrodes are stimulated to offer non-functionality to its surrounding brain region while the patients perform routine day-to-day conversations or related tasks. This helps to delineate the margin of surgical resection as well as predict any possible post-resection disability that may be acquired by the patient. Finally, in the second and final surgery these electrodes as well as the part of the brain with epileptogenic focus are resected.

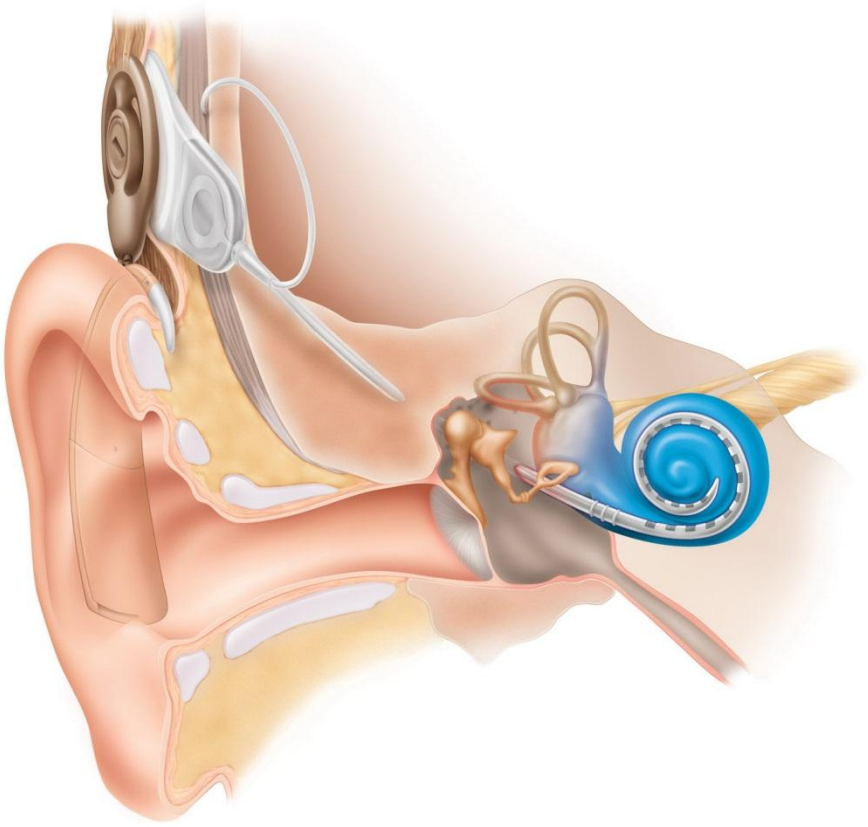

Figure 6.2: Schematic diagram of a cochlear implant (Reproduced from: National Institute of Health, part of the United States Department of Health and Human Services)

Considerable research has been conducted in the past decade on the active development of permanent cortical implants (Chapin and Moxon 2001; Nicolelis, Chapin, and Wessberg 2007;

Giszter et al. 2001; Carmena et al. 2003; Schwartz et al. 2006). Some sensorimotor implants are undergoing active human trials to restore the function of the denervated limb or replacement of the resected limb with a robotic limb that is controlled by the brain signals (Donoghue 2002; Hochberg et al. 2006; Patil et al. 2004; Andersen, Musallam, and Pesaran 2004). This neural prosthetic device may be a pure recording device, the signals from which might be used to move the limb or a robot. It might also be a combination of recording and stimulating units which would also send the state information of the limb or a robot back to the brain, thus closing the loop and enabling more access and freedom to the user. This differs from the visual or auditory cortical implants where the implanted microelectrodes are used purely to stimulate the neural substance based on the visual/auditory signals that the external sensors may be receiving(Schmidt et al. 1996; Niparko et al. 1989). Here the micro-stimulation site may be located in the central nervous system, namely cerebral cortex or a deep structure like lateral or medial geniculate nucleus instead of the peripheral nervous system organ like the cochlea in case of the cochlear implant or the retina in case of the retinal implant(Wilson et al. 1991; Skinner et al. 1994; Humayun et al. 2003; Margalit et al. 2002).

Recently there has been an increased interest in the peripheral nervous system neural prostheses among the clinical and research community. In essence, a microelectrode array in the same or slightly modified configuration as used for the brain is implanted in a peripheral nerve(Hillman et al. 2003) like the sciatic nerve(Branner, Stein, and Normann 2001) for a lower limb or member of the brachial plexus in the upper limb. Through this implant, the nerve fascicles can be monitored or stimulated in order to receive the sensory information it is carrying or feed motor commands that the muscles can use in order to move the limb, respectively.

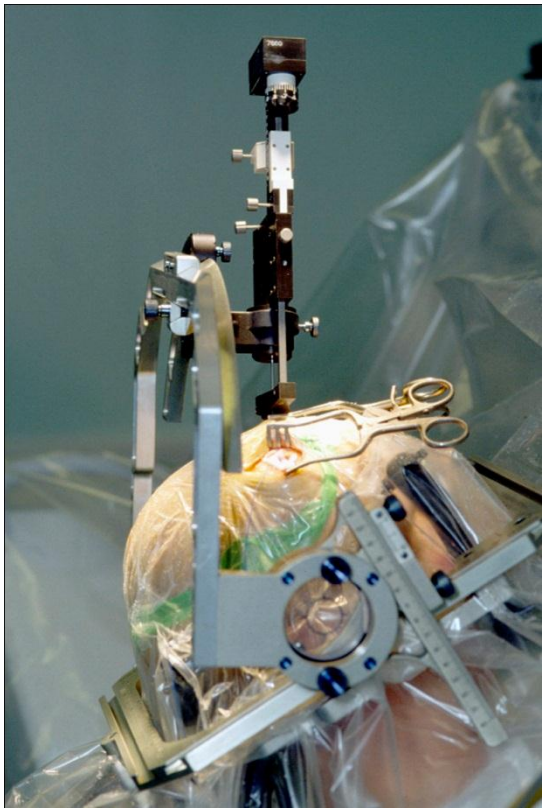

Figure 6.3: A parkinsonian patient undergoing a subthalamic implant procedure with a framed stereotaxy. Newer methods of such implantation procedures don't involve such frames, and thus are called frameless stereotaxy. Here the precise location of an electrode tip is determined by pre-operative or intra-operative MRI. An even newer method is intra-operative 3D USG. (image from Wikimedia Commons)

A slight extension of the peripheral nervous system neural prostheses, which is not a neural prosthesis in the pure sense but resembles it enough to be mentioned here, is a myoelectric prosthesis(Kuiken, Miller, et al. 2007). Here the diversion and implantation of the nerves feeding the resected limb is performed on the pectoral muscles. The patient can use his EMG signals to control the multiple degree of freedom robotic arm. The sensory counterpart of it would be a tactile stimulator on the chest, neck, or cheek used on an amputee with or without the diversion and implantation of the nerves feeding the resected limbs on the skin as the tactile stimulation site(Kuiken, Marasco, et al. 2007). In a nutshell, the touch pattern generated by the tactile stimulator would be received on these diverted nerves and thus the patient feels the sensations which are similar to the sensations on the amputed limb. This can be compared with the peripheral nervous stimulating type prosthesis, but the quality and richness heavily depend on the innervations of the diverted nerve and the spatiotemporal resolution of the tactile

stimulator that is partly controlled by its physical properties. Many such diversions and the extensions of the peripheral nervous or myoelectric prostheses are being investigated with varying degrees of success.

6.3 Current and potential uses of neural prostheses

As of now, very few neural prostheses are being used successfully on a commercial basis. Some examples are cochlear implants in patients with profound sensorineural deafness and subthalamic implants in patients with drug-refractory Parkinsonism. Cochlear implants(Geers et al. 2000; Waltzman et al. 1994) have contributed significantly to improving the users' quality of life and have a long track record regarding their safety and efficacy, but long term effects and failure rates of the newer techniques like subthalamic implants (Romito et al. 2002; Pahwa et al. 2003; Lyons et al. 2004) are still not well established. There is also some but insufficient evidence in humans on the neural control of external devices(Hochberg et al. 2006) like a computer cursor, and its simple technological extensions like moving a limited degree of freedom hand and wheelchairs.

Implantable visual prosthetic devices for the future may have prosthesis implanted in the retina(Zrenner 2002) or sub retinal region(Schwahn et al. 2001), optic nerve(Veraart et al. 1998; Veraart et al. 2003), lateral geniculate nucleus(Pezaris and Reid 2007; Suaning et al. 1998) or visual cortex(Campbell et al. 1989) itself. This would help blind people to have at least a 'pixelated' view of the outside world, just like the way cochlear implants seem to give tones of limited frequency values. But this application, once sophisticated technologically, might also serve as an accessory visual stimulation pattern where a person can actually get additional relevant information based on the location and the scene one is looking at.

Similarly, attempts have been made to create implants for hearing impaired patients where the cochlea is non-functional or inert for electrical stimulation. Future auditory prostheses may include a cochlear nerve implant(Hillman et al. 2003), auditory brainstem implant(ABI)(Rauschecker and Shannon 2002), inferior colliculus (IC) implant, medial geniculate nucleus (MGN) implant, and auditory cortex implant(Howard III 1998).

The very idea behind the development of such prostheses is to restore or improve the function of a disabled person, just like having glasses for eye refraction improvement (disability improvement) or having cataract surgery (restoration of a function). But going a step further, the integration of visual, auditory, somatosensory and motor neural prostheses application can lead to new applications that may change drastically the way we think and live. Just contemplating about the consequences of such futuristic developments might give a bewildering feeling given the current state of technology use. Just to illustrate some examples, visual prostheses might obviate the need for a television set. With the help of sensorimotor prostheses we may not need a keyboard or a mouse to operate the computers. Given the dynamic nature of sensorimotor cortex, it can be trained to operate buttons ranging from a simple light switch to complicated cell phones without buttons or a touch screen.

Telecommunication devices like cell phones possibly communicate wirelessly with auditory implants to send the voice and may be able to get speech signals from an implant in Broca's area to send it to the party on the other end. Because of a generic nature of the neural implants and transfer protocols, it might be possible to use a somatosensory implant to enjoy the texture as well as the feel of the cloth that one is about to buy in a store. Hippocampal implants with micro needles can help to selectively forget traumatic experiences or events by using substances like PKMζ(Sacktor 2008; Serrano et al. 2008), decreasing the chances of being affected by psychiatric

problems like acute or post-traumatic stress disorder. The programmed peripheral muscular stimulation might mean smaller, shorter workout sessions with manifold and speedy build-up of the muscle mass without actually having neural fatigue caused by presynaptic neurotransmitter exhaustion. It might also be able to give an additional boost to the muscles of a soldier to reach towards or away from the enemy at a little faster speed or little farther distance. Motor cortical activity might control multiple prosthetic arms at the same time, effectively using the very neural signals to control a variety of instruments. This can range from big cranes and bulldozers for routine construction chores to precision work like robotic microsurgery (Mack 2001; Lanfranco et al. 2004) where activity from a larger brain area can be used for a lesser degree of freedom task. Use of multiple different instruments like handling multiple machine guns, rocket launchers, missiles while controlling fighter airplane or a tank while simultaneously communicating with the other soldiers might be possible. In short, it can take over the dexterous hand/feet maneuvers with increased precision. This all might sound like a fairy tale, but we strongly believe that the possibilities are infinite and that realization of it is the question of when rather than if. After the discussion on the current state of neural prostheses below, we hope to make the above-stated claims sound somewhat feasible, if not a trivial extension of the current technology.

6.4 Current research on development of neural prosthetic devices

Our senses are divided into two broad categories: general senses and special senses. General senses include touch, pressure, pain, temperature, vibration etc., broadly covering the sensations that we get through our skin and underlying tissue which have various sensory nerve endings. Vision, hearing, taste and smell are classified as special senses. As of today, the majority of the work on neural prostheses is related to the field of vision and hearing part of

special senses and touch part of general senses. Recently proprioception has started getting a lot of attention because of its role in artificial limb, but relatively little work has been conducted in the field of taste, smell, temperature or pain in terms of restoration of these modalities in prosthetic devices. This is possibly because of their limited role in terms of rehabilitation (taste, smell) and easy detection by simple sensors (temperature).

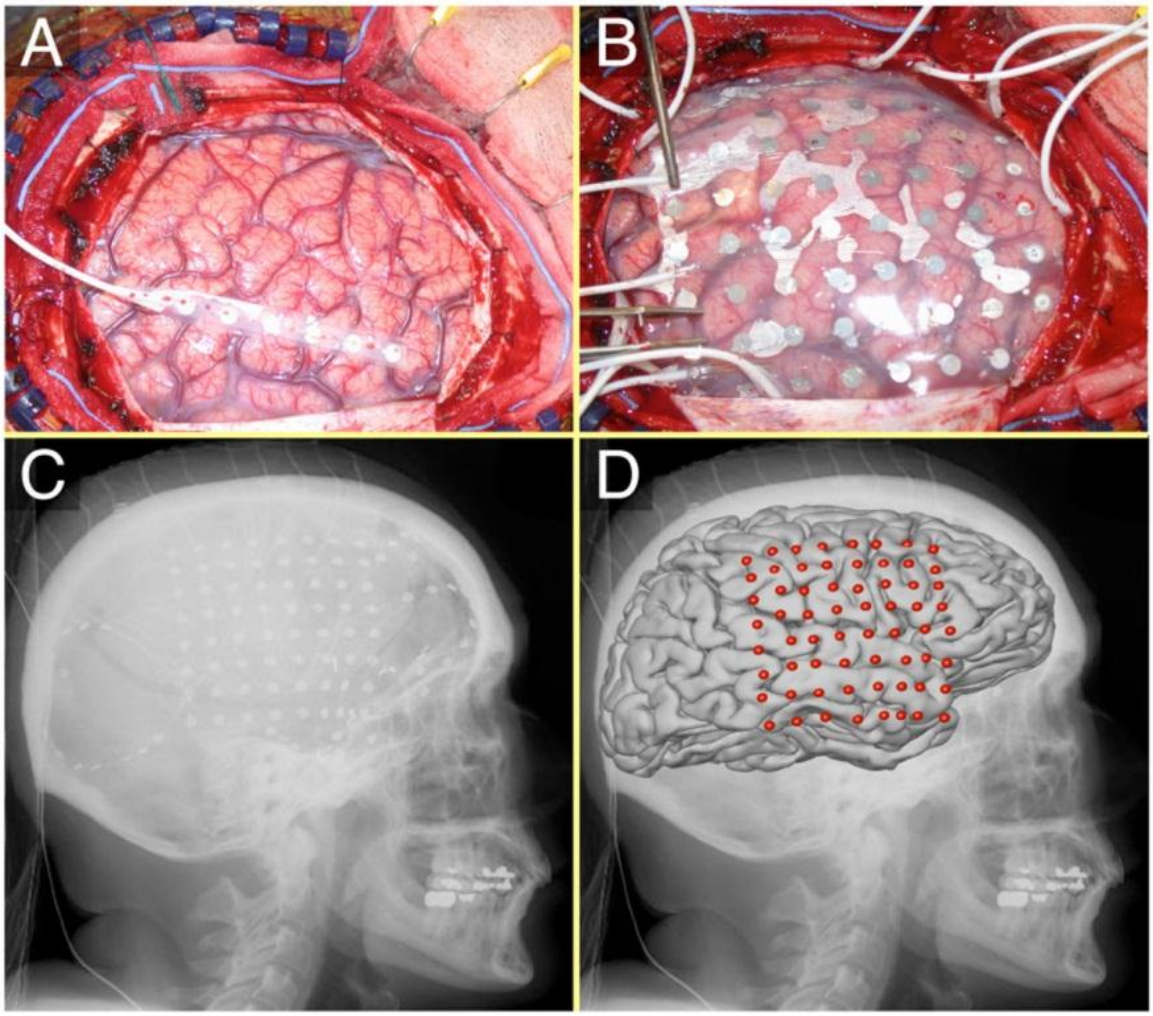

Figure 6.4: ECoG array in situ. A: Exposed brain after craniotomy. B: 8×8 electrode grid on the surface of the brain. C: Lateral x-ray image. The electrode grid and several strips are visible. D: Average brain template and electrode locations co-registered to the x-ray image. (Reproduced with permission (Schalk et al. 2008))

For decades, there has been a tremendous amount of interest in neural prostheses as evidenced by many movies, serials, novels etc. based on or relating to some sort of brain-machine interface. But considering the progress we have made in this field in past couple of decades, it is no exaggeration to confess that the real status of the technology is still in its infancy. There are many hurdles on the way to perfecting this technology, many breakthroughs to achieve before we shall actually start to enjoy its benefits. It doesn't seem impossible to achieve some of the benefits considering the rapid progress the science has made. However it is definitely a much more difficult task as most might reasonably consider.

The possibility of having full-fledged visual or auditory prosthetic devices is still a long way off, considering its limited trials in humans(Delbeke, Oozeer, and Veraart 2003; Wilson et al. 1991) and the difficulty of inferring the perceptions and thus behavioral studies after implantation in animal models(Troyk et al. 2003; Shinohara et al. 2002). On the other hand, in animal models(Schwartz et al. 2006; Carmena et al. 2003; Patil et al. 2004; Wessberg et al. 2000; Talwar et al. 2002) and in human experimentation(Hochberg et al. 2006; Serruya et al. 2002) use of chronic multi-electrode array implantation in sensorimotor cortices has been demonstrated. Here the virtual or prosthetic limb movement by the switching between the brain control mode and hand control mode has been established. This makes the implementation of sensorimotor prostheses a more likely possibility in near future.

The use of non-invasive EEG recordings to control a remote robot has been attempted(Millán et al. 2003). Similar signals are used to control the wheelchair also(Felzer and Freisleben 2002). Stimulating the spinal cord, peripheral nerves or even muscle directly to generate limb movements has also been investigated, sometimes with successful patient application(Stein et al. 2002). Electrocorticography (ECoG) has recently been tried to control the

cursor with the leads over the sensory and/or motor cortex(Felton et al. 2007). ECoG is considered superior to EEG because of higher signal-to-noise ratio (SNR) attributed to subdural lead placement or needle electrodes. However it is a less likely choice because of its invasive nature. Evidence of possible brain-computer interfacing (BCI) using thalamic/subthalamic recordings in some awake human subjects under acute setup(Patil et al. 2004) has shown some exciting possibilities. Chronic cortical multi-electrode implant(Hochberg et al. 2006) also has a comparable success rate, but definitely needs further investigation.

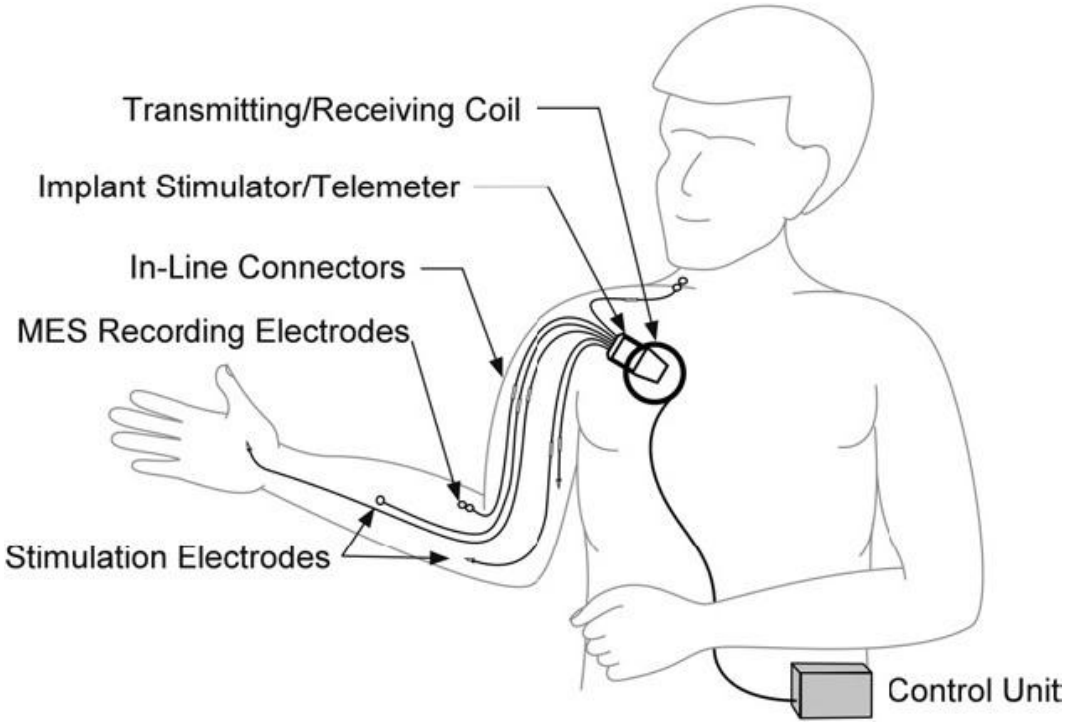

Figure 6.5: Drawing of the second-generation neuroprosthetic system. The internal components include the IST-12, 12 stimulating electrodes (not all shown), and 2 recording electrodes. The external components include the control unit and the transmit/receive coil. This system provides grasp/release, forearm pronation, and elbow extension with myoelectric control for improved function in the tetraplegic spinal cord–injured individual. MES, myoelectric signal. (Reproduced with permission from (Kilgore et al. 2008))

The ultimate goal of these neural prostheses would be to successfully implement real-time BCI. The use of non-invasive EEG recordings on humans has been demonstrated by various groups(Millán et al. 2003; Guger, Ramoser, and Pfurtscheller 2000) and also some patients have been able to control the orthosis (Pfurtscheller et al. 2000). The use of EEG signals is extending towards the video gaming(Mason et al. 2004) and some real-life problem solution for paralytics like switching(Borisoff et al. 2004). The success in the EEG technology can be attributed to its non-invasive nature allowing the experimenter access to a higher number of subjects and volunteers and thus more opportunity to optimize the signal interpreting algorithm. Compared to this, the high SNR invasive implantable devices require surgery and strict protocol. This significantly limit the number of subjects and experiments. Also, behavioral training to non-human primates(Wessberg et al. 2000) takes at least a few months to make them reasonably proficient in the particular task.

6.5 Manufacturing and different implications

The neuroprostheses currently used are made from a wide variety of components that directly or distally record from or stimulate the neural substance. These include familiar EEG metal leads(Mason et al. 2004) to recently FDA approved temporary devices like Cereport (Hochberg et al. 2006) made of Platinum with or without Iridium Oxide coating. A vast variety of electrodes are in use currently on humans for finding epileptic focus(Spencer et al. 1990) or to treat drug-refractory parkinsonism (Simuni et al. 2002) as mentioned earlier. Here we will briefly discuss only the aspects and parts of the manufacturing processes which directly deal with the health of the end-user and the personnel involved in such processes.

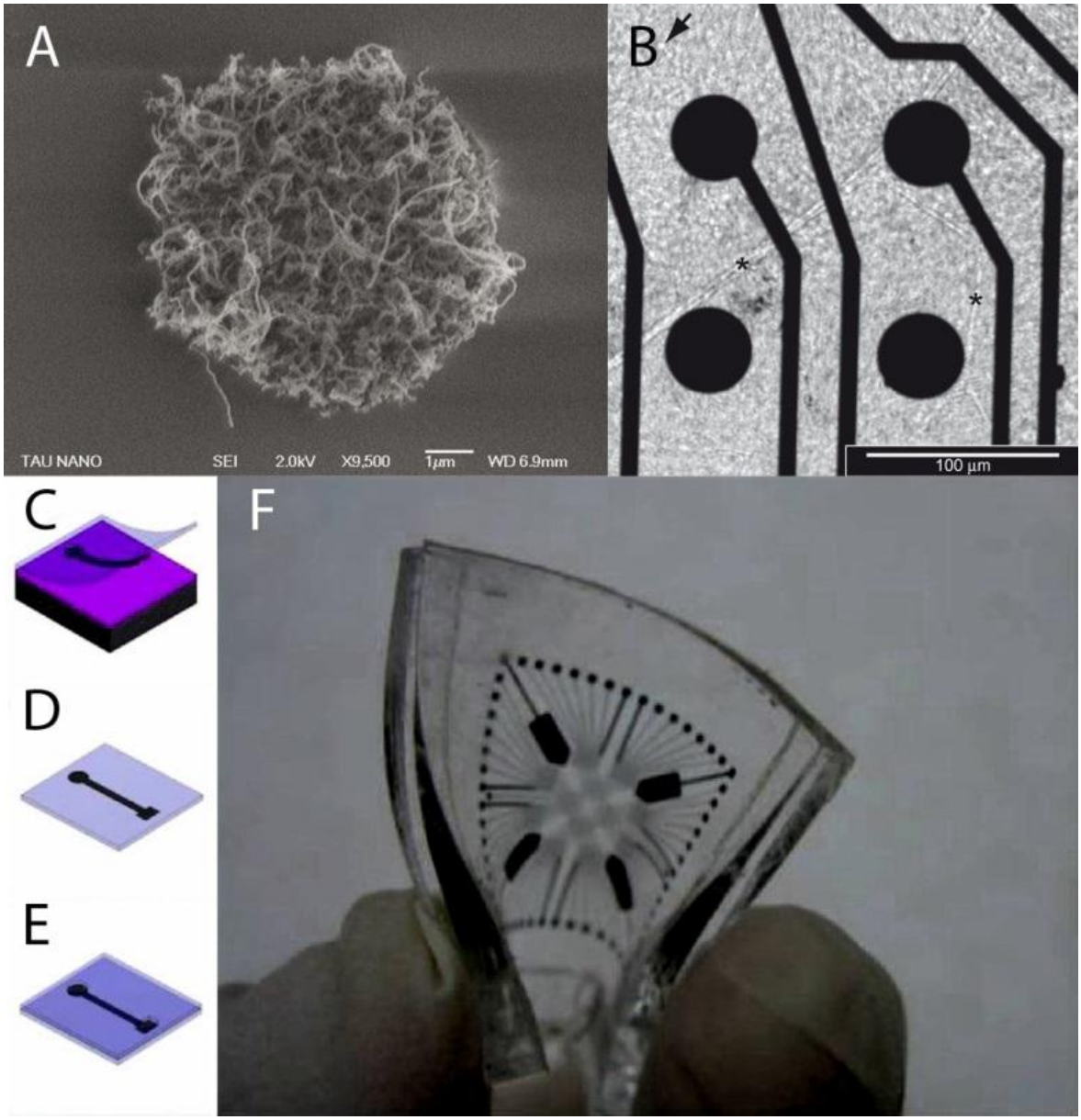

Figure 6.6: (A) Carbon nanotube (CNT) island on a single microelectrode (x9500). Note the porous nature of the CNT island. (B) Four of such islands can be seen with a retina laid on such a microelectrode array in vitro (x32). An arrow points to a retinal ganglion cell and asterisks to blood vessels. (C-E) Design of flexible CNT MEA in preparation and (F) finished product. (Reproduced from (Shoval et al. 2009; Hanein 2010)).

Like any other manufacturing process, neuroprostheses have to undergo different stages of development to reach final state. The processes involve molding, hybridization, functionalization, coating etc. The most important things of concern here is proven bio-friendly

and non-hazardous quality of the material, and proven eco-friendliness of the manufacturing process as a whole. Both these issues can be exemplified by new potentially promising technology of carbon nanotubes.

Carbon nanotubes as an integral material of implantable microelectrodes has been used for recording purposes in neuronal cultures in vitro (Lovat et al. 2005; Keefer et al. 2008), in small animals (Keefer et al. 2008), and even in non-human primates (Keefer et al. 2008). There are some reports to stimulate the neural substrate through carbon nanotubes after appropriate functionalization as well (Wang et al. 2006). The results look exciting and promising, but the overall effect of carbon nanotubes on health is still unknown. Some recent reports document the effects of carbon nanotubes on different systems of the body (Smart et al. 2006; Carrero-Sanchez et al. 2006; Fraczek et al. 2008; Mooney et al. 2008; Salvador-Morales et al. 2008; Florczyk and Saha 2007; Vallero 2007), but they might still not be adequate to actually advocate the use of carbon nanotubes for different applications, including neuroprostheses, for populations at large. Similarly, the reports on the manufacturing process of carbon nanotubes and its effect on the health of the personnel involved (Shvedova et al. 2003; Lam et al. 2006; Robichaud et al. 2005; Köhler et al. 2008) should be considered with utmost scrutiny since the only way to deal with the potential hazards of new unknown technology is to prevent them.

6.6 Animal trials

Just like most new medicine or surgical techniques, thorough animal experimentation should be conducted before a new technology of neuroprosthetics is used on humans. One can always question and object to the need for animal trials, but at the same time one has to consider the benefits of such trials in terms of higher success rate for human use, the non-

hazardous nature of such new technology also needs to be demonstrated by controlled experiments on other species.

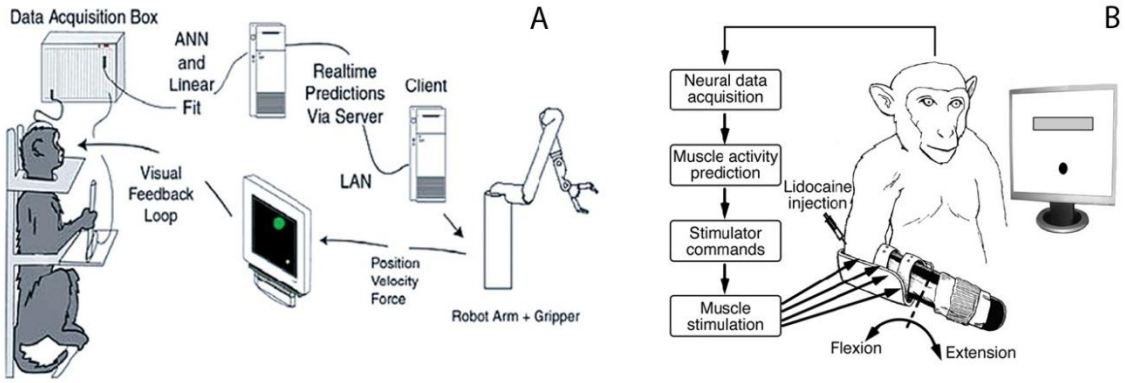

Figure 6.7: Schematic diagrams of some of the currently used experimental setup of closed-loop brain-machine interface, controlling robotic arm (A, reproduced from (Carmena et al. 2003)) or the paralyzed limb (B, reproduced from (Pohlmeyer et al. 2009))

It would be humane to respect every form of life, and thus the animal trials have to be designed in a way to minimize the number of compromised animals with maximum amount of results obtained from a single animal. Apart from being frugal on use and duration of use of animals, we should consider it more appropriate to use animals of lower taxonomical classification whenever possible. With technological advancement especially in the field of computers, modeling of a biological system in a more realistic way has sometimes been possible. If by utilizing mathematical modeling we can estimate the results that we can get from an animal experimentation, this can drastically decrease the need of animal trials. Such modeling may allow the investigator to test only a few animals to demonstrate the proof of the principle that has been developed through extensive simulation and calculations. Similarly, in vitro experiments should be encouraged over in vivo trials wherever possible.

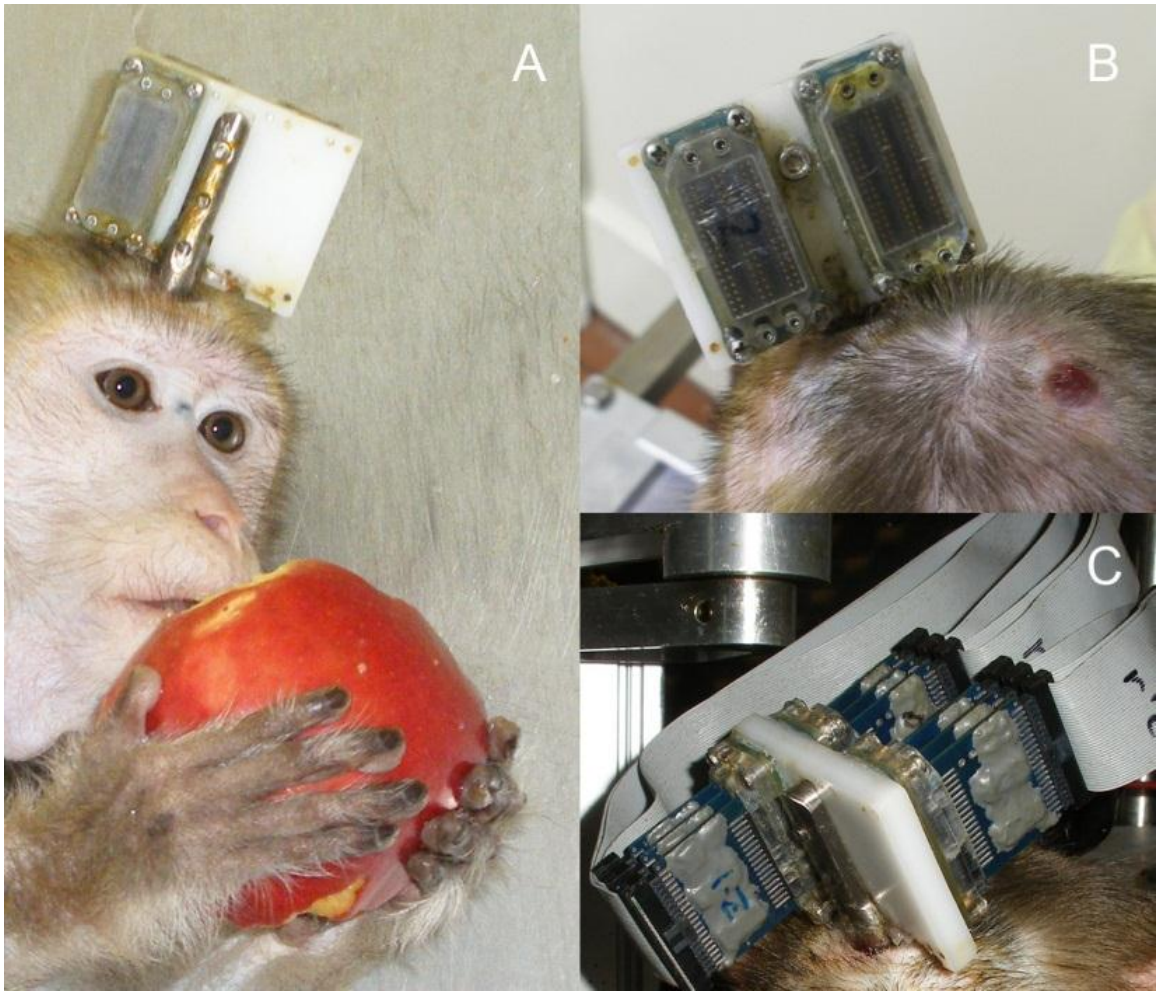

Figure 6.8: An experimental implant device that is capable of carrying connectors from multiple microelectrode arrays thus giving access to hundreds of implanted microelectrodes while limiting the exposed scalp skin margin and thus decreasing the chances of infections and other complications. A, monkey enjoying an apple; B, view from the back while seated; C, assembly with headstages plugged in. (Reproduced from (Chhatbar et al. 2010)).

6.7 Clinical trials

Once the animal trials are completed, the next step for most technology before being marketed to the general population is to undergo clinical trials, which is testing of the technology on a limited number of people to prove its non-hazardous nature and efficacy. Fortunately for the field of neural prosthetics, cochlear implants have been used routinely for

decades on deaf patients (House and Willstedt 1957) and long term reports on subthalamic implants are also being reported(Pahwa et al. 2003). Trials of sensorimotor prosthesis for tetraplegic humans have been approved by FDA (Hochberg et al. 2006; Donoghue et al. 2007), with some limitations with the duration of implants. It has generated high hopes for such and other neuroprosthetic devices. It might not be an exaggeration to state that the days of routine neural prosthetic implants in disabled, or even healthy, people may not be far away.

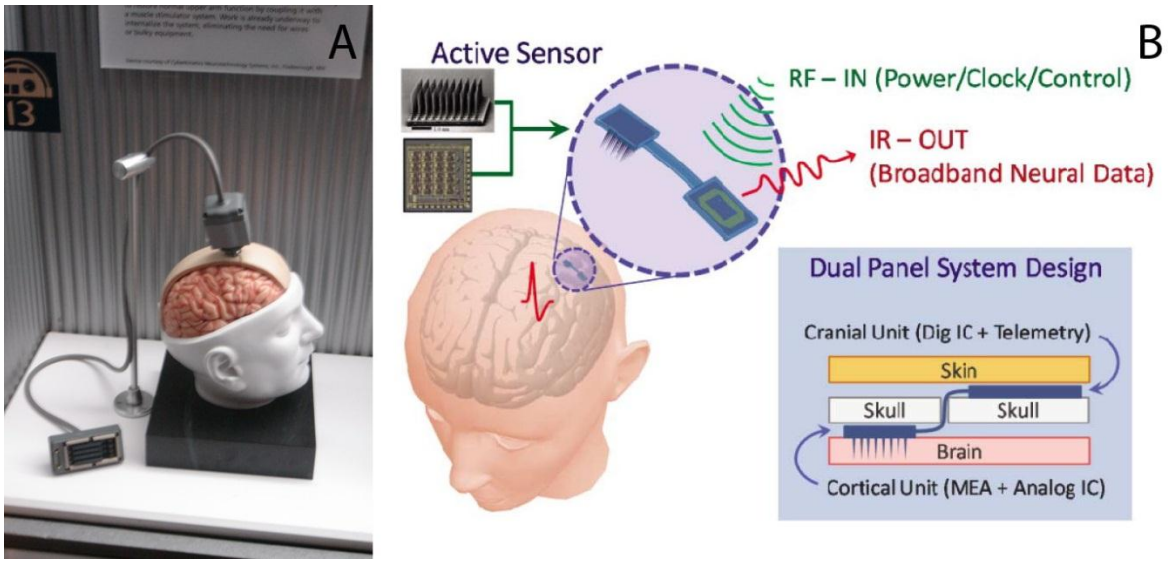

Figure 6.9: Braingate (A) and recent Braingate2 (B): two of the most famous clinical trials of sensorimotor neuroprostheses (Reproduced from: http://www.braingate.org/ and (Song et al. 2009))

Even in such an advanced stage of development of neuroprostheses, one should point out that such implants may have their own complications. Gliosis and infection with invasive neural interfaces and relatively lower precision with non-invasive methods of neural interfaces need careful evaluation before considering this technology as self-sufficient, independent and accountable for short and long term use. IRBs, HIPAA and other agencies dealing directly or indirectly with clinical trials have to be cautious in reviewing the clinical trial proposals, in the light of the rapidly ever changing and growing field of neural prostheses. This is because new

products and their extensions and/or modifications are being introduced rapidly and sometimes these may not even have FDA approval for clinical trials before being marketed to the physicians, and thus their hospitals and patients.

Another major consideration in clinical trials is the need for informed consent for the newer technology. One problem here is that the informed consent cannot be fully 'informed' in a true sense because no one can predict the outcome of this new 'treatment'. So, one should include as many possibilities of favorable and unfavorable outcomes and potential remedies to deal with them. This possibly will minimize the confusions and apprehensions that can arise out of unexpected events during the clinical trials.

Compensation for the clinical trial participants is the other sensitive issue that needs to be addressed carefully. With growing awareness about the newer technologies and faster means of communications, today's patient is more informed than ever. Considering the potential benefits of the neural prostheses, there is a good chance that the investigator would get the genuine volunteers who are interested to enjoy the favorable outcome of the new technology and would consider that as compensation itself. But the investigator and the design of the clinical trial has to make it clear that it is merely a clinical trial and not the treatment option. In fact, clinical trials should not be highlighted as a treatment option as that might be considered unethical and misleading. This will avoid creating unrealistic hopes for the potential candidates of the new technology who may like to participate in the clinical trial of the new technology that may produce uncertain outcomes.

6.8 Humane use of tomorrow's neural prostheses

Today's widely used neural prostheses are primarily used to correct the disability. Cochlear implants give a crude sense of hearing, while subthalamic implants provide tremor free movements with relatively rapid onset compared to a debilitated parkinsonian state. But newer developments in the field of neuroprosthetics might make it possible for anyone not only to regain the vision, muscle power or mobility, but potentially gain a link of today's electronics world with the brain as mentioned earlier. This includes neural control on telecommunications which makes the possibilities infinite. This might make it very difficult to keep track of full functionality provided by this so called 'brain-machine interface' when compared with the simple electronic circuit which can have functionality to track and log all the activities. Thus, the technology might be misused if fallen into wrong hands.

6.9 Restoration vs. Supplementation

Another sensitive issue with the use of the neural prostheses is the need to limit its use to a certain extent. With the development of new technologies, the possibility to use the functionality today might grow beyond anyone's expectations. To illustrate, cochlear implants when launched decades ago had a single channel. That gave the deaf patient an ability to have a binary sense of sound of certain frequency range above a certain amplitude. The number of channels has increased today ranging from 16-channels to 32-channels in cochlear implants, which now enables the patient with profound hearing loss to actually enjoy the music and actively participate in regular conversations. Similar assumptions and projections can be safely made for visual and other neural prostheses a few decades down the line. Perhaps after a few decades, a person can be able to see with resolution comparable to a healthy eye or supplement the vision sense to make the experience as vibrant as observed in birds. The olfaction sense might be supplemented using the same technology thus making biosensors capable of sending

information directly into the brain, in real time. Sensorimotor neural prostheses can control an exoskeletal robotic system that may be stronger and more robust than the human musculoskeletal system.

Beyond our five modalities of senses, neural prostheses can be used to give us a totally novel modality of a sense. For example, ultrasound or sonar system can be designed to send signals to the brain. Put simplistically, frequency coding of a single micro-stimulation channel in the brain can be a function of the distance of an object as detected by an ultrasound. This way a person can have a sense of distance of an object, not through the stereotactic vision but through a new modality that bats use primarily to map out the surroundings and locate the prey. This suggests that the neuroprosthetics can be used not only for improvement or restoration of the disability, but supplementation, or super-ability achievement. A person with supplementation may become superior to others because of the special senses or powers that the novel use of neural prostheses can provide. With this additional ability comes additional freedom for the person to use it in a productive or destructive way. A vivid example of it would be Dr. Octopus as portrayed in the movie based on a famous comic character Spiderman (Carmena 2004). This is a potential issue of tomorrow that needs attention today considering the pace at which this technology is making progress.

6.10 Implications of neural prostheses usage and conclusion

We already have touched upon many current and potential uses of neural prostheses for today's use and tomorrow's applications. The only thing we can say about the future of this field with certainty is that the field is growing faster than ever. Our five bodily senses, namely vision, hearing, smell, taste and touch can all have external interface that can restore or supplement their function. With the advancement in the electronics and telecommunications

combined with the dynamicity and plasticity of our nervous system, the novel uses of neural prostheses can easily exceed the functions of the highly specialized biological sensors like the organ of Corti of the cochlea or rods and cons of Retina. A telecommunication chip with adequate neural connections can obviate the need not only of a cell phone but also the hearing, speaking mechanism. The amount of information transferred this way might be much less than traditional talking, which can save a large amount of dedicated neural substrate required purely for the act of talking and also would be lighter on both energy consumption and electronic data transfers. The possibilities are infinite. The question doesn't seem to be of 'if', but 'when' for reaching from current 'nanoscale' level of technological progress in neural prostheses to 'gigascale' level of proficient implementation (De Man 2005).

7 Appendix : Hardware Setup

The description of the hardware setup we developed here at SUNY Downstate hopefully will serve as a ready reference for new users getting introduced to the system and also to disseminate one possible method of setting up a closed-loop brain-machine interface system.

A schematic diagram of the system is explained below:

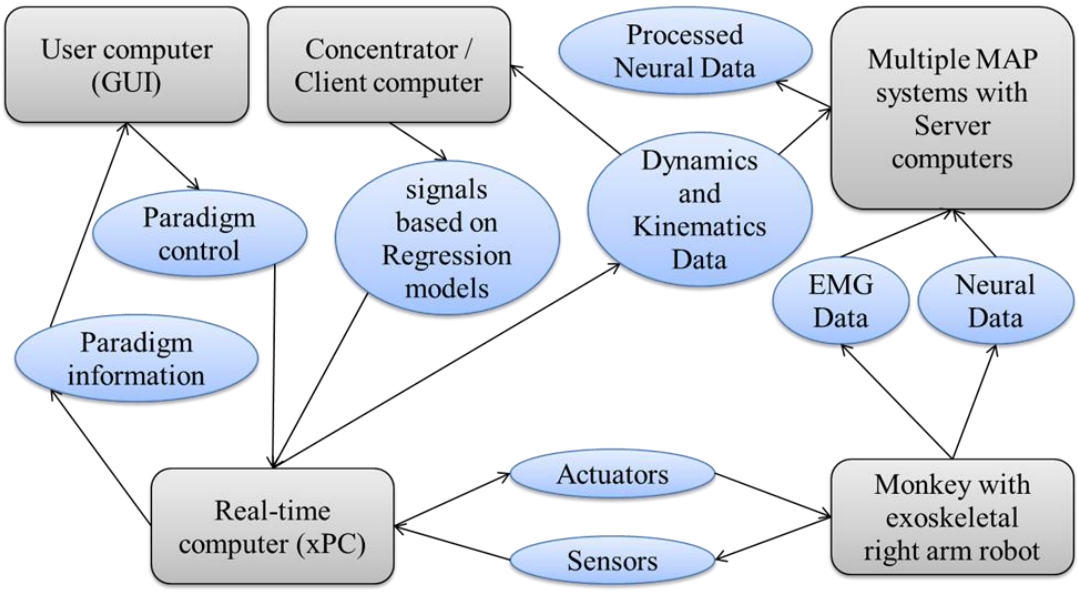

Figure 7.1: Schematic diagram of the hardware used for the experimental setup.

Every block of Figure 7.1 and its role is covered below.

7.1 Real-time computer (xPC):

This computer is the one that runs the experimental paradigm, and thus has control on the KINARM robot's sensors and actuators (using Python script). It receives movement-related kinematic and dynamic parameter information from KINARM's sensors, and in turn determines the state of the task paradigm that monkey is working on. It sends out information

to user computer (GUI) using UDP (Universal Data Protocol) packets, and also broadcasts certain state information, relevant paradigm parameters and also the motor control as well as movement-related information over the network. The program that drives xPC is written using multiple toolboxes of Matlab and Simulink like real-time workshop, xPC Target, Stateflow etc.

7.2 User computer (GUI):

This computer controls the paradigm that monkey works on. It also provides the visual feedback of the task on the screen that is mounted in the KINARM setup. It sends paradigm control signals to xPC and receives paradigm state information from it using UDP packets. This computer gives operator a comprehensive view of almost real-time progression of the task paradigm that monkey is performing and an option to start, stop, change or record task performance.

7.3 Monkey with exoskeletal right arm robot:

The robot we use is KINARM (Scott 1999) and schematic diagram is explained in Figure 7.2. Hinge joints are adjustable and can be aligned with the center of rotation of the monkey's shoulder and elbow joints. The linkage allows the monkey to move its hand in the horizontal plane by making combined flexion and extension movements at the shoulder and elbow. Each motor is attached to the device using timing belts and can modify the mechanical load at the shoulder and/or elbow joints. Accelerometers are located underneath the monkey's hand and torque sensors are attached to the base of the torque motors. A computer projection system including a semi-transparent mirror display spatial targets onto the plane of the motor task.

Eye-tracking algorithm was developed in-house where broad classification of eye-position has been made as monkey is looking at the workspace or not. This is based on supervised

training of algorithm using ~30 seconds of eye-movements. The data is synched with xPC target timer using import of timer UDP packets from xPC target at every ~3 second interval.

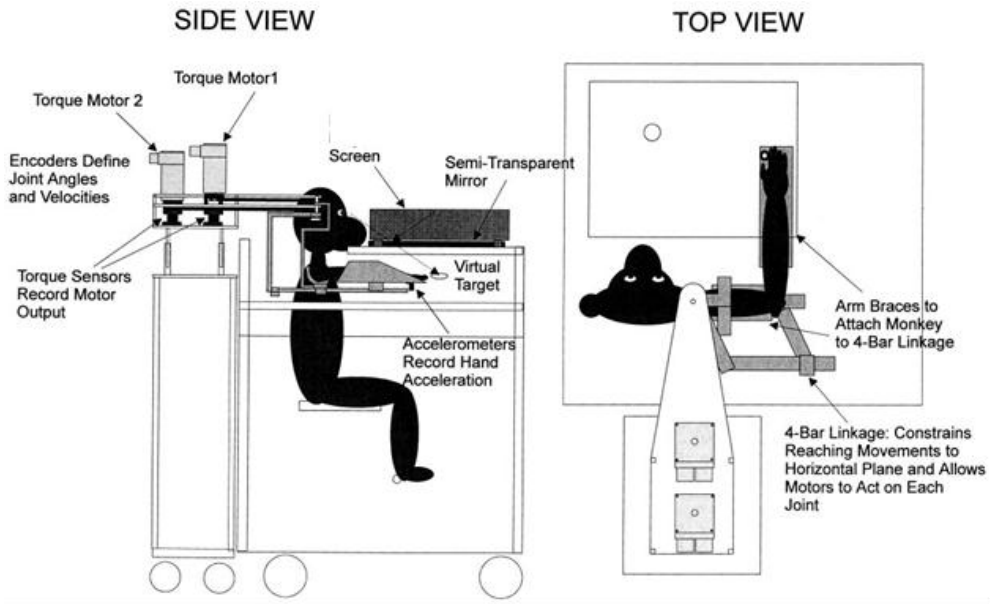

Figure 7.2: Schematic diagram of 'monkey with exoskeletal right arm robot' block in the Figure 7.1 above. Side(left) and top(right) views of monkey using KINARM(Scott 1999).

7.4 EMG Data:

EMG data is collected from Pectoralis Major (PM), Latissimus Dorsi (LD), Deltoid-anterior (DA) and posterior (DP) fibers, Biceps Brachii (BB), Triceps Brachii (TB) of both the arms, and optionally Forearm flexors (FF) and extensors (FE) using 12-channel EMG headstage system (Plexon, Dallas, TX). EMGs are band-pass filtered at 0.7 Hz – 170 Hz and sampled at 2 KHz. We use 6 mm surface electrodes (Grass Technologies, West Warwick, RI) in pairs by differential recording. The skin is prepared by abrasive gel before application of the electrode

lids with conductive gel. Monthly trimming of hair on the EMG recording sites is also performed.

7.5 Neural Data:

Neural data is collected from different cortical regions of the brain. The most commonly recorded regions are contralateral primary motor cortex (M1), dorsal premotor area (PMd), areas 3b, 1 and 2 of primary somatosensory cortex (S1). We use Microwire arrays (32 micro-electrodes per array and inter electrode spacing ~500 μm or ~1000 μm at the tip) and/or Cyberkinetics arrays (36 or 100 micro-electrodes per array and inter-electrode spacing ~400 μm at tip). Cyberkinetics arrays can be of 1.0 mm or 1.5 mm depth and is made of Platinum with/without Iridium Oxide (IrOx) coating.

7.6 Multiple MAP systems with Server computers

Three Multiple Acquisition Processor (MAP, Plexon Inc., Dallas, TX) systems with 128 spike channels and 64 LFP channel capacity each (total 384 spike channels and 192 LFP channels) are synchronized with external 2 MHz clock(Nicolelis et al. 2003). The spiking neuronal activity, after high pass filtering (154 Hz – 8.8 KHz) is sampled digitally at 40 KHz, gained, thresholded, sorted in these MAPs and then sent to the server computers to record. LFP data is filtered at 0.7 Hz – 300 Hz and sampled at 2 KHz. The analog data, in way of EMG activity and other movement related parameters are also sent to these server computers through Plexon Break-out Box (P-BOB or C-HUB), synchronized with one of the MAP system.

7.7 Concentrator/Client Computer:

This computer gets the spike timestamps from all the server computers through TCP/IP connection (PlexNetConc), and can also receive the paradigm information, instantaneous state of different kinematic and dynamic parameters from xPC.

Since all the spike-timestamps from multiple MAP systems are cumulated here, this is the computer that processes them in real-time and sends out predicted movement-related parameter value back to xPC using UDP packets, which in turn controls the GUI computer or KINARM actuator motors accordingly to run the brain-controlled task paradigm.

References

Adams, D. L., J. R. Economides, C. M. Jocson, and J. C. Horton. 2007. A biocompatible titanium headpost for stabilizing behaving monkeys. *J Neurophysiol* 98 (2):993-1001.

Albrektsson, T., and L. Linder. 1984. Bone injury caused by curing bone cement. A vital microscopic study in the rabbit tibia. *Clin Orthop Relat Res* (183):280-7.

Andersen, R. A., J. W. Burdick, S. Musallam, B. Pesaran, and J. G. Cham. 2004. Cognitive neural prosthetics. *Trends Cogn Sci* 8 (11):486-93.

Andersen, R. A., S. Musallam, and B. Pesaran. 2004. Selecting the signals for a brain-machine interface. *Curr Opin Neurobiol* 14 (6):720-6.

Behrens, E., J. Zentner, D. van Roost, A. Hufnagel, C. E. Elger, and J. Schramm. 1994. Subdural and depth electrodes in the presurgical evaluation of epilepsy. *Acta Neurochir (Wien)* 128 (1-4):84-7.

Borisoff, J. F., S. G. Mason, A. Bashashati, and G. E. Birch. 2004. Brain-computer interface design for asynchronous control applications: improvements to the LF-ASD asynchronous brain switch. *IEEE Trans Biomed Eng* 51 (6):985-92.

Branner, A., R. B. Stein, and R. A. Normann. 2001. Selective stimulation of cat sciatic nerve using an array of varying-length microelectrodes. *J Neurophysiol* 85 (4):1585-94.

Buldyrev, S. V., L. Cruz, T. Gomez-Isla, E. Gomez-Tortosa, S. Havlin, R. Le, H. E. Stanley, B. Urbanc, and B. T. Hyman. 2000. Description of microcolumnar ensembles in association cortex

and their disruption in Alzheimer and Lewy body dementias. *Proc Natl Acad Sci U S A* 97 (10):5039-43.

Cabel, D. W., P. Cisek, and S. H. Scott. 2001. Neural activity in primary motor cortex related to mechanical loads applied to the shoulder and elbow during a postural task. *J Neurophysiol* 86 (4):2102-8.

Campbell, P. K., R. A. Normann, K. W. Horch, and S. S. Stensaas. 1989. A chronic intracortical electrode array: preliminary results. *J Biomed Mater Res* 23 (A2 Suppl):245-59.

Carmena, J. M., M. A. Lebedev, R. E. Crist, J. E. O'Doherty, D. M. Santucci, D. F. Dimitrov, P. G. Patil, C. S. Henriquez, and M. A. Nicolelis. 2003. Learning to control a brain-machine interface for reaching and grasping by primates. *PLoS Biol* 1 (2):E42.

Carmena, Jose M. 2004. Brain versus Machine Control. *PLoS Biol* 2 (12):e430.

Carrero-Sanchez, J. C., A. L. Elias, R. Mancilla, G. Arrellin, H. Terrones, J. P. Laclette, and M. Terrones. 2006. Biocompatibility and toxicological studies of carbon nanotubes doped with nitrogen. *Nano Lett* 6 (8):1609-16.

Chapin, J. K., K. A. Moxon, R. S. Markowitz, and M. A. Nicolelis. 1999. Real-time control of a robot arm using simultaneously recorded neurons in the motor cortex. *Nat Neurosci* 2 (7):664-70.

Chapin, John K., and Karen A. Moxon. 2001. *Neural Prostheses for Restoration of Sensory and Motor Function*, *Methods & new frontiers in neuroscience series*. Boca Raton: CRC Press.

Chase, S. M., A. B. Schwartz, and R. E. Kass. 2009. Bias, optimal linear estimation, and the differences between open-loop simulation and closed-loop performance of spiking-based brain-computer interface algorithms. *Neural Netw* 22 (9):1203-13.

Cheng, E. J., and S. H. Scott. 2000. Morphometry of Macaca mulatta forelimb. I. Shoulder and elbow muscles and segment inertial parameters. *J Morphol* 245 (3):206-24.

Chhatbar, P. Y., L. M. von Kraus, M. Semework, and J. T. Francis. 2010. A bio-friendly and economical technique for chronic implantation of multiple microelectrode arrays. *J Neurosci Methods* 188 (2):187-94.

Chhatbar, Pratik Y., and Joseph T. Francis. 2010. Comparison of force and power generation patterns and their predictions under different external dynamic environments. Paper read at Engineering in Medicine and Biology Society (EMBC), 2010 Annual International Conference of the IEEE, Aug. 31 2010-Sept. 4 2010.

Chib, V. S., M. A. Krutky, K. M. Lynch, and F. A. Mussa-Ivaldi. 2009. The separate neural control of hand movements and contact forces. *J Neurosci* 29 (12):3939-47.

Danziger, Z., A. Fishbach, and F. Mussa-Ivaldi. 2009. Learning Algorithms for Human-Machine Interfaces. *IEEE Trans Biomed Eng*.

Dawson, T.P. 2004. Method and system for generating sensory data onto the human neural cortex. edited by U. S. Patent. USA: Sony Corporation, Tokyo (JP); Sony Electronics Inc., Park Ridge, NJ (US).

De Man, H. 2005. Ambient intelligence: gigascale dreams and nanoscale realities.

Delbeke, J., M. Oozeer, and C. Veraart. 2003. Position, size and luminosity of phosphenes generated by direct optic nerve stimulation. *Vision Res* 43 (9):1091-102.

Digiovanna, J., P. Rattanatamrong, M. Zhao, B. Mahmoudi, L. Hermer, R. Figueiredo, J. C. Principe, J. Fortes, and J. C. Sanchez. 2010. Cyber-workstation for computational neuroscience. *Front Neuroengineering* 2:17.

Dolbakyan, E., N. Hernandez-Mesa, and J. Bures. 1977. Skilled forelimb movements and unit activity in motor cortex and caudate nucleus in rats. *Neuroscience* 2 (1):73-80.

Donoghue, J. P. 2002. Connecting cortex to machines: recent advances in brain interfaces. *Nat Neurosci* 5 Suppl:1085-8.

Donoghue, J. P., A. Nurmikko, M. Black, and L. R. Hochberg. 2007. Assistive technology and robotic control using motor cortex ensemble-based neural interface systems in humans with tetraplegia. *J Physiol* 579 (Pt 3):603-11.

Fagg, A. H., G. W. Ojakangas, L. E. Miller, and N. G. Hatsopoulos. 2009. Kinetic Trajectory Decoding Using Motor Cortical Ensembles. *Neural Systems and Rehabilitation Engineering, IEEE Transactions on* 17 (5):487-496.

Fellows, Matthew, and Selim Suner. 2006. Cyberkinetics Array Surgical Implant Procedure Training Manual. Salt Lake City, UT: Cyberkinetics, Inc.

Felton, E. A., J. A. Wilson, J. C. Williams, and P. C. Garell. 2007. Electrocorticographically controlled brain-computer interfaces using motor and sensory imagery in patients with temporary subdural electrode implants. Report of four cases. *J Neurosurg* 106 (3):495-500.

Felzer, Torsten, and Bernd Freisleben. 2002. HaWCoS: The "Hands-free" Wheelchair Control System. Paper read at Fifth International ACM SIGCAPH Conference on Assistive Technologies, at Edinburgh, Scotland.

Florczyk, S. J., and S. Saha. 2007. Ethical issues in nanotechnology. *J Long Term Eff Med Implants* 17 (3):271-80.

Fraczek, A., E. Menaszek, C. Paluszkiewicz, and M. Blazewicz. 2008. Comparative in vivo biocompatibility study of single- and multi-wall carbon nanotubes. *Acta Biomater* 4 (6):1593-602.

Francis, J. T., S. Xu, and J. K. Chapin. 2008. Proprioceptive and cutaneous representations in the rat ventral posterolateral thalamus. *J Neurophysiol* 99 (5):2291-304.

Fukunaga, K. 1990. *Introduction to statistical pattern recognition*: Academic Pr.

Ganguly, K., and J. M. Carmena. 2009. Emergence of a stable cortical map for neuroprosthetic control. *PLoS Biol* 7 (7):e1000153.

Ganguly, K., L. Secundo, G. Ranade, A. Orsborn, E. F. Chang, D. F. Dimitrov, J. D. Wallis, N. M. Barbaro, R. T. Knight, and J. M. Carmena. 2009. Cortical representation of ipsilateral arm movements in monkey and man. *J Neurosci* 29 (41):12948-56.

Geers, A. E., J. Nicholas, N. Tye-Murray, R. Uchanski, C. Brenner, L. S. Davidson, G. Toretta, and E. A. Tobey. 2000. Effects of communication mode on skills of long-term cochlear implant users. *Ann Otol Rhinol Laryngol Suppl* 185:89-92.

Georgopoulos, A. P., J. Ashe, N. Smyrnis, and M. Taira. 1992. The motor cortex and the coding of force. *Science* 256 (5064):1692-5.

Gilja, V., P. Nuyujukian, C. Chestek, J. Cunningham, B. Yu, S. Ryu, and K. Shenoy. 2010. High-performance continuous neural cursor control enabled by a feedback control perspective.

Gilja, V., P. Nuyujukian, C. A. Chestek

J. P. Cunningham, B. M. Yu, S. I. Ryu, and K. V. Shenoy. 2010. A high-performance continuous cortically-controlled prosthesis enabled by feedback control design. Paper read at Society for Neuroscience, 2010, at San Diego, CA.

Giszter, Simon F., Karen A. Moxon, Ilya A. Rybak, and John K. Chapin. 2001. Neurobiological and neurorobotic approaches to control architectures for a humanoid motor system. *Robotics and Autonomous Systems* 37:219–235.

Graham, K. M., K. D. Moore, D. W. Cabel, P. L. Gribble, P. Cisek, and S. H. Scott. 2003. Kinematics and kinetics of multijoint reaching in nonhuman primates. *J Neurophysiol* 89 (5):2667-77.

Greger, B, and B Kateb. 2004. Chronically implantable hybrid cannula-electrode system for continuously monitoring electrophysiological signals during infusion of a chemical or pharmaceutical agent. Google Patents.

Guger, C., H. Ramoser, and G. Pfurtscheller. 2000. Real-time EEG analysis with subject-specific spatial patterns for a brain-computer interface (BCI). *IEEE Trans Rehabil Eng* 8 (4):447-56.

Gupta, R., and J. Ashe. 2009. Offline Decoding of End-Point Forces Using Neural Ensembles: Application to a Brain-Machine Interface. *Neural Systems and Rehabilitation Engineering, IEEE Transactions on* 17 (3):254-262.

Hanein, Y. 2010. Carbon nanotube integration into MEMS devices. *physica status solidi (b) DOI: 10.1002/pssb.201000109*:n/a-n/a.

Heliot, R., K. Ganguly, J. Jimenez, and J. M. Carmena. 2010. Learning in Closed-Loop Brain-Machine Interfaces: Modeling and Experimental Validation. *Systems, Man, and Cybernetics, Part B: Cybernetics, IEEE Transactions on* 40 (5):1387-1397.

Herter, T. M., T. Korbel, and S. H. Scott. 2009. Comparison of neural responses in primary motor cortex to transient and continuous loads during posture. *J Neurophysiol* 101 (1):150-63.

Herter, T. M., I. Kurtzer, D. W. Cabel, K. A. Haunts, and S. H. Scott. 2007. Characterization of torque-related activity in primary motor cortex during a multijoint postural task. *J Neurophysiol* 97 (4):2887-99.

Hillman, T., A. N. Badi, R. A. Normann, T. Kertesz, and C. Shelton. 2003. Cochlear nerve stimulation with a 3-dimensional penetrating electrode array. *Otol Neurotol* 24 (5):764-8.

Hochberg, L. R., M. D. Serruya, G. M. Friehs, J. A. Mukand, M. Saleh, A. H. Caplan, A. Branner, D. Chen, R. D. Penn, and J. P. Donoghue. 2006. Neuronal ensemble control of prosthetic devices by a human with tetraplegia. *Nature* 442 (7099):164-71.

House, D, and U Willstedt. 1957. Fundamental Frequency Control and Voice Quality in Cochlear Implant Users. *Working Papers*.

Howard III, MA. 1998. Wireless prosthetic electrode for the brain. edited by USPTO: The University of Iowa Research Foundation.

Humayun, M. S., J. D. Weiland, G. Y. Fujii, R. Greenberg, R. Williamson, J. Little, B. Mech, V. Cimmarusti, G. Van Boemel, G. Dagnelie, and E. de Juan. 2003. Visual perception in a blind subject with a chronic microelectronic retinal prosthesis. *Vision Res* 43 (24):2573-81.

Jarosiewicz, B., S. M. Chase, G. W. Fraser, M. Velliste, R. E. Kass, and A. B. Schwartz. 2008. Functional network reorganization during learning in a brain-computer interface paradigm. *Proc Natl Acad Sci U S A* 105 (49):19486-91.

Jones, E. G. 1998. Viewpoint: the core and matrix of thalamic organization. *Neuroscience* 85 (2):331-45.

Jones, E. G. 2000. Microcolumns in the cerebral cortex. *Proc Natl Acad Sci U S A* 97 (10):5019-21.

Keefer, E. W., B. R. Botterman, M. I. Romero, A. F. Rossi, and G. W. Gross. 2008. Carbon nanotube coating improves neuronal recordings. *Nat Nanotechnol* 3 (7):434-9.

Khamassi, M., A. B. Mulder, E. Tabuchi, V. Douchamps, and S. I. Wiener. 2008. Anticipatory reward signals in ventral striatal neurons of behaving rats. *Eur J Neurosci* 28 (9):1849-66.

Kilgore, K. L., H. A. Hoyen, A. M. Bryden, R. L. Hart, M. W. Keith, and P. H. Peckham. 2008. An implanted upper-extremity neuroprosthesis using myoelectric control. *J Hand Surg Am* 33 (4):539-50.

Kim, H. K., J. M. Carmena, S. J. Biggs, T. L. Hanson, M. A. Nicolelis, and M. A. Srinivasan. 2007. The muscle activation method: an approach to impedance control of brain-machine interfaces through a musculoskeletal model of the arm. *IEEE Trans Biomed Eng* 54 (8):1520-9.

Köhler, AR, C Som, A Helland, and F Gottschalk. 2008. Studying the potential release of carbon nanotubes throughout the application life cycle. *Journal of Cleaner Production* 16 (8-9):927-937.

Kuiken, T. A., P. D. Marasco, B. A. Lock, R. N. Harden, and J. P. Dewald. 2007. Redirection of cutaneous sensation from the hand to the chest skin of human amputees with targeted reinnervation. *Proc Natl Acad Sci U S A* 104 (50):20061-6.

Kuiken, T. A., L. A. Miller, R. D. Lipschutz, B. A. Lock, K. Stubblefield, P. D. Marasco, P. Zhou, and G. A. Dumanian. 2007. Targeted reinnervation for enhanced prosthetic arm function in a woman with a proximal amputation: a case study. *Lancet* 369 (9559):371-80.

Kurtzer, I., T. M. Herter, and S. H. Scott. 2005. Random change in cortical load representation suggests distinct control of posture and movement. *Nat Neurosci* 8 (4):498-504.

Kurtzer, I., T. M. Herter, and S. H. Scott. 2006. Nonuniform distribution of reach-related and torque-related activity in upper arm muscles and neurons of primary motor cortex. *J Neurophysiol* 96 (6):3220-30.

Lam, C, JT James, R McCluskey, S Arepalli, and RL Hunter. 2006. A review of carbon nanotube toxicity and assessment of potential occupational and environmental health risks. *CRC Critical Reviews in Toxicology* 36 (3):189-217.

Lam, Y. W., and S. M. Sherman. 2010. Functional organization of the somatosensory cortical layer 6 feedback to the thalamus. *Cereb Cortex* 20 (1):13-24.

Lanfranco, A. R., A. E. Castellanos, J. P. Desai, and W. C. Meyers. 2004. Robotic surgery: a current perspective. *Ann Surg* 239 (1):14-21.

Loizou, P. C. 1999. Introduction to cochlear implants. *IEEE Eng Med Biol Mag* 18 (1):32-42.

London, B. M., L. R. Jordan, C. R. Jackson, and L. E. Miller. 2008. Electrical stimulation of the proprioceptive cortex (area 3a) used to instruct a behaving monkey. *IEEE Trans Neural Syst Rehabil Eng* 16 (1):32-6.

Lovat, V., D. Pantarotto, L. Lagostena, B. Cacciari, M. Grandolfo, M. Righi, G. Spalluto, M. Prato, and L. Ballerini. 2005. Carbon nanotube substrates boost neuronal electrical signaling. *Nano Lett* 5 (6):1107-10.

Ludvig, N, and L Kovacs. 2002. Hybrid neuroprosthesis for the treatment of brain disorders. Google Patents.

Ludvig, N, R Rizzolo, HM Tang, RI Kuzniecky, and WK Doyle. 2009. Microelectrode-equipped subdural therapeutic agent delivery strip. Google Patents.

Luppino, G., and G. Rizzolatti. 2000. The Organization of the Frontal Motor Cortex. *News Physiol Sci* 15:219-224.

Lyons, K. E., S. B. Wilkinson, J. Overman, and R. Pahwa. 2004. Surgical and hardware complications of subthalamic stimulation: a series of 160 procedures. *Neurology* 63 (4):612-6.

Mack, M. J. 2001. Minimally invasive and robotic surgery. *JAMA* 285 (5):568-72.

Mahmoudi, B., J. C. Principe, and J. C. Sanchez. 2009. An Actor-Critic architecture and simulator for goal-directed Brain-Machine Interfaces. *Conf Proc IEEE Eng Med Biol Soc* 2009:3365-8.

Margalit, E., M. Maia, J. D. Weiland, R. J. Greenberg, G. Y. Fujii, G. Torres, D. V. Piyathaisere, T. M. O'Hearn, W. Liu, G. Lazzi, G. Dagnelie, D. A. Scribner, E. de Juan, Jr., and M. S. Humayun. 2002. Retinal prosthesis for the blind. *Surv Ophthalmol* 47 (4):335-56.

Mason, S. G., R. Bohringer, J. F. Borisoff, and G. E. Birch. 2004. Real-time control of a video game with a direct brain--computer interface. *J Clin Neurophysiol* 21 (6):404-8.

Maynard, E. M., C. T. Nordhausen, and R. A. Normann. 1997. The Utah intracortical Electrode Array: a recording structure for potential brain-computer interfaces. *Electroencephalogr Clin Neurophysiol* 102 (3):228-39.

Millán, JR, F Renkens, J Mouriño, and W Gerstner. 2003. Non-Invasive Brain-Actuated Control of a Mobile Robot. Paper read at *Proceedings of the 18th Joint International Conference on Artificial Intelligence*, 8/9/2003 - 8/15/2003.

Mooney, E., P. Dockery, U. Greiser, M. Murphy, and V. Barron. 2008. Carbon nanotubes and mesenchymal stem cells: biocompatibility, proliferation and differentiation. *Nano Lett* 8 (8):2137-43.

Murata, Y., N. Higo, T. Oishi, A. Yamashita, K. Matsuda, M. Hayashi, and S. Yamane. 2008. Effects of motor training on the recovery of manual dexterity after primary motor cortex lesion in macaque monkeys. *J Neurophysiol* 99 (2):773-86.

Musallam, S., B. D. Corneil, B. Greger, H. Scherberger, and R. A. Andersen. 2004. Cognitive control signals for neural prosthetics. *Science* 305 (5681):258-62.

Nicolelis, M. A., D. Dimitrov, J. M. Carmena, R. Crist, G. Lehew, J. D. Kralik, and S. P. Wise. 2003. Chronic, multisite, multielectrode recordings in macaque monkeys. *Proc Natl Acad Sci U S A* 100 (19):11041-6.

Nicolelis, M. A., A. A. Ghazanfar, C. R. Stambaugh, L. M. Oliveira, M. Laubach, J. K. Chapin, R. J. Nelson, and J. H. Kaas. 1998. Simultaneous encoding of tactile information by three primate cortical areas. *Nat Neurosci* 1 (7):621-30.

Nicolelis, M.A.L., J. K. Chapin, and J. Wessberg. 2007. Closed loop brain machine interface. edited by USPTO. USA: Duke University.

Niparko, J. K., R. A. Altschuler, D. A. Evans, X. L. Xue, J. Farraye, and D. J. Anderson. 1989. Auditory brainstem prosthesis: biocompatibility of stimulation. *Otolaryngol Head Neck Surg* 101 (3):344-52.

Nordhausen, C. T., E. M. Maynard, and R. A. Normann. 1996. Single unit recording capabilities of a 100 microelectrode array. *Brain Res* 726 (1-2):129-40.

Normann, R. A., E. M. Maynard, P. J. Rousche, and D. J. Warren. 1999. A neural interface for a cortical vision prosthesis. *Vision Res* 39 (15):2577-87.

Nozaki, D., I. Kurtzer, and S. H. Scott. 2006. Limited transfer of learning between unimanual and bimanual skills within the same limb. *Nat Neurosci* 9 (11):1364-6.

Nozaki, D., and S. H. Scott. 2009. Multi-compartment model can explain partial transfer of learning within the same limb between unimanual and bimanual reaching. *Exp Brain Res* 194 (3):451-63.

O'Doherty, J. E., M. A. Lebedev, T. L. Hanson, N. A. Fitzsimmons, and M. A. Nicolelis. 2009. A brain-machine interface instructed by direct intracortical microstimulation. *Front Integr Neurosci* 3:20.

Pahwa, R., S. B. Wilkinson, J. Overman, and K. E. Lyons. 2003. Bilateral subthalamic stimulation in patients with Parkinson disease: long-term follow up. *J Neurosurg* 99 (1):71-7.

Patil, P. G., J. M. Carmena, M. A. Nicolelis, and D. A. Turner. 2004. Ensemble recordings of human subcortical neurons as a source of motor control signals for a brain-machine interface. *Neurosurgery* 55 (1):27-35; discussion 35-8.

Pezaris, J. S., and R. C. Reid. 2007. Demonstration of artificial visual percepts generated through thalamic microstimulation. *Proc Natl Acad Sci U S A* 104 (18):7670-5.

Pfurtscheller, G., C. Guger, G. Muller, G. Krausz, and C. Neuper. 2000. Brain oscillations control hand orthosis in a tetraplegic. *Neurosci Lett* 292 (3):211-4.

Piccione, F., F. Giorgi, P. Tonin, K. Priftis, S. Giove, S. Silvoni, G. Palmas, and F. Beverina. 2006. P300-based brain computer interface: reliability and performance in healthy and paralysed participants. *Clin Neurophysiol* 117 (3):531-7.

Pohlmeyer, E. A., E. R. Oby, E. J. Perreault, S. A. Solla, K. L. Kilgore, R. F. Kirsch, and L. E. Miller. 2009. Toward the restoration of hand use to a paralyzed monkey: brain-controlled functional electrical stimulation of forearm muscles. *PLoS ONE* 4 (6):e5924.

Qiang, W., O. Sourina, and N.M. Khoa. A Fractal Dimension Based Algorithm for Neurofeedback Games.

Rauschecker, J. P., and R. V. Shannon. 2002. Sending sound to the brain. *Science* 295 (5557):1025-9.

Rizzolatti, G., G. Luppino, and M. Matelli. 1998. The organization of the cortical motor system: new concepts. *Electroencephalogr Clin Neurophysiol* 106 (4):283-96.

Robichaud, CO, D Tanzil, U Weilenmann, and MR Wiesner. 2005. Relative risk analysis of several manufactured nanomaterials: An insurance industry context. *Environ. Sci. Technol* 39 (22):8985-8994.

Romito, L. M., M. Scerrati, M. F. Contarino, A. R. Bentivoglio, P. Tonali, and A. Albanese. 2002. Long-term follow up of subthalamic nucleus stimulation in Parkinson's disease. *Neurology* 58 (10):1546-50.

Rousche, P. J., and R. A. Normann. 1998. Chronic recording capability of the Utah Intracortical Electrode Array in cat sensory cortex. *J Neurosci Methods* 82 (1):1-15.

Sacktor, T. C. 2008. PKMzeta, LTP maintenance, and the dynamic molecular biology of memory storage. *Prog Brain Res* 169:27-40.

Salvador-Morales, C., E. V. Basiuk, V. A. Basiuk, M. L. Green, and R. B. Sim. 2008. Effects of covalent functionalization on the biocompatibility characteristics of multi-walled carbon nanotubes. *J Nanosci Nanotechnol* 8 (5):2347-56.

Sanchez, J. C., B. Mahmoudi, J. DiGiovanna, and J. C. Principe. 2009. Exploiting co-adaptation for the design of symbiotic neuroprosthetic assistants. *Neural Netw* 22 (3):305-15.

Schalk, G, KJ Miller, NR Anderson, JA Wilson, MD Smyth, JG Ojemann, DW Moran, JR Wolpaw, and EC Leuthardt. 2008. Two-dimensional movement control using electrocorticographic signals in humans. *Journal of Neural Engineering* 5:75-84.

Schmidt, E. M., M. J. Bak, F. T. Hambrecht, C. V. Kufta, D. K. O'Rourke, and P. Vallabhanath. 1996. Feasibility of a visual prosthesis for the blind based on intracortical microstimulation of the visual cortex. *Brain* 119 (Pt 2):507-22.

Schwahn, H. N., F. Gekeler, K. Kohler, K. Kobuch, H. G. Sachs, F. Schulmeyer, W. Jakob, V. P. Gabel, and E. Zrenner. 2001. Studies on the feasibility of a subretinal visual prosthesis: data from Yucatan micropig and rabbit. *Graefes Arch Clin Exp Ophthalmol* 239 (12):961-7.

Schwartz, A. B., X. T. Cui, D. J. Weber, and D. W. Moran. 2006. Brain-controlled interfaces: movement restoration with neural prosthetics. *Neuron* 52 (1):205-20.

Scott, S. H. 1997. Comparison of onset time and magnitude of activity for proximal arm muscles and motor cortical cells before reaching movements. *J Neurophysiol* 77 (2):1016-22.

Scott, S. H. 1999. Apparatus for measuring and perturbing shoulder and elbow joint positions and torques during reaching. *J Neurosci Methods* 89 (2):119-27.

Scott, S. H., and J. F. Kalaska. 1997. Reaching movements with similar hand paths but different arm orientations. I. Activity of individual cells in motor cortex. *J Neurophysiol* 77 (2):826-52.

Scott, S. H., L. E. Sergio, and J. F. Kalaska. 1997. Reaching movements with similar hand paths but different arm orientations. II. Activity of individual cells in dorsal premotor cortex and parietal area 5. *J Neurophysiol* 78 (5):2413-26.

Serrano, P., E. L. Friedman, J. Kenney, S. M. Taubenfeld, J. M. Zimmerman, J. Hanna, C. Alberini, A. E. Kelley, S. Maren, J. W. Rudy, J. C. Yin, T. C. Sacktor, and A. A. Fenton. 2008. PKMzeta maintains spatial, instrumental, and classically conditioned long-term memories. *PLoS Biol* 6 (12):2698-706.

Serruya, M. D., N. G. Hatsopoulos, L. Paninski, M. R. Fellows, and J. P. Donoghue. 2002. Instant neural control of a movement signal. *Nature* 416 (6877):141-2.

Shinohara, T., G. Bredberg, M. Ulfendahl, I. Pyykko, N. P. Olivius, R. Kaksonen, B. Lindstrom, R. Altschuler, and J. M. Miller. 2002. Neurotrophic factor intervention restores auditory function in deafened animals. *Proc Natl Acad Sci U S A* 99 (3):1657-60.

Shoval, A., C. Adams, M. David-Pur, M. Shein, Y. Hanein, and E. Sernagor. 2009. Carbon nanotube electrodes for effective interfacing with retinal tissue. *Front Neuroengineering* 2:4.

Shvedova, AA, V Castranova, ER Kisin, D Schwegler-Berry, AR Murray, VZ Gandelsman, A Maynard, and P Baron. 2003. Exposure to carbon nanotube material: assessment of nanotube cytotoxicity using human keratinocyte cells. *Journal of toxicology and environmental health. Part A* 66 (20):1909.

Simuni, T., J. L. Jaggi, H. Mulholland, H. I. Hurtig, A. Colcher, A. D. Siderowf, B. Ravina, B. E. Skolnick, R. Goldstein, M. B. Stern, and G. H. Baltuch. 2002. Bilateral stimulation of the subthalamic nucleus in patients with Parkinson disease: a study of efficacy and safety. *J Neurosurg* 96 (4):666-72.

Skinner, M. W., D. R. Ketten, M. W. Vannier, G. A. Gates, R. L. Yoffie, and W. A. Kalender. 1994. Determination of the position of nucleus cochlear implant electrodes in the inner ear. *Am J Otol* 15 (5):644-51.

Smart, SK, AI Cassady, GQ Lu, and DJ Martin. 2006. The biocompatibility of carbon nanotubes. *Carbon* 44 (6):1034-1047.

Song, Y. K., D. A. Borton, S. Park, W. R. Patterson, C. W. Bull, F. Laiwalla, J. Mislow, J. D. Simeral, J. P. Donoghue, and A. V. Nurmikko. 2009. Active microelectronic neurosensor arrays for implantable brain communication interfaces. *IEEE Trans Neural Syst Rehabil Eng* 17 (4):339-45.

Spencer, S. S., D. D. Spencer, P. D. Williamson, and R. Mattson. 1990. Combined depth and subdural electrode investigation in uncontrolled epilepsy. *Neurology* 40 (1):74-9.

Stein, R. B., Y. Aoyagi, V. K. Mushahwar, and A. Prochazka. 2002. Limb movements generated by stimulating muscle, nerve and spinal cord. *Arch Ital Biol* 140 (4):273-81.

Suaning, G. J., N. H. Lovell, K. Schindhelm, and M. T. Coroneo. 1998. The bionic eye (electronic visual prosthesis): a review. *Aust N Z J Ophthalmol* 26 (3):195-202.

Suminski, A. J., D. C. Tkach, A. H. Fagg, and N. G. Hatsopoulos. 2010. Incorporating feedback from multiple sensory modalities enhances brain-machine interface control. *J Neurosci* 30 (50):16777-87.

Talwar, S. K., S. Xu, E. S. Hawley, S. A. Weiss, K. A. Moxon, and J. K. Chapin. 2002. Rat navigation guided by remote control. *Nature* 417 (6884):37-8.

Taylor, D. M., S. I. Tillery, and A. B. Schwartz. 2002. Direct cortical control of 3D neuroprosthetic devices. *Science* 296 (5574):1829-32.

Todorov, E. 2004. On the role of primary motor cortex in arm movement control. *Progress in Motor Control: Effects of age, disorder, and rehabilitation*:125.

Todorov, E. 2000. Direct cortical control of muscle activation in voluntary arm movements: a model. *Nat Neurosci* 3 (4):391-8.

Troyk, P., M. Bak, J. Berg, D. Bradley, S. Cogan, R. Erickson, C. Kufta, D. McCreery, E. Schmidt, and V. Towle. 2003. A model for intracortical visual prosthesis research. *Artif Organs* 27 (11):1005-15.

Vallero, D. A. 2007. Beyond responsible conduct in research: new pedagogies to address macroethics of nanobiotechnologies. *J Long Term Eff Med Implants* 17 (1):1-12.

Velliste, M., Z. Zohny, S. T. Clanton, S. M. Jeffries, A. J. C. McMorland, J.-W. Sohn, G. W. Fraser, and A. B. Schwartz. 2010. Toward robust continuous decoding for prosthetic arm control. Paper read at Society for Neuroscience, 2010, at San Diego, CA.

Venkatraman, S., K. Elkabany, J. D. Long, Y. Yao, and J. M. Carmena. 2009. A system for neural recording and closed-loop intracortical microstimulation in awake rodents. *IEEE Trans Biomed Eng* 56 (1):15-22.

Veraart, C., C. Raftopoulos, J. T. Mortimer, J. Delbeke, D. Pins, G. Michaux, A. Vanlierde, S. Parrini, and M. C. Wanet-Defalque. 1998. Visual sensations produced by optic nerve stimulation using an implanted self-sizing spiral cuff electrode. *Brain Res* 813 (1):181-6.

Veraart, C., M. C. Wanet-Defalque, B. Gerard, A. Vanlierde, and J. Delbeke. 2003. Pattern recognition with the optic nerve visual prosthesis. *Artif Organs* 27 (11):996-1004.

Waltzman, S. B., N. L. Cohen, R. H. Gomolin, W. H. Shapiro, S. R. Ozdamar, and R. A. Hoffman. 1994. Long-term results of early cochlear implantation in congenitally and prelingually deafened children. *Am J Otol* 15 Suppl 2:9-13.

Wang, K., H. A. Fishman, H. Dai, and J. S. Harris. 2006. Neural stimulation with a carbon nanotube microelectrode array. *Nano Lett* 6 (9):2043-8.

Wessberg, J., C. R. Stambaugh, J. D. Kralik, P. D. Beck, M. Laubach, J. K. Chapin, J. Kim, S. J. Biggs, M. A. Srinivasan, and M. A. Nicolelis. 2000. Real-time prediction of hand trajectory by ensembles of cortical neurons in primates. *Nature* 408 (6810):361-5.

Wilson, B. S., C. C. Finley, D. T. Lawson, R. D. Wolford, D. K. Eddington, and W. M. Rabinowitz. 1991. Better speech recognition with cochlear implants. *Nature* 352 (6332):236-8.

Zrenner, E. 2002. Will retinal implants restore vision? *Science* 295 (5557):1022-5.